DISSERTATION FOR DOCTORAL (PHD) DEGREE

Omar Saber Zinad

University of Sopron

Faculty of Wood Engineering and Creative Industries
Sopron

2026

Dissertation for Doctoral (PhD) Degree

University of Sopron

Faculty of Wood Engineering and Creative Industries

Cziráki József Doctoral School of Wood Sciences and Technologies

Head: Prof. Dr. László Bejó

Doctoral programme: F2 Creative Design and Technologies

Head of programme: Prof.Dr. Kovács Zsolt CSc and Prof. Dr. Zalavári József

Discipline: material sciences and technologies

ANALYSIS OF WATER VAPOR DIFFUSION IN STRUCTURAL WOOD ADHESIVE BOND

Written by: Omar Saber Zinad

Supervision: Mrs. Dr. habil. Csilla CSIHA

Sopron

2026

ANALYSIS OF WATER VAPOR DIFFUSION IN STRUCTURAL WOOD ADHESIVE BOND

Dissertation for doctoral (PhD) degree

Written by:

Omar Saber Zinad

Made in the framework of the József Cziráki Doctoral School , University of Sopron
F2 Creative Design and Technologies

Supervisor: Mrs. Dr. habil. Csilla CSIHA

I recommend for acceptance (**yes** / no)

(signature)……

Final debate:

As assessor I recommend the dissertation for acceptance:

First assessor (Dr. .....) yes/no ……..
(signature)

Second assessor (Dr. .....) yes/no ……
(signature)

(Possible third assessor (Dr. .....) yes/no ……
(signature)

The candidate reached .....% in the public debate of the dissertation

Sopron,

.....
Chairman of the Assessor Committee

Qualification of the doctoral (PhD) degree ….....

.....
Chairman of the University Doctoral
and Habilitation Council (UDHC)

DECLARATION

I, he undersigned **Omar Saber Zinad** by signing this declaration declare that my PhD thesis entitled "**Analysis of Water Vapor Diffusion In Structural Wood Adhesive Bond**" was my own work; during the dissertation I complied with the regulations of Act LXXVI of 1999 on Copyright and the rules of the doctoral dissertation prescribed by the Cziráki József Doctoral School, especially regarding references and citations.[1]

Furthermore, I declare that during the preparation of the dissertation I did not mislead my supervisor(s) or the programme leader with regard to the independent research work.

By signing this declaration, I acknowledge that if it can be proved that the dissertation is not self-made or the author of a copyright infringement is related to the dissertation, the University of Sopron is entitled to refuse the acceptance of the dissertation.

Refusing to accept a dissertation does not affect any other legal (civil law, misdemeanour law, criminal law) consequences of copyright infringement.

Sopron, ... 2026

……..

Omar Saber Zinad

[1] **Act LXXVI of 1999** Article 34 (1) Anyone is entitled to quote details of the work, to the extent justified by the nature and purpose of the recipient work, by designating the source and the author specified therein.

Article 36 (1) Details of publicly lectures and other similar works, as well as political speeches, may be freely used for the purpose of information to the extent justified by the purpose. For such use, the source, along with the name of the author, shall be indicated, unless this is impossible.

Acknowledgments

In the name of God, the Most Gracious, the Most Merciful.

No words can fully express my gratitude to the place that embraced me, supported my ambitions, and became my second home **Hungary**. I am equally grateful to my homeland, **Iraq**, for the trust it placed in me to represent it abroad and for granting me the honor of serving as a bridge of knowledge between the two countries.

My sincere appreciation goes to the **University of Sopron**, especially the **Faculty of Wood Sciences and creative industry**, whose academic, technical, and administrative staff were unfailingly kind, supportive, and cooperative throughout every stage of this journey.

In the spirit of the saying, "He who taught me a letter, I became forever indebted to him," I extend my deepest respect and admiration to the person who illuminated my path and shaped my knowledge my supervisor, **Dr. Csilla Csiha**. Her scientific guidance, wisdom, generosity, and human values have left a lasting mark on my life. She has been my role model in professionalism, integrity, and compassion, and I owe her more than words can convey.

My special appreciation goes to **Kasuba-Tóth Endr**e from **Hottinger Brüel & Kjaer GmbH** – the measurement experts, whose contribution played a major role in the success of the experimental work in this dissertation.

I am also grateful to **BorsodChem Zrt.** for providing essential research materials.

My gratitude is also extended to **Ms. Tolvaj Vera**, faculty doctoral office , and **Ms. Laktos Barbara**, from the International Office, whose continuous support made countless academic and administrative steps easier and smoother.

I would also like to sincerely thank the skilled technicians and colleagues **Mr. Labozar Antal**, **Horvath Imre**, **Mr. Kun Gabor**, **Mr. Hanzseros Oliver**, and **Dr. Csanády Viktória** and all academic and technical staff at the Faculty of Wood Sciences and creative industry for their invaluable collaboration.

I dedicate this work to the soul of my late **father**, to my beloved **mother**, and to my **brothers** and **sisters**, whose prayers, love, and support have always been my strength.

No words are sufficient to express my gratitude to my wife, **Hend Badr** my partner, my support, and the pillar that carried me through every hardship. She bore the weight of life's responsibilities during the most demanding moments of this journey. To her, I dedicate every effort in this dissertation.

And to my son, **Ameer**, the light of my life, this achievement is for you as well.

Finally, to everyone who stood beside me, supported me, or shared even a small part of the challenges of this path thank you. And all praise is due to God.

Omar Zinad

Table of contents

Table Of Figures

Table Of Tables

Abstract

Water-vapor diffusion in layer-bonded wood panels used for structural purposes plays a critical role in the long-term performance and durability of engineered wood products such as cross-laminated timber (CLT) used for residential houses and multistorey buildings. While the diffusion behavior of solid wood has been widely studied, far less is known about vapor diffusion through adhesive layers, the extent to which adhesives block diffusion, and the internal strains generated as a result. This thesis investigates these missing aspects by examining seven wood species: spruce, grey poplar, beech, oak, Smaragdfa, eucalyptus, and oil-palm wood under four surface conditions: uncoated, lasure-coated, commercial adhesive-coated, and coated with custom-made polymer resins of varying molecular weights (2000–6000 MW).

Water-vapor diffusion was evaluated using an accelerated cup method following ISO 12572 and ASTM E96. A total of 315 specimens were tested, and permeability behavior was analyzed under both pre-steady-state and steady-state conditions. Although steady-state water vapor permeability among uncoated wood samples appeared similar (2.62–3.81 $\times 10^{-14}$ kg/(m·s·Pa)), the pre-steady zone revealed large differences strongly governed by structure and density, with mass change at the transition point serving as the most reliable indicator of early-stage permeability. Structural adhesives exhibited significant blocking effects. The commercial adhesive produced the lowest permeability values and the highest strains, confirming its strong vapor-blocking property. In contrast, lasure coatings specially formulated to moderate vapor transport allowed semi-permeable diffusion with smooth and stable strain profiles. Custom-made polymers showed systematic molecular weight (MW) dependent behavior: low-MW systems restricted permeability, intermediate MW enabled selective vapor passage, and high-MW systems supported enhanced vapor transport while reducing internal strains. Internal-strain measurements demonstrated a direct correlation between permeability resistance and strain development, with the highest strains occurring in impermeable adhesives and the lowest in uncoated or semi-permeable coatings. The findings reveal that vapor permeability in wood bonded in layer is governed by the coupled interaction of wood anatomy, density and adhesive molecular weight. The results suggest that the development of structural wood adhesives should account for molecular weight design to enable moderate water-vapor diffusion, which can reduce moisture-induced stresses and enhance the long-term performance of CLT and other bonded in layer engineered wood systems.

Kivonat

A szerkezeti célokra alkalmazott, rétegragasztott fa panelekben lejátszódó vízgőz-diffúzió alapvető szerepet játszik az olyan mérnöki faipari termékek hosszú távú teljesítményében és tartósságában, mint a lakóépületekben és többszintes épületekben használt keresztirányban rétegelt fa (CLT). Míg a tömör fa diffúziós viselkedését széles körben vizsgálták, jóval kevesebb ismeret áll rendelkezésre a ragasztórétegeken keresztüli gőzdiffúzióról, a ragasztók diffúziógátló hatásának mértékéről, valamint az ennek következtében kialakuló belső feszültségekről.

A disszertáció e hiányzó területeket vizsgálja hét fafaj elemzésével: lucfenyő, szürke nyár, bükk, tölgy, smaragdfa, eukaliptusz és olajpálmafa. A vizsgálatok négy felületi állapot mellett történtek: bevonat nélküli, lazúrral bevont, kereskedelmi ragasztóval bevont, valamint egyedi fejlesztésű, különböző molekulatömegű (2000–6000 MW) polimer gyantákkal bevont minták esetében.

A vízgőz-diffúzió értékelése gyorsított csészemódszerrel történt az ISO 12572 és az ASTM E96 szabványok előírásai szerint. Összesen 315 próbatest került vizsgálatra, és az áteresztőképességi viselkedést mind az elő-stacionárius, mind az állandósult (stacionárius) állapotban elemeztük. Bár az állandósult állapotban mért vízgőz-áteresztőképesség a bevonat nélküli faminták esetében hasonló értékeket mutatott (2,62–3,81 $\times 10^{-14}$ kg/(m·s·Pa)), az elő-stacionárius szakasz jelentős különbségeket tárt fel, amelyeket nagymértékben a szerkezeti felépítés és a sűrűség befolyásolt. Az átmeneti pontban mért tömegváltozás bizonyult a kezdeti diffúziós viselkedés legmegbízhatóbb indikátorának.

A szerkezeti ragasztók számottevő diffúziógátló hatást mutattak. A kereskedelmi ragasztó eredményezte a legalacsonyabb áteresztőképességi értékeket és a legnagyobb belső alakváltozásokat, ami erőteljes vízgőz-záró tulajdonságát igazolja. Ezzel szemben a kifejezetten mérsékelt vízgőz-transzport biztosítására fejlesztett lazúrbevonatok félig áteresztő diffúziót tettek lehetővé, egyenletes és stabil alakváltozási profil mellett.

Az egyedi fejlesztésű polimerek esetében szisztematikus, molekulatömeg-függő viselkedés volt megfigyelhető: az alacsony molekulatömegű rendszerek korlátozták az áteresztőképességet, a közepes molekulatömeg szelektív vízgőz-áteresztést tett lehetővé, míg a magas molekulatömegű rendszerek fokozott vízgőz-transzportot biztosítottak a belső feszültségek csökkentése mellett.

A belső alakváltozások mérései közvetlen összefüggést igazoltak az áteresztési ellenállás és a feszültségképződés között: a legnagyobb alakváltozások az impermeábilis ragasztók esetében jelentkeztek, míg a legalacsonyabb értékek a bevonat nélküli vagy félig áteresztő bevonatoknál voltak megfigyelhetők.

Az eredmények rámutatnak arra, hogy a rétegragasztott faanyag vízgőz-áteresztőképességét a fa anatómiai szerkezete, sűrűsége és a ragasztó molekulatömege közötti

kölcsönhatás együttesen határozza meg. A vizsgálat megállapításai szerint a szerkezeti faragasztók fejlesztése során figyelembe kell venni a molekulatömeg-tervezést annak érdekében, hogy mérsékelt vízgőz-diffúzió biztosítható legyen, ezáltal csökkentve a nedvesség okozta belső feszültségeket és növelve a CLT, valamint más rétegragasztott mérnöki faszerkezetek hosszú távú teljesítményét..

1. Introduction and literature review

1.1. Research background

Using sustainable materials and technologies has become a global focus, implying research also. This commitment involves preserving non-renewable resources, reducing industrial waste, and lowering greenhouse gas emissions etc.. In the construction sector, both for structural and non-structural work, finding alternatives to concrete has become essential (Clements-croome, 2021). With its potential to fully or partially replace concrete in construction work, wood is a promising option that can contribute to sustainability principles. It can reduce structural costs, minimize the use of non-renewable natural resources, and lower carbon emissions (Gustavsson et al., 2006). Using wood as a construction material can help reduce cement consumption, a significant source of environmental pollution. Structural and non-structural wood, derived from forests, is used to construct large and small-scale structures (Zinad & Csiha, 2024).

The extensive adoption of engineered wood products (EWPs) in sustainable construction encounters obstacles due to the wood's moisture-sensitive physical and mechanical attributes (Christen, 1988; Karagüler & Kaya, 2017; Robert, 2010). It has become necessary to understand the behavior of wood used for buildings when the moisture content or environmental characteristics change (Gereke, 2009). Throughout the operational lifespan of timber products, the ambient temperature and relative humidity (RH) seldom remain constant. The non-uniform fluctuation in moisture content (MC) may trigger moisture-induced swelling/shrinkage strains, leading to subsequent distortion and deformation of the timber (Amaral et al., 2022; Gereke, 2009; Lennart & Elina, 2009; Rafsanjani et al., 2012, 2014). Many factors can affect the moisture diffusivity in wood-based products, such as the drying method, additives, sample thickness, composition etc.(Joščák et al., 2012; Sonderegger et al., 2010, 2011). A water molecule consists of two hydrogen atoms and one oxygen atom, and the three atoms form an angle of approximately 104.5 degrees (H-O-H angle)(Chidambaram, 1962). However, the bond angle changes when considering water vapor, leading to different behavior in the vapor phase. The challenge is managing this shift in bond angle and facilitating water vapor passage through the voids within the adhesive polymer without altering its effectiveness. In load-bearing wood assemblies, structural adhesives often restrict water-vapor transmission because their high molecular weight and dense polymer networks form an effective permeability barrier.

The central challenge, therefore, is to develop adhesive systems that permit controlled vapor passage without reducing bond strength or compromising structural performance.

Wooden structures are widely used, particularly in earthquake zones, owing to their lightweight, ease of application, and resistance to the external environment. Wood, an environmentally friendly and sustainable building element, will be more economical and safer than the current reinforced concrete and steel elements (Ozdemir et al., 2023). Water vapor permeability through the adhesive layer in structural wood is a complex phenomenon influenced by multiple factors related to the environment surrounding it, adhesive material characteristics, or the wood itself. Exploring various interconnected topics relevant to this research is essential to understanding this process and analyzing this subject comprehensively. This includes an in-depth review of previous studies that have examined similar or related aspects, such as wood properties, adhesive properties, the influence of adhesive type, thickness, and environmental conditions on water vapor diffusion through the adhesive layer. This critical evaluation will enable us to pinpoint the research gap this study aims to address, thereby contributing new insights to the field. Gaining a comprehensive understanding of the principles underlying diffusion in wood holds significance across diverse disciplines, such as forestry and construction / non-construction engineering work, due to its potential impact on the properties and functionality of wood products (H. K. Burr & A. J. Stamm, 1946).

Diffusion within wood involves the passage of water, nutrients, and diverse substances through its intricate cellular structure. Timber consists of numerous pores, which serve as small channels that enable the movement of water and other substances, as shown in Fig. 1.1. Nevertheless, it is essential to highlight that when the moisture content within wood surpasses 20%, it experiences a notable rise in vulnerability to insect infestations and fungal attacks (Van Meel et al., 2011). Water diffusion plays a vital role in the sustenance and glowing of living trees by facilitating the transport of essential nutrients and minerals throughout the plant (Chen et al., 2020; Jakes, 2019; Utsumi et al., 1998). The diffusion process within wood is subject to numerous factors, including wood species, pore size and shape, temperature, humidity, and pressure.

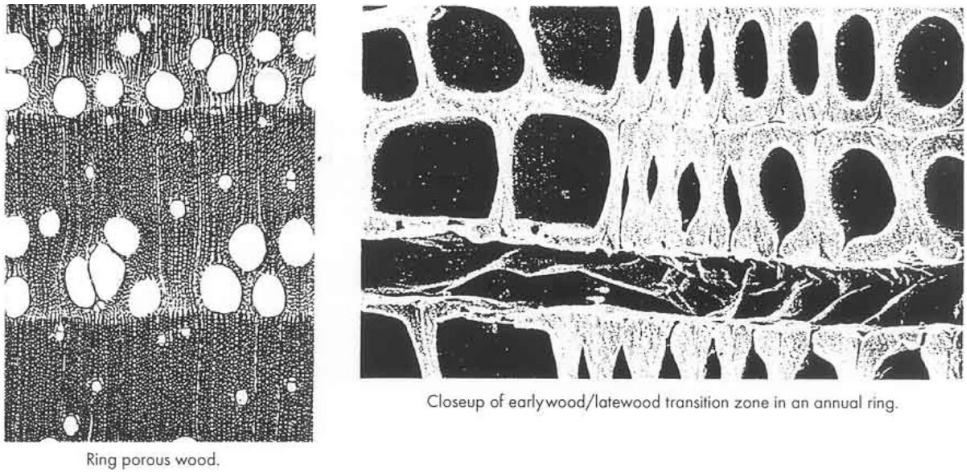

Figure 1.1 The porous channels in wood (Chaney, 2000)

1.2. Water distribution and transport mechanisms within the wood microstructure

Within the wood, water is present in two distinct locations: the cell walls and the porous macro-void structure of the material, as illustrated in Fig. 1.2. The water molecules residing within the cell walls are commonly known as "cell wall water" or "bound water" because of their close association with the polymers constituting the cell walls (Thybring et al., 2022). Cell wall water: the water particles found inside the wood cells in nano-voids also interact with cellulose, hemicelluloses, and lignin by hydrogen bonds with hydroxyl chemical groups [OH] (Lindh et al., 2017; Matthews et al., 2006). While cellulose possesses a large concentration of [OH] (Tang et al., 2013; Thybring et al., 2017). Hemicelluloses (one of the cell wall constituents) are the most responsible for bonding hydrogen with water. This occurs because a high number of hydroxyl groups in cellulose prevents water particle penetration in optimum environmental conditions (Hofstetter et al., 2006; Lennart & Elina, 2009). Capillary Water: This type of water is found in the void structure of wood. The water particles enter the wood body through capillary action or capillary condensation. Capillary condensation refers to the mechanism by which water vapor can undergo condensation in tiny empty spaces, even when the relative humidity (RH) levels are below 100% (Thomson, 1872). The occurrence of capillary condensation is influenced by the size and shape of the voids and also by the relative humidity at which it takes place (Sing et al., 1999).

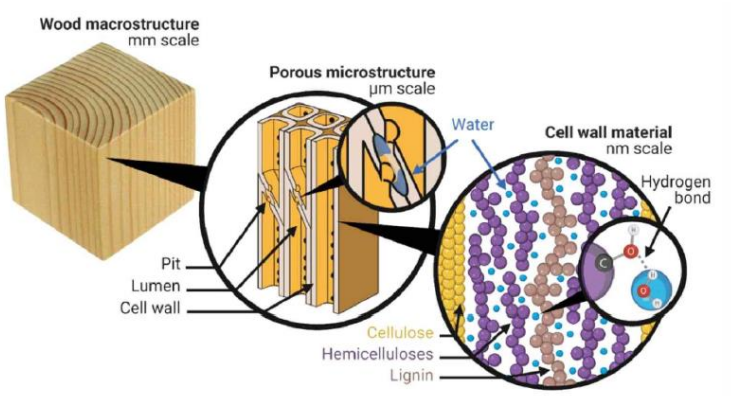

Figure 1.2 The location of water within the microstructure of wood. Adapted from Thybring et al. (2022) with CC-BY

Water transportation in wood occurs through various pathways depending on the location of water particles within the wood structure. Water transportation in wood can be categorized into three main mechanisms: water vapor diffusion, diffusion through the cell walls, and capillary water transport. The diffusion involves mass movement due to random molecular motions and can occur in the vapor phase and within the wood cell walls. In the hygroscopic range and at a constant temperature, the overall diffusion of water through wood can be mathematically described by considering the gradient in various assumed potentials, including concentration, moisture content, vapor pressure, relative humidity, chemical potential, osmotic pressure, and spreading pressure (Siau, 1984; Skaar, 1988). Fick's law is commonly used to explain water transport through diffusion (Fick, 1855). The diffusion characteristics of bonded wood samples are assessed through sorption experiments following the specification standard (ISO 12572-1, 2016) and (ASTM E96/95M). These experiments involve dry cup/wet cup setups. It is well-established that gluten-based adhesives exhibit greater moisture absorption compared to other types of adhesives, and they also demonstrate higher diffusion coefficients (Mannes et al., 2012).

1.3. Influence of wood species on water diffusion behavior

Some species of wood, such as teak (Opoku, 2007) and IPE (Tabebuia sp.) (Jankowska, 2017), have high natural resistance to water due to their high density and oil content. Other species, such as pine and fir, have a lower density and are more porous, making them more susceptible to water absorption. The amount of water a particular species of wood can absorb also varies. For example, hardwoods like oak and maple can absorb more water than softwoods like pine and cedar. This is because hardwoods have a more complex cellular structure, which

allows them to hold more water. This leads to the conclusion that wood density is a factor influencing water diffusion through wood, affecting absorption rates. The diffusion of water through wood is influenced by factors such as temperature, humidity, and the type of wood. Some woods have a higher diffusion coefficient, meaning they can absorb water more quickly than others. For example, pine has a higher diffusion coefficient than oak, meaning it can absorb water more rapidly and to a greater extent (Jankowska, 2017). When selecting wood for outdoor projects, such as decks and fences, it is essential to understand the relationship between wood species and water diffusion. By choosing a wood species that is naturally resistant to water and with a low diffusion coefficient, you can help ensure that your project will withstand moisture exposure over time.

1.4. The effect of wood moisture content on water diffusion in wood

The moisture content of the wood also affects the performance of the adhesive. High moisture content can reduce the adhesive's bonding strength and increase the water diffusion rate (Bekhta et al., 2015). The moisture content of the wood is also influenced by the relative humidity and the environment's temperature. For example, wood stored in a high-humidity climate will absorb moisture and have a higher moisture content than wood kept in a low-humidity environment.

1.5. The effect of temperature on water diffusion in wood

The surrounding environmental temperature influences the performance of water diffusion through wood or glued wood. Higher temperatures can accelerate the rate of water diffusion, leading to faster degradation of the glue line. Conversely, lower temperatures can slow water diffusion, increase brittleness, and reduce adhesive flexibility. These were the results obtained from (Heshmati et al., 2016), temperature plays a crucial role in both the rate of water vapor diffusion and the overall durability and properties of the adhesive.

Kang & Hart (1997) focuses on the relationship between drying temperature and the moisture diffusion characteristics of the wood specimens by examining the impact of drying temperature on the unsteady-state moisture diffusion process. In this experiment, small wood species from Poplar and Oak, with a thickness of 25 mm, were dried at four different temperatures: 32.2°C, 43.3°C, 54.4°C, and 65.6°C with two different rates of moisture content 10% and 5%. The linearity observed in the plot provides evidence that moisture diffusion through wood is a process that is activated. This finding suggests that temperature plays a

crucial role in influencing the rate of moisture movement within the wood material (Kang & Hart, 1997).

Chiniforush et al.(2019) conducted a comprehensive investigation on the effects of glue lines, moisture content, and temperature on diffusion coefficients of various engineered wood products. The study involved measuring diffusion coefficients in three orthogonal directions for glued laminated timber (Glulam) made from Blackbutt (Eucalyptus pilularis), Pacific Teak (Tectona grandis), Tasmanian Oak (Eucalyptus regnans/oblique/delegates), Radiata Pine (Pinus radiata), Slash Pine (Pinus elliottii), as well as Laminated Veneer Lumber made from Radiata Pine and Cross Laminated Timber made from Norwegian Spruce (Picea abies). Specimens were prepared both with and without glue line, and the experiments were conducted at four different temperatures: 15°C, 25°C, 35°C, and 45°C, along with three different relative humidity gradients. The findings demonstrated that the diffusion coefficient significantly difference depended on temperature (direct relationship) and moisture content (direct relationship). This highlights the importance of considering these factors when modeling moisture transport, analyzing drying stresses, distortion, and warping, and conducting long-term serviceability assessments of timber elements (Chiniforush, Valipour, et al., 2019).

The influence of temperature on moisture-induced shrinkage and swelling in the longitudinal direction was studied by Chiniforush et al., (2019).This investigation delved into the hygroscopic behavior of engineered timber, focusing on two distinct categories: a) glued-laminated timber comprising Teak, oak, blackbutt, Scotspine, and slash pine) laminated veneer lumber constructed from Radiata Pine. The study entailed a comprehensive experimental regimen designed to scrutinize timber's moisture-induced swelling and shrinkage at two distinct temperatures: 15°C and 50°C. The outcomes highlighted noteworthy distinctions in the swelling and shrinkage characteristics between extensive glued-laminated timber (glulam) and laminated veneer lumber (LVL) specimens compared to their smaller clear wood counterparts. Furthermore, temperature significantly difference influenced the moisture-induced swelling and shrinkage of glulam and LVL beams in the transverse direction. Specifically, there was an observed decrease in the coefficient of moisture expansion and/or moisture contraction in the transverse direction with escalating temperatures. Increasing the temperature from 15 °C to 50 °C increased the coefficient of moisture expansion and coefficient of moisture contraction in the longitudinal (parallel to the grain) direction of the glulam and LVL. Moreover, engineered timber's coefficient of moisture expansion and/or moisture contraction experienced a substantial drop (exceeding 90%) for moisture content alterations beyond the fiber saturation point (FSP). Temperature fluctuations demonstrated a limited impact on the moisture content

at which the wood fibers attain full saturation in these specific engineered timber species. In contrast, the swelling and shrinkage coefficients in the longitudinal direction exhibited an opposing pattern.

Chedeville et al., (2012) observed that the diffusion coefficient increases exponentially as temperature rises, with the effect of temperature being more pronounced in the longitudinal direction. Conversely, the longitudinal diffusion coefficient decreases exponentially with increasing moisture content, while the transverse diffusion coefficient follows the opposite trend. Furthermore, longitudinal to transverse diffusion coefficient ratios decrease exponentially as moisture content increases. These ratios are higher at higher temperatures and eventually converge to the same value with further increases in moisture content. At lower volumetric moisture content, the coefficient of diffusion in the longitudinal direction is approximately an order of magnitude greater than that in the transverse direction (Ganne-Chedeville et al., 2012).

1.6. Adhesive behavior and insights from neutron imaging studies

To clarify the adhesive's behavior, Franke et al., (2016) conducted a study examining the hygroscopic behavior of wood and the resulting changes in its physical and mechanical properties, specifically in the glue lines of glulam and block-glued cross sections (Franke et al., 2016). Similarly, Mannes et al., (2014) focused on investigating the absorption and diffusion of moisture behavior of traditionally significant adhesives with gluten as the base material, such as fish glue, hide glue, and bone glue (Mannes et al., 2014). Fundamental differences between the adhesives that had gluten, as determined by the analysis of absorption isotherms on specimens, were observed between the base material and the artificial adhesives, such as polyurethane.

To analyze moisture transport with greater precision, neutron radiography, a method for measuring and localizing water inside the wood sample, evaluates how moisture moves (Mannes et al., 2009). Compared with previously published research utilizing neutron scans, Mannes's article showed an upgraded method for measuring and localizing water inside the wood sample (beech and spruce). Nonzero starting moisture rates were allowed and accounted for any improvement or changes in specimen morphology brought by swelling or shrinking, allowing for a description of the diffusion process inside the glue layer. The neutron imaging-derived diffusion coefficients were characterized as part of a theoretical model that accounts for the glue line microstructure. They demonstrated that the neutron imaging can be used to

measure the diffusion parameters, comparing it with the traditional method (mass change), with the difference being only 3%. Interestingly, the gluten-based adhesive had larger diffusion coefficient values than the polyurethane adhesive; this difference was not reflected in the sorption measurement .This was due to excessive penetration of the adhesive materials inside the wood with the fiber direction. It prevents adhesive layer formation, and the reason for this phenomenon can be traced to the wood surface roughness, causing significant localized tensions, resulting in tracheid bending and distortion. Csiha & Gurau (2011) found that wood surface roughness (resulting from both manufacturing processes and anatomical structure) and adhesive penetration are interrelated and dependent on wood species (Csiha & Gurau, 2011) .

In continuation of neutron imaging applications, Sonderegger et al., (2010) conducted a study on water diffusion through the spruce sample, which contained more than one layer exposed to varying climatic conditions (dry side / wet side). This study utilized neutron imaging to examine the impact of different adhesives on the diffusion process. Neutron radiography was used to detect the water content within wood. Various adhesives were investigated, including polyvinyl acetate, urea-formaldehyde resin, epoxy resin, and one-component polyurethane. The number of layers in the samples and the thickness of the adhesive were varied. The time-dependent water profiles in the diffusion direction were measured utilizing neutron transmission imaging. This article explores the diffusion coefficients of (one-component polyurethane, epoxy resin) adhesive at high moisture content levels lower than three times the magnitude of that diffusion coefficient in spruce wood (Sonderegger et al., 2010). On the other hand, a lower barrier effect appears compared with wood in polyvinyl acetate and urea-formaldehyde resin. The advantage of this non-destructive method is its high sensitivity to hydrogen, allowing visualization of time-dependent water diffusion processes in wood. Recently, several investigations with neutron radiography were carried out to analyze capillary water absorption by partial immersion of wood specimens into water. (Mannes et al., 2009) demonstrated that even small amounts of water absorbed from air moisture can be detected and quantified.

Dietsch et al., (2015) examined various commonly used methods for determining wood moisture content and assessed their suitability for monitoring purposes. Their research revealed an additional consequence of changes in wood moisture content, namely, the resultant shrinkage or swelling of the material . High moisture content in wood can create favorable conditions for fungal decay or growth. As a result, accurately estimating the moisture content of timber and taking appropriate measures in response are critical tasks in planning,

constructing, and maintaining buildings constructed with wood or wood-based products (Dietsch et al., 2015).

1.7. The impact of water diffusion on CLT and bond lines

Understanding moisture diffusion through solid wood has a significant role in wood drying. Still, it is also crucial from the point of view of internal strains, especially in the case of adhesive-bonded structural wood products. The adhesive layer may act as a barrier to moisture diffusion, causing strain on the sides of the bond line. The internal strains weaken the performance of a structural adhesive wood bond. This review is a resource for enhancing our understanding of water vapor diffusion through wood adhesive layers.

Considering the practical consequences, due to the inherent impermeability of most commercial structural adhesives to water vapor, water vapor transfer through the panel becomes highly non-uniform. When one side of a CLT panel typically the exterior-facing side is exposed to higher water vapor, it accumulates and is absorbed primarily by the wood layers adjacent to that surface. In contrast, the opposing side often facing a drier indoor climate experiences limited water vapor uptake. This asymmetric water vapor distribution induces differential swelling and shrinkage behavior in the wood, leading to internal strain development along the adhesive bond lines. This creates a scenario where tensile or shear stresses concentrate at the glue lines, potentially exceeding the adhesive's mechanical limits and initiating delamination or micro-cracking. Over time, repeated moisture cycling exacerbates this phenomenon, compromising the CLT elements' long-term bond durability and structural reliability.

Several studies have addressed this moisture-induced degradation mechanism in CLT systems to address this challenge. For example, Kläusler et al., (2013) highlighted adhesive types and application thicknesses' crucial role in mitigating strain concentrations (Kläusler et al., 2013).

1.8. Diffusion in wood systems

Mannes et al., (2009) evaluated the diffusion through wood according to Fick's law, incorporating the wood moisture content factor as a key parameter affecting wood's diffusion coefficient. Theoretically, diffusion can occur at the bond line, and it was found that several factors, including wood moisture content, influence the diffusion process. Importantly, the adhesive type or the thickness of the adhesive layer (bond line) has a minor impact, with

diffusion coefficients increasing as thickness increases. The results of these experiment conducted according to the standard represents an average value valid for the entire sample, i.e., wood coated with an adhesive layer, regardless of the properties and type of wood species or the specifications and type of adhesive, Gluten-based adhesives are known to absorb more moisture than others and also have higher diffusion coefficients (Mannes et al., 2012). Complementary to this, Olek & Weres, (2007) investigated the diffusion coefficient using inverse modeling to solve the inverse diffusion problem. In this research, they assumed that the moisture content would better determine the diffusion coefficient for bound water in Scots pine wood. Their study highlighted that traditional diffusion methods may fall short in accuracy by ignoring these factors and recommended studying the heat and moisture coupling for greater simulation fidelity. Thybring et al., (2022) provides a comprehensive overview for understanding of the basic principles of water within wood, which is divided as cell wall water (bound water), capillary water (free water), while emphasizing significant gaps in knowledge related with the diffusion through adhesive material. The review encompasses various aspects, including water distribution in wood, phase changes by diffusion of water in wood, and equilibrium states of water within the material. Also, it clarified that there is a non-Fickian diffusion behavior in wood that occurs especially at high relative humidity levels like 95%. Unlike Fickian diffusion, where moisture diffuses in response to a steady gradient, non-Fickian behavior involves slow, delayed water uptake due to interactions between water molecules and the polymers inside the wood cell wall.

Supporting evidence from Wadsö (1993) reinforces these insights. His doctoral research revealed that diffusion coefficients derived from steady-state "cup methods" differ from those obtained through unsteady-state "sorption method". For these differences, he described many factors affecting effectiveness, such as surface resistance, non-Fickian behavior, and temperature effects due to sorption heat. Wadsö concluded that while cup methods provide reliable values for use in Fickian models, sorption-based methods require careful calibration and may not accurately reflect moisture behavior in adhesive-bonded systems due to slow water uptake dynamics in the cell wall. Finally, parallel insights can be drawn from research on water vapor transmission in cementitious materials, where it was shown that vapor transmission does not strictly follow linear gradients of vapor pressure. Rather, absorption states, surface diffusion, and microstructural interactions dominate the transport mechanism an analogy that aligns with the behavior of bonded wood systems, further justifying the need for advanced modelling beyond classical Fickian assumptions.

1.9. Penetration of adhesive materials

There are various adherent and adhesive types and different processes to bond materials. Nowadays, wood adhesives are used in over 70% of wood products worldwide. This widespread usage can be attributed to their indispensable role in fastening furniture joints and facilitating the creation of wood composite materials (Gardner, 2018).

In the research conducted by Ülker, (2016) The technical properties of various types of wood adhesives were examined, including environment-friendly adhesives. Furthermore, the article discusses the penetration of wood adhesives. This aspect is explored in the section dedicated to the technical properties of wood adhesives. The penetration of adhesive into wood can be classified into two distinct groups:

Gross penetration: This type of penetration occurs when liquid resin flows into the porous structure of wood, primarily filling the cell lumens. Gross penetration can be attributed to hydrodynamic flow and capillary action.

Cell wall penetration: In this case, resin diffuses into the cell wall or flows into micro fissures within the wood structure.

Given that vessels in hardwoods lack pit membranes and are connected end-to-end with perforation plates, they play a significant role in the penetration of adhesives. This particular cell type tends to dominate adhesive penetration in hardwoods. Through optical microscopy, the author observed resin present in pit chambers of both hardwood and softwood species, as well as in cell lumens. Notably, the sole pathway for resin entry into these cells was through the pit structure (Hwang et al., 2022).

1.10. Adhesive types for structural bonding of wood

Various wood adhesives are available, each with unique properties and ideal applications. Natural polymer-based adhesives, such as gluten-based ones, fish glue, hide glue, and bone glue, have traditionally been widely employed in non-structural applications like furniture, veneering, and instrument making. Casein-based resins do not have creep but have low water resistance. Only a limited number of adhesives are suitable for structural bonding with the general expectation to exhibit negligibly low or no creep and preferably high-water resistance. EPI Polyurethanes are frequently used in CLT production. Similar studies were done by Hwang et al., (2022) on the effects of manufacturing in the environment on the bonding performance of CLT using a polyurethane (PUR) adhesive; many other studies were also

conducted on CLT and adhesive. Here are some of the most common structural types of wood adhesives and their general properties:

Phenol-resorcinol-formaldehyde (PRF) glue: RF glue is a two-part adhesive made from resorcinol and formaldehyde. It is known for its exceptional strength and is often used for bonding structural components in boats and aircraft (Schwandt & Gound, 2003).

Phenol formaldehyde (PF) glue is a type of adhesive commonly used as a wood glue; a synthetic polymer formed through the chemical reaction of phenol (an alcohol derived from benzene) with formaldehyde (derived from methane). These resins are renowned for their exceptional adhesive properties and find extensive application as wood adhesives, particularly in the construction industry. They are commonly employed in producing waterproof wood panels like plywood and oriented strand boards, making them indispensable for various construction-grade applications (Kaboorani & Riedl, 2011).

Emulsion polymer with isocyanate (EPI) glue is a highly effective adhesive for wood-to-wood bonding. It comprises two components: a water-based emulsion and a hardener. EPI glue formulations can vary, offering different combinations of emulsion and hardener. This adhesive is particularly suitable for wood with high moisture content. It finds wide applications for parquet adhesive, finger joint adhesive, and bonding wood panels. Moreover, EPI glue is suitable for doors, windows, wood veneer, and edge-glued panels, making it a versatile choice for various woodworking applications (Sandberg, 2016).

One-component polyurethane (PUR) glue: curing these types of adhesives is initiated by the moisture content of the environment, most of all the water vapor of the environmental air. The bond is known for its good water resistance and is often used for outdoor applications (Kong et al., 2011). The material components of each adhesive can vary depending on the specific type and manufacturer. However, common components include synthetic polymers.

In a study conducted by Sernek et al., (2008), the bonding performance of heat-treated wood using different adhesives was examined. The researchers utilized untreated wood, intermediate (hydro thermolysis) wood, and fully heat-treated wood, bonding them with melamine urea formaldehyde (MUF),(PRF), and (PUR) adhesives. The results indicated that the shear strength and delamination of the laminated wood were influenced by the adhesive system employed and the degree of heat treatment. The PUR and MUF adhesives demonstrated similar performance, which was generally superior to the PRF adhesives. When bonded with MUF and PRF adhesives, the shear strength decreased for specimens made from hydro-thermolysis and fully heat-treated timber. However, the difference in shear strength between untreated, intermediate, and fully treated wood was less significant for the PUR adhesive.

Delamination of the PRF bond line substantially decreased for all heat-treated specimens. Overall, the study revealed that the bonding performance of heat-treated wood depended on the adhesive system, with PUR and MUF adhesives meeting the requirements for Norway spruce and heat-treated poplar. The researchers recommended further investigation into improving the bonding performance of heat-treated wood, including modifications to adhesive composition and bonding processes, hardeners, solvents, and fillers.

1.11. Wood adhesive mechanisms

The mechanisms by which wood adhesives work can be broadly categorized into two groups: mechanical and chemical bonding.

Mechanical bonding mechanisms rely on the physical interlocking of adhesive molecules with wood fibers to establish a mechanical bond. This bond is achieved through the penetration of the adhesive into the porous wood surface, resulting in a network of adhesive molecules that interlock with wood fibers. Adhesives such as polyvinyl acetate (PVA) glue commonly employ mechanical bonding mechanisms, enabling them to form robust and flexible bonds with wood, particularly for furniture bonding applications (Dunky, 2017).

Adhesive bonding involves chemical mechanisms resulting from the reaction between the adhesive and the surface of the wood, leading to the formation of a robust bond. This bonding process is facilitated by the chemical interaction between the adhesive and specific functional groups found within the wood, like hydroxyl (-OH) groups. Various adhesive types, including one-component polyurethane, EPI, phenol-resorcinol-formaldehyde, and phenol-formaldehyde, utilize chemical bonding mechanisms to establish enduring and resilient connections with wood surfaces (Dunky, 2017).

1.12. Water resistance of adhesives

Various factors, including adhesive type, wood species, moisture content, and temperature, influence wood adhesives' performance in wet environments. The choice of adhesive type is critical, as different adhesives have different properties that affect their ability to resist water diffusion or to be used as structural adhesives. For example, polyvinyl acetate (PVA) adhesives are commonly used in bonding non-structural wood-based products due to their selectable water resistance, high bonding strength, and low cost. Still, being subject to creep, they are not recommended for structural bonding of wood. Phenol formaldehyde (PF) adhesives, on the other hand, have excellent water resistance and structural strength. However,

they require hot pressing, which limits their application for glulam production; thus, they are commonly used in exterior-grade plywood (Bomba et al., 2014).

1.13. The effect of wood coating materials on water diffusion

Wood coating materials, like paints, can block or support water and water vapor diffusion since they are synthetic resin formulations, and depending on their characteristics. Contrary to adhesives, water vapor and water resistance are under research. Coatings manufactured for outdoor applications, like lacquer, are formulated with molecule size adjusted conveniently to allow water vapor diffusion. Waterborne outdoor lasure has rapidly become the majority of wood surface coatings (Han et al., 2022; Huang et al., 2022; Pan et al., 2022) due to their eco-friendly features (Qin & Yan, 2022; Yang et al., 2022). Considering their chemical structure, the majority of aqueous wood coatings are polyurethanes (Panda et al., 2018). However, the physical and chemical properties of one-component polyurethane products, such as water resistance (Gunesoglu et al., 2017; Wang et al., 2020) and chemical resistance (Athawale & Nimbalkar, 2010; García-Pacios et al., 2013), are somewhat inferior to those of two-component products (Yin et al., 2017). (De Meijer & Militz, 2000) conducted a study on the sorption of liquid water in coated spruce. They test of the change in the overall moisture content of the wood over time and analyzed the moisture content results at different intervals. The study involved various outdoor coatings, including a solvent-borne alkyd coating and two waterborne acrylic coatings with varying layer thicknesses, uncoated wood was used as a reference, these diffusivities were inadequate in predicting the moisture content profiles in the coated wood, particularly near the surface where a significant increase in moistening was observed. The most accurate prediction of the moisture content profile was achieved by incorporating the changing surface concentration and the diffusion coefficient derived from the sorption data of uncoated wood. In general, diffusion was identified as the primary driving force influencing water transport in the wood. On the other hand, capillary flow had a noticeable impact on sorption only near the wood surface. This phenomenon was more significant for uncoated wood.

Sonderegger et al., (2015) conducted a research study to investigate the diffusion of water into spruce wood coated with an acrylate/polyurethane and a silica-based coating system. The humidity conditions varied during the experiment. Non-destructive neutron imaging techniques measured and analyzed MC. The results showed that the acrylate/polyurethane-based coating exhibited a stronger barrier effect against water diffusion than the silica-based

coating. After ten days, the silica-based coating showed similar behavior to the uncoated reference, while the acrylate/polyurethane-based coating still displayed significant deceleration in sorption. Furthermore, the acrylate/polyurethane-based coating specimens demonstrated a strong barrier against water sorption into the wood throughout the entire measurement period, even when subjected to changing humidity conditions and direct water contact.

Despite the differences between coatings and adhesive materials, recent results indicate that PUR adhesives (specifically, those commonly used CLT) may exhibit a similar water diffusion-blocking effect to some paints. Consequently, their water diffusion-blocking status also needs to be analyzed.

1.14. Adhesive layer under vapor diffusion and evidence internal strain development

Structural adhesive material is used widely to make a mechanical link between joints or materials; it has advantageous properties according to the material that is the synthesis or based material types, but the major deficit in studies of this material through long-term behavior is the disadvantage of it (Heinrich, 2019; Kinloch, 1997). Water is the most frequently encountered harmful medium, and warm, damp environments significantly difference by reduce the strength of adhesive junctions. The physicochemical changes at the interface (or interphase) between the substrate and adhesive may be responsible for the reduction in mechanical resistance caused by water infiltration (Gledhill & Kinloch, 1974; Sharpe, 1972).

Zanni-Deffarges & Shanahan, (1995) conducted a classic gravimetric analysis on the diffusion of water into a bulk epoxy adhesive at 70°C under approximately 100% relative humidity. They observed that as the diffusion progressed, the elastic modulus of the adhesive decreased so this is the most important point to prove that there was a strain inside the adhesive material itself caused by the water vapor diffusion. Similar effects were observed in torsional adhesive joints, but the phenomenon appeared to occur more rapidly. Since gravimetric analysis is not practical for bonded joints, a "composite" model was developed to estimate water ingress by analyzing changes in the overall elastic behavior of the polymer.

The elastic moduli are influenced by the combination of rigidities resulting from the proportions of "wet" and "dry" polymer under load. The composite model provided values for the coefficient of diffusion, D, of the bulk adhesive that were in satisfactory agreement with those obtained through gravimetric analysis. However, the value of D for torsional joints was significantly difference higher. The researchers supposed that a phenomenon called "capillary

diffusion" exacerbates water ingress. Surface tension effects near the metal (oxides) polymer interfacial region increase the effective driving force for water diffusion.

Leger et al., (2010) tested industrial rubber-toughened epoxy adhesive to understand its diffusion behavior in water at different temperatures. Density measurements and gravimetric experiments were performed on bulk specimens at 25, 40, 60, and 70°C. The investigations revealed non-classical mass uptake and swelling phenomena, which will create internal strain inside the adhesive layer. During aging, it was observed that the adhesive's glass transition was surpassed, and cavities developed due to diffusion. Some water diffused into the adhesive matrix, decreasing the adhesive's glass transition temperature (Tg), while the remaining water entered the cavities. The study encompassed experimental work and phenomenological modeling to investigate water diffusion as a temperature function. The diffusion behavior exhibited non-classical characteristics at temperatures above 40°C, with significant water uptake. At a 5% uptake, the adhesive's Tg decreased to 60°C, indicating a change in the physical state and diffusion kinetics during aging in water at 60°C and 70°C. The development of cavities was attributed to a cavitation phenomenon that occurred during aging, resulting in substantial water uptake. The swelling caused by water ingress was considered the most likely cause of the formation of these cavities.

Extensive research has been conducted by Huacuja-Sánchez et al., (2016) on the interaction of water with PUR, but the exploration in the case of PU networks remains limited. In this study, a chemically simple yet well-defined PUR is employed as a starting point to investigate the influence of water on this type of polymer. During immersion in water for up to 15 days, no changes in the chemical composition of the PUR were observed in the infrared (IR) spectra. However, the water saturation in the PUR samples occurred earlier depending on the temperature. This saturation resulted in plasticization, as evidenced by a significant decrease in the mechanical modulus and a shift of the glass transition to lower temperatures in the polymer. Surprisingly, it was found that achieving approximately 70% water saturation was sufficient for maximum plasticization. The IR spectra analysis suggested that water weakens the interactions between MW within the network. The hydrogen bonds originally present in the urethane groups are partially substituted by hydrogen bonds formed between water and the urethane moieties.

1.15. Measuring the water diffusion through the adhesive layers

Various techniques have been developed for measuring water diffusion through wood adhesive layers. One commonly used method of nuclear magnetic resonance (NMR) spectroscopy can be used to measure the distribution of water within the adhesive layer. This method can use theoretically to calculate the diffusion behavior, but it takes time and there is a challenge in taking a lot of images over time (Herbst, MARK D. & Goldstein, 1989; Tsushima S., K. Teranishi, 2005). Also, Chiniforush et al., (2019) quantitatively describe the rate of moisture movement in wood as being governed by molecular diffusion, which is generally controlled by two mechanisms: vapor diffusion through lumens and bond water diffusion through the cell walls. In this case, moisture movement is divided into two parts: above the saturation point and below it, which are mainly controlled by free water (Robert, 2010; Time, 1998). Below the saturation point, moisture movement is governed by the diffusion process due to the vapor pressure gradient and other parameters, such as temperature and moisture content. These two behaviors depend on the classical Fickian theory (Skaar et al., 1969; Wadsö, 1993). The moisture transport below the saturation point is traditionally evaluated using Fick's law, which relies on the gravimetric analysis technique. This involves measuring a wood-based product sample's weight gain or loss over time as it is exposed to water. According to the main standards (ISO 12572 and ASTM E96/E96M), water or water vapor diffusion through materials can be characterized using two primary approaches: steady-state and unsteady-state methods. The steady-state method assumes constant environmental conditions throughout the test, such as temperature and humidity. In contrast, the unsteady-state method accounts for variations in these conditions over time. In this context, two experimental techniques are commonly used to evaluate diffusion behavior: the cup and the sorption methods. The following sections provide a brief description and discussion of both approaches. These methods are widely applied to determine the diffusion coefficient based on experimental environmental conditions.

1.15.1. Cup method

The cup method determines a material's diffusion coefficient by measuring steady-state water vapor flow through a sample. In this standardized test (outlined in ISO 12572 and ASTM E96), the specimen is sealed over a cup or chamber that creates two fixed humidity environments on each side (e.g. desiccant or dry air on one side and higher humidity or water on the other). This constant humidity difference drives a continuous vapor flux across the material. After an initial transient period, the rate of mass change (gain or loss of water in the cup) becomes constant and linear with time, indicating steady state. By measuring this constant

rate (mass transfer per area) and knowing the vapor pressure difference, one can calculate the diffusion coefficient or an equivalent permeability for the material (essentially applying Fick's first law in steady conditions). In essence, the cup method directly gauges how easily water vapor permeates the sample under a sustained gradient, yielding an apparent diffusion coefficient linked to that fixed set of conditions. A thin layer of wood is attached to a cup containing a saturated salt solution to create constant RH_1 on one side of the specimen. The whole assembly is conditioned inside an environmental chamber to generate a constant relative humidity RH_2 outside the cup. The seams between the cup and sample are sealed to enforce vertical transportation of the water vapor through the thin layer as shown in Fig. 2.3. Both RH are kept constant to create a constant relative humidity gradient that simulates a steady-state diffusion required for the calculation of diffusion coefficients according to Fick's first law. Depending on RH1 and RH2 values, the water vapor can diffuse in/outside the cup and change the whole assembly's weight. The water vapor permeance and diffusion coefficient with vapor pressure as a driving potential is deemed to be the slope of weight change vs. time plots as per ASTM E96/E96M.

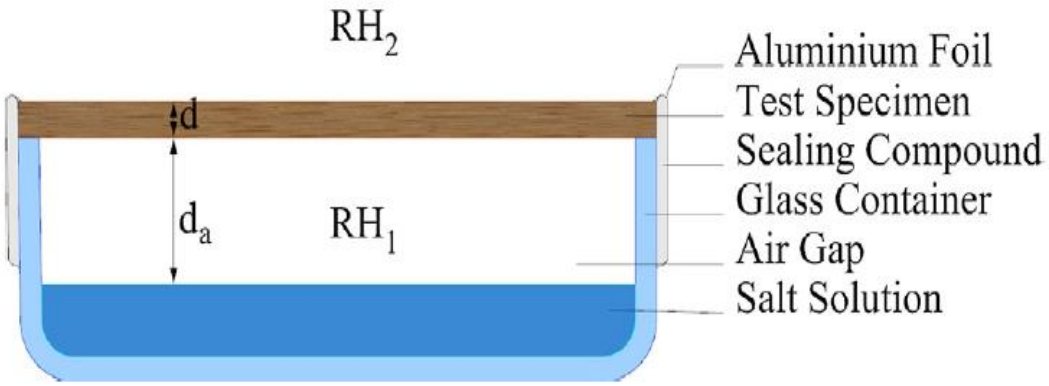

Figure 1.3Cup test set up

1.15.2. Sorption method

The sorption method, by contrast, infers the diffusion coefficient from a material's time-dependent moisture uptake or release behavior. In this unsteady-state test, the sample is first equilibrated at a known humidity, then the ambient humidity is suddenly changed (for example, from dry to humid air) so that the material begins absorbing or desorbing water vapor. The specimen's mass is recorded regularly as it gains or loses moisture, reflecting how quickly water vapor diffuses through it. Conceptually, the sorption method captures the kinetics of moisture transport: instead of a constant flux, it looks at how fast the material moves toward a

new equilibrium. This approach highlights how the diffusion coefficient governs the rate of moisture penetration, distinguishing it from the cup method's steady flux interpretation and often allowing assessment of diffusion under different humidity ranges or moisture contents (Guindeira et al., 2005)

1.16. Research gap in vapor diffusion through adhesive layers

The literature review reveals a substantial gap in understanding water-vapor diffusion through adhesive layers in CLT and the strains generated by hindered water vapor diffusion within these layers.

Research has also not sufficiently examined the development of vapor-permeable adhesive systems, despite their potential importance. Conventional structural adhesives typically exhibit low vapor permeability, causing moisture to accumulate at the bond line, which increases internal strains and elevates the risk of delamination or long-term mechanical degradation. Designing adhesive formulations that allow controlled water-vapor transmission without compromising bond strength represents a key advancement in improving CLT durability.

This research gap underscores the need for innovative adhesive technologies that combine robust mechanical performance with enhanced vapor permeability. Progress in this area would improve CLT behavior under varying environmental conditions, reduce moisture-induced failures, and strengthen the material's sustainability and service life in modern construction.

1.17. Scope of the thesis

The demand for sustainable and high-performance building materials is steadily increasing in the construction industry. CLT panels have gained significant attention as an innovative and eco-friendly alternative to conventional prefabricated wall construction elements.

Their lightweight nature, high strength-to-weight ratio, and thermal and acoustic insulation properties and sustainable renewable material make them ideal for contemporary construction. However, one of the critical challenges in utilizing wood for construction purposes lies in its hygroscopic nature. Unlike metals, glass, or other non-porous materials, wood continuously interacts with the environment by absorbing or releasing moisture based on

the surrounding humidity. This interaction leads to dimensional changes such as swelling or shrinking, impacting structural integrity and durability of wood-based building elements.

Water vapor diffusion through the adhesive material and laminated solid wood is crucial in wood bonding processes. In the case of CLT panels, where multiple layers of wood are bonded using adhesive layers, the diffusion behavior becomes even more complex. The adhesive layer may impede water vapor diffusion when it occurs perpendicular to the bond line, leading to an imbalance in moisture content between the bonded layers. This imbalance causes differential strain on either side of the bond line, inducing internal strains within the bonded assembly caused by the blocked voids of adhesive materials against water vapor diffusion. Over time, these strains may compromise the integrity of the CLT structure, affecting its performance and longevity. Thus, a pressing question arises: how long can the bonded structure maintain its integrity under the influence of moisture diffusion blockage induced strains, and what strategies can mitigate the inevitable tensions that develop within the adhesive layer?

The significance of this issue is magnified in the context of contemporary construction, where CLT panels are increasingly being used in multi-story buildings, residential complexes, and other structural applications. Ensuring these panels' long-term performance and stability is essential for safety, durability, and overall building efficiency. Despite its importance, there is a noticeable gap in literature regarding the interaction between water vapor diffusion and adhesive layers in bonding wood for structural purposes. Current studies are limited and do not fully explore the complex relationship between the adhesive's molecular weight, the bonded layers' diffusion properties, and the wood species used.

This study aims to fill this gap, considering both the diffusion properties of the adhesive and the strains caused for advancing sustainable building practices and optimizing structurally bonded wood material’s performance in the construction industry.

1.18. The research pillars

This thesis explores the relationship between water vapor diffusion through the adhesive layer, by:

1.) Evaluating the diffusion mechanisms in accelerated conditions on seven wood species with and without an adhesive layer, in similar conditions to examine the diffusion properties when vapor movement is perpendicular to the bond line, in order to find that adhesive, which has the most appropriate diffusion characteristic to lasure coated wood.

2.) Adjusting the diffusion properties of adhesive materials:
one commercial structural adhesive frequently used also in CLT manufacturing and one custom-made adhesive manufactured by BorsodChem company were evaluated for their water vapor diffusion characteristics, compared with five custom-made adhesives specially designed to these experiments, formulated with different molecular weight (MW) by BorsodChem, to monitor how different polymer structures influence diffusion rates and how blocked voids within the adhesive layers contribute to strain development.

3.) Investigation of the strains:
Internal strain measurements in the adhesive layer were performed to investigate the water vapor diffusion–blocking effect of the commercial adhesives. Similar measurements with custom-made adhesives were also performed to evidentiate the difference.

4.) Comparative evaluation of the results:
By analyzing water vapor diffusion and strain development across multiple wood species with and without adhesive layer, the research can identify wood species, -and MW specific behaviors and their implications for adhesive formulation/manufacturing and selection.

5.) Identification of knowledge gaps and future research directions:
results are provided on different MW adhesive formulations, water vapor diffusion mechanisms on structurally bonded wood assemblies, within the circumstances of accelerated diffusion testing. Further research might be needed to follow the real case scenario.

This thesis aims to highlight that contrary to the actual practice structural adhesives should be formulated by the producer considering their water vapor diffusion performance. It is suggested that water vapor diffusion should be aligned with the diffusion characteristics of the lasures, which are formulated for decades upon these principles.

2. Material and method

2.1. Materials

2.1.1. Wood species

The wood species utilized in this study were obtained from healthy trees, with careful consideration given to the position of each sample within the tree trunk. All specimens were selected and prepared to ensure they were free from fungal contamination, visible defects, or signs of disease. Any dirt or surface impurities were thoroughly removed before processing. Each specimen was cut perpendicular to the annual growth rings in a way that preserved the natural anatomical features of the wood. The detailed methodology for specimen preparation is described in the following section, together with the description of the 7 selected wood species. A diverse selection of wood types was intentionally used in this research, based on a comprehensive evaluation of several criteria: frequency of industrial utilization, reports in existing literature, underrepresentation in scientific studies, regional availability or scarcity, and the presence of unique or well-established physical properties was also considered. Both frequently utilized and underutilized wood species were selected.

Spruce (*Picea abies*) was chosen for investigations as it is one major wood species of most structural construction products, such glulam and CLT. Whilst there is a large mass of CLT production both in Europe and in Türkey and other countries, there are no tests reported on the water vapor diffusion through the panels. Contrary to the glulam, where a water vapor blockage is protecting the load bearing internal core, the strains caused by water vapor blocking in CLT might reduce it's lifespan. By studying and optimizing the water vapor permeability in bonded spruce assemblies, we might contribute to prolonging the lifespan of the CLT prefabricated wall elements.

Beech wood (*Fagus sylvatica*) besides its widespread application and well-documented characteristics (Schadauer & Freudenschuss, 2023) was selected for our tests for its uniform microstructure reflected also in the fact that it is the suggested wood species for the EN 301 and 302 tests as a very suitable wood species and there are attempts to be used also for CLT manufacturing. Grey poplar (*Populus* × *canescens*) was included in the tests because it was selected in 2023 as a target wood species for research at the Faculty of Wood Science and Creative Industries, due to its significant underutilization, combined with its abundant availability in Hungary and many other countries of this climate zone, relatively underexplored in terms of its industrial utilization (Pokorná et al., 2020). Furthermore, the Hungarian research

aims to evaluate its potential suitability as a substitute for the declining availability of coniferous wood materials. Oak *(Quercus robur)* was evaluated because it is a commonly used wood species and has also been employed in CLT production, for example in Spain (Lana et al., 2022).

Eucalyptus (*Eucalyptus camaldulensis*) was chosen in search for a wood species to support the economy of Iraq, Middle East and Africa as it is being explored for CLT in Brasil, Australia and many more, though it's not yet as widespread as the typical softwoods. Oil palm (*Elaeis guineensis*) was incorporated between the studied wood species as oil palm plantations reach their rotation age and a massive amount of palm wood trunks is generated (Csiha et al., 2025). According to international union of forest research organizations (IUFRO) data, about 100–120 million m^3 of palm trunks per year are generated globally when oil palm plantations are cleared for replanting (Arno Frühwald, 2017). A pilot study tested 3-layer CLT panels made using oil palm (*Elaeis guineensis*) trunk waste. They used melamine-urea formaldehyde adhesive. They found that density and pressing force strongly affect the performance of the panels. Some mechanical properties of selected trunks (like compressive strength in certain directions) met CLT standards, suggesting use in low-rise buildings might be possible (Srivaro et al., 2019). Samaragdfa (× paulownia in vitro 112) was selected for experiments as it is a fast-growing hybrid, developed in Hungary and searches its utilization


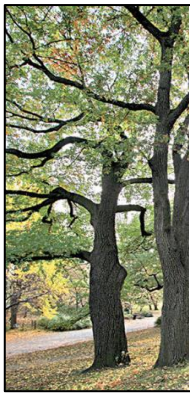



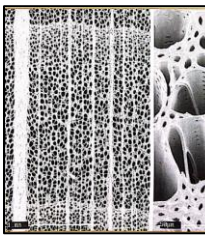
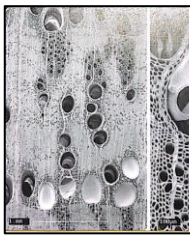
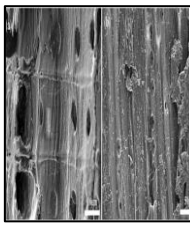
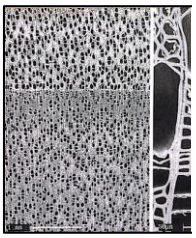

Beech OAK Spruce Grey Poplar

Samaragdfa wood Eucalyptus Oil Palm

Figure 2.1Wood Species type used in the study

2.1.1.1.Beech (BW)*(Fagus silvatica l.)*

Beech wood is a temperate hardwood species native to Central and Western Europe, with a vast natural distribution in countries such as central Europe, Hungary, Germany, France, Poland, and parts of the Balkans. It is regarded as one of the most abundant and sustainably managed hardwoods in Europe, making it highly accessible for commercial and research

applications. Structurally, beech wood features a uniform, fine texture and a straight grain, lacking the vascular bundle complexity seen in other wood species. Beech wood is characterized by being easy to machine, finish, and bond with adhesives, making it ideal for joinery, furniture, and engineered wood products. This might be the reason as being suggested suitable wood species for different bonding tests in many standards like EN301, EN302, EN204, EN205. The average dry density of beech wood was 759.9 kg/m³. Mechanically, the characteristics of beech wood were as follows: modulus of elasticity (MOE): ~13.5 GPa, modulus of rupture (MOR): ~110 MPa, compressive strength (parallel to grain): ~54–56 MPa, tensile strength (parallel to grain): ~100–130 MPa. These values reflect the wood's capability to withstand significant mechanical loads in structural applications. (Molnár & Bariska, 2006). The samples were conditioned to an average moisture content of 12.2% by storing them at 20 ± 1 °C and 65% relative humidity.

2.1.1.2.Oak (OW) *(Quercus spp.)*

Oak wood, taxonomically classified under the *Quercus genus*, is a durable hardwood species native to Europe, North America, and parts of Asia. In Europe, *Quercus robur* and *Quercus petraea* are among the most prominent, with wide availability in countries such as France, Germany, and Poland. The species is sustainably managed and widely used in the construction, furniture, and flooring industries due to its excellent strength and resistance characteristics. Structurally, oak wood is characterized by a coarse texture and prominent medullary rays, which enhance both its mechanical performance and visual appeal. Unlike diffuse-porous woods, oak has a ring-porous anatomy, contributing to its notable anisotropic behavior. The wood is moderately easy to machine and bonds well with adhesives, though the presence of tyloses and high tannin content can influence drying and finishing behavior. The average dry density of oak wood is approximately 682.1 kg/m³. Mechanically, the oak wood specimens used in this study exhibited the following average properties: MOE ~12 GPa , MOR ~102 MPa, compressive Strength (parallel to grain): ~51.2 MPa, tensile Strength (parallel to grain): ~97 MPa (Molnár & Bariska, 2006). The samples were conditioned to an average moisture content of 12.8% by storing them at 21 ± 1 °C and 65% relative humidity.

2.1.1.3.Spruce (SW) *(Picea abies)*

Spruce is a widely distributed softwood species native to Central and Northern Europe, particularly abundant in countries such as Norway, Sweden, Germany, Austria, and the Czech

Republic. It is one of the most economically significant coniferous trees in Europe, extensively cultivated and sustainably managed for both industrial and structural applications. Structurally, spruce is a softwood characterized by a fine, uniform texture and straight, consistent grain. Its wood consists primarily of longitudinal tracheid's and scattered resin canals, giving it a clean and even appearance with minimal figure. The transition between earlywood and latewood within the annual growth rings is noticeable but smooth, contributing to its reliable mechanical behavior. Wood is easy to machine, plane, and bond, although it has limited natural durability and is prone to biological degradation unless properly treated. The average dry density of spruce was 511.4 kg/m³, while the basic density ranges between 0.32 and 0.41 g/cm³. Mechanically, spruce demonstrates favorable strength-to-weight properties: MOE ~11–12 GPa, MOR ~75–80 MPa, compressive strength (parallel to grain): ~40 MPa, tensile strength (parallel to grain): ~90 MPa. These values reflect the species' suitability for light to moderate structural applications, particularly in timber framing, trusses, and laminated elements (Caudullo et al., 2016)(Jansson et al., 2013)(Galka et al., 2014). The spruce sample was also conditioned to an average moisture content of 12.2% at 20 ± 1 °C and RH ~ 65%.

2.1.1.4.Grey poplar (GPW**)** *(Populus canescens)*

Grey poplar is one of the fastest-growing deciduous species in Europe and is widely available in regions like Hungary. Despite its abundance, grey poplar is underutilized industrially, making it an appealing candidate for innovative applications in engineered wood products. Grey poplar features a straight grain and even, soft texture. It is light in color and machines easily, although it is prone to warping and discoloration over time. Its fast growth rate and moderate mechanical properties make it attractive for both structural and non-structural uses. The average dry density of grey poplar was 449.3 kg/m³. Its mechanical characteristics are as follows: MOR ~67.5 MPa, tensile strength (parallel to grain): ~82.3 MPa, compressive strength (parallel to grain): ~38.3 MPa, pull-off adhesion strength (with 2-component lacquer): ~3.42 MPa (Csiha et al., 2025). The grey poplar samples were obtained from KEFAG Ltd. (Hungary) and conditioned to MC=12.65% in a controlled environment at 21 ± 1 °C and 65% RH.

2.1.1.5.Smaragdfa® (SMW) *(× Paulownia Clone in vitro 112)*

Smaragdfa® (× Paulownia Clone in vitro 112), a fast growing plantation-grown hybrid was a lightweight raw material with an average dry density of approximately 379.4 kg/m³.

SMW is characterized by high porosity, large vessels, and thin-walled fibres, which distinguish it from conventional hardwoods and softwoods. These anatomical features result in low hardness and pronounced swelling and shrinkage even under minor water vapor changes. Its high sensitivity to moisture makes it a perfect candidate for the investigation of moisture induced dimensional changes, supporting reliable detection of moisture diffusion effects. The mechanical properties with a MOR ≈ 38.8 MPa, MOE ≈ 3.78 GPa, compressive strength parallel to grain ≈ 19.3 MPa, and impact bending strength ≈ 1.88 J/cm² justifiy its low-strength classification (István et al., 2023). All boards were taken from a uniform region and conditioned to a moisture content of 10.8–12% at 20–21 °C and 65% RH prior to testing.

2.1.1.6.Eucalyptus (EUW) *(Eucalyptus camaldulensis)*

Eucalyptus wood, particularly eucalyptus camaldulensis, is a fast-growing hardwood species native to Australia and widely cultivated in tropical and semi-arid regions, including the Middle East, Africa, and parts of Europe. In Iraq, eucalyptus is locally abundant and promoted for afforestation projects due to its heat, salinity, and drought tolerance, making it highly sustainable and suitable for structural wood production. Structurally, eucalyptus is dense and durable, with an interlocked grain and medium texture. It contains abundant extractives and resins that contribute to its resistance to decay but may interfere with adhesive bonding unless properly treated. The heartwood is typically reddish to brown, with distinct color variation and high oil content. The average dry density of Eucalyptus was 952.18 kg/m³, reflecting its high mass and strength. Mechanically, the wood performs exceptionally well: modulus of rupture (MOR): ~88 MPa, tensile strength (parallel to grain): ~60 (Cheng et al., 2021), pull-off adhesion strength (with 2K lacquer): ~5.25 MPa (Csiha et al., 2025). These values demonstrate eucalyptus's high suitability for flooring, wall cladding, and structural members requiring superior bonding capacity. Samples were cut from straight-grained boards collected in Iraq and conditioned to an average moisture content of 12.8% by storing them at 21 ± 1 °C and 65% relative humidity for two weeks.

2.1.1.7.Oil Palm (OPW) *(Elaeis guineensis)*

A low-density wood species, being very sensitive to the changes of the moisture content of the environment, shrinking and swelling considerably even by minor water vapor variation, thus was considered suitable to support a stable detection of the effect of vapor permeability. Its wood is characterized by a fibrous structure with vascular bundles embedded in a

parenchymatous matrix, leading to notable variability in mechanical properties(Pournou, 2020). The average wet density of palm wood is approximately 0.46 g/cm³, while the saturated density reaches about 0.69 g/cm³. Another study reports on a density of 0.32 g/cm³, indicating variability based on moisture content and sampling location (Elkhal et al., 2022). According to Amirou et al., (2014) wood exhibited a flexural MOE of approximately 6,647 MPa, reflecting notable stiffness under bending loads. The MOR, which indicates the maximum load the wood can endure before failure, was measured around 35.04 MPa. In parallel-to-grain compression tests, the wood showed a compression modulus of approximately 5.35 MPa and a maximum compressive strength of about 2.338 MPa. These values were measured on boards extracted from a uniform region along the mid-height of a single trunk. The average dry density of OPW was 301.1 kg/m³

2.1.2. Coating materials

2.1.2.1. OBI 2201465 Ajtó és ablaklazúr

Lasures are penetrative but film forming wood finishes and proposed for outdoor use in Europe and also in Hungary, due to their specially designed molecule size/structure, which offer control over promoted water vapor permeability parallel with hindering (levelling) the water uptake through the layer, enabling a promoted vapor permeability associated with a moderate water uptake

Due to their specially tailored molecular structure, lasures are able to facilitate a controlled high diffusion of water vapor while restricting the free diffusion of liquid water, which could otherwise cause internal strains, premature delamination, and degradation of the layer. This seemingly contradictory behavior can be addressed by lasures based on the fact, that water molecules exhibit different shapes and properties in the vapor phase compared to the liquid state. Water vapor can easily penetrate channels in the lasure layer that are approximately the size of its molecules, whereas liquid water is effectively hindered. The solution to promoting vapor diffusion while blocking liquid water lies in the precise adjustment of the lasure's molecular size. In this way, lasures allow the wood substrate to "breathe," enabling moisture exchange by permitting water vapor to diffuse through the coating. Several studies have demonstrated the effectiveness of lasures in reducing moisture uptake and improving UV resistance (Temiz et al., 2005) .

Lasures also protect the wood surface from the UV radiation by containing a minimal amount of pigments, which does not cover the wood pattern completely like paints would do (Valent et al., 2017).

Lasures are often organic solvent or water-based, and there are of two types: so called “thin lasures” and “thick lasures”. Thin lasures were developed for non-dimensionally stable structures (such as benches, etc.), whereas thick lasures, in contrast, were developed for dimensionally stable structures (such as doors and windows). The best process to apply lasures includes; preparation of the surface, by standing and smoothing the surface. A thin primer lasure layer is applied on the surface. For top results, two to three intermediate layers are recommended, and it is also recommended to allow each layer to dry completely before applying the next one. As top coat it is recommended a thick lasure layer to be applied. The highest quality can be achieved by spraying. The wood density, porosity, and extractive content also influence how deeply the lasures penetrate and how well adheres over time (George et al., 2005). The drying time also varies based on the product and environmental conditions.

Figure 2.2 OBI 2201465 Ajtó és ablaklazúr used in study

The lasure used for experiments was purchased from OBI Hungary (Sopron, Hungary) as shown in Fig. 2.2. It has a density of 1300 g/L, and contains binders (linseed oil and acrylic polymers), pigments (iron oxides and titanium dioxide), solvent, and aqueous phases for application. It allows water vapor diffusion but has high resistance to soaking in water.

2.1.2.2.Adhesive JOWAPUR 681-60 (AJ)

JOWAPUR 681-60 is a structural adhesive (Jowat SE Co., Detmold, Germany). This adhesive is a joint-filling, fiber-reinforced, one-component commercial polyurethane adhesive specifically designed for load-bearing wood structures. According to the manufacturer’s data sheet (attached in Appendix I), the recommended application rate of adhesive was 120–200

g/m². This particular adhesive was selected not only for its structural performance but also due to its commercial availability. According to the data sheet provided by Jowat SE, the recommended adhesive applying amount with range 140–200 g/m² and must be selected to ensure full-surface wetting. The assembly time for two surfaces is determined by several factors, e.g., by humidity, wood moisture, temperature, and the adhesive application amount. The maximum assembly time for Jowapur® 681.60 at a temperature of 20 °C, a wood MC 12%, and a RH 65% is max. 60 minutes. If finger jointing procedures are to be carried out, the prescribed pressure is approximately. 7.5-10.0 MPa, must be applied onto the joint for at least 1 or 2 seconds, depending on the applicable product standard. After that, parts bonded with Jowapur® 681.60 are to be stored for a minimum curing time of 100 minutes (20 °C, MC 12%). During curing, it is imperative to prevent any mechanical load/strain on the bonded parts. If GLT or CLT, the recommended pressure is 0.6-1.0 MPa.

2.1.2.3. Adhesive XP 1166 (AX)

This was a custom-made adhesive available by BorsodChem Ltd, under the name Original XP 1166, with brown colour and high viscosity. The recommended applying amount of adhesive was 120–200 g/m².

2.1.2.4. Custom-made synthesized resins series (S_i; i = 1-5)

Five custom-made adhesives specially designed to these experiments were formulated with different MW by BorsodChem Gödöllő (Hungary). These resins were synthesized through controlled variation in the MW and structure of polyether polyols (PPG diols and triols), specifically by modifying the MW. All samples contained free monomeric MDI and structurally distinct prepolymer. The MDI component used in these formulations consisted solely of monomeric MDI, devoid of high-molecular-weight oligomers.

As shown in Table 2.1, and Fig. 2.3, the five custom-made synthesized polymers samples were developed with varying polyol MW, as listed below:

Series 1: Prepolymer based on PPG diol, MW = 2000

Series 2: Prepolymer with partial PPG triol, MW = 3000

Series 3: Balanced diol/triol blend, MW = 4000

Series 4: Triol-dominant blend, MW = 5000

Series 5: Pure PPG triol system, MW = 6000

Table 2-1 Custom-made synthesized polymers used according to the manufacturer

Series	Polyol Type	Mixing Ratio (%)	Average MW
Series 1 (S1)	2000 MW Diol	100% (2000 Mw Diol) / 0% (6000 Mw Triol)	2000
Series 2 (S2)	2000 Diol+6000 MW Triol	75% (2000 Mw Diol) / 25% (6000 Mw Triol)	3000
Series 3 (S3)	Mixed Diol/Triol	50% (2000 Mw Diol) / 50% (6000 Mw Triol)	4000
Series 4 (S4)	Triol-Dominant	25% (2000 Mw Diol) / 75% (6000 Mw Triol)	5000
Series 5 (S5)	Pure 6000 Triol	0% (2000 Mw Diol) / 100% (6000 Mw Triol)	6000

Figure 2.3Wood samples with adhesive cans

By adjusting the molecular weight (MW) of the synthetic resin formulations, the polyol systems were conceptually modified resulting different water vapor diffusion while different hindering liquid water uptake through the adhesive layer. This design approach was inspired by the manufacturing concept of lasures, which are known to allow controlled vapor permeability while restricting liquid water penetration. The underlying hypothesis assumes that the diffusion behavior can be tailored through precise control of the adhesive's molecular size, enabling selective permeability toward water vapor while limiting liquid water transport.

2.1.3. Other materials utilized in the study

2.1.3.1.Silica gel

In this study, an indicator-type silica gel desiccant was used. The product used was FIO-1533 silica gel 1 kg per sack, orange, commercially purchased from Fiorex Packaging Kft, Hungary. Was supplied in granular form with an integrated humidity indicator that changes color from orange to green as it becomes saturated with moisture. This visible color transition provides a reliable method for assessing desiccant efficiency in real-time. Fig. 2.4 shows a

visual representation of the silica gel's colour change upon exposure to humidity, which was used as a qualitative indicator of environmental moisture levels during the experiment.

Figure 2.4Silica gel in a cup before and after water absorption

2.1.3.2.Sealing materials

A grey silicone sealant LOCTITE® SI 5699, manufactured by Henkel Corporation, USA was used to ensure a tight and vapor-impermeable connection between the aluminum cup and the wood specimen Fig. 3.5. This specific sealant was selected due to its elasticity, excellent heat resistance and its ability to prevent water vapor transmission. The silicone effectively sealed the interface between the aluminum cup and the wooden disk, as illustrated in Fig. 3.8, thereby ensuring the integrity of the vapor diffusion measurement.

Figure 2.5 Silicon used for sallied wood disk with cup

2.2. Method

2.2.1. Experimental setup

Wood samples were taken from healthy, defect-free trees, free from fungal infection or decay (no knots). Boards were then prepared by cutting the samples from a radial position within the trunk, ensuring uniform grain orientation and minimizing variation in physical and mechanical properties. The wood boards were conditioned in a drying chamber at 40 °C until they reached an equilibrium moisture content of

approximately 12%. Following this, the boards were sanded using a sanding machine (aligator 630 by houfek co., Czech Republic) until a uniform thickness of 1 cm was achieved, as illustrated in Fig. 2.6.

Figure 2.6 Sanding Machine

After sanding the boards were carefully dedusted. The sanded boards were coated on one side using adhesive material, lasure, and different MW of custom-made synthesized polymers. Before applying the adhesive, the edges of each sample were masked with paper tape to control the amount of coated material forming the layer on the surface of the board. A sponge roller was used for applying the lasure adhesive and the custom-made synthesized polymers, using different application amounts. The coated samples were then left to dry for 24 hours. This sample preparation aligns with the sample preparation outlined in ISO 13061-2:2014. For some materials, such as lasure, the application amount followed the manufacturer's datasheet recommendation (e.g., 150 g/m²). For other materials like adhesives and resins, the optimal application amount was determined experimentally. This process involved avoiding the formation of foaming bubbles, which could negatively affect the test results. The target was to achieve a uniform, bubble-free coating as illustrated in Fig. 2.7, in contrast to the flawed application shown in Fig. 3.7a. Through a trial-and-error approach, the final application amount for resins and adhesive materials was set at 150 g/m². To avoid bubble formation the adhesives were applied in several consecutive thin layers, in a 120 second interval.

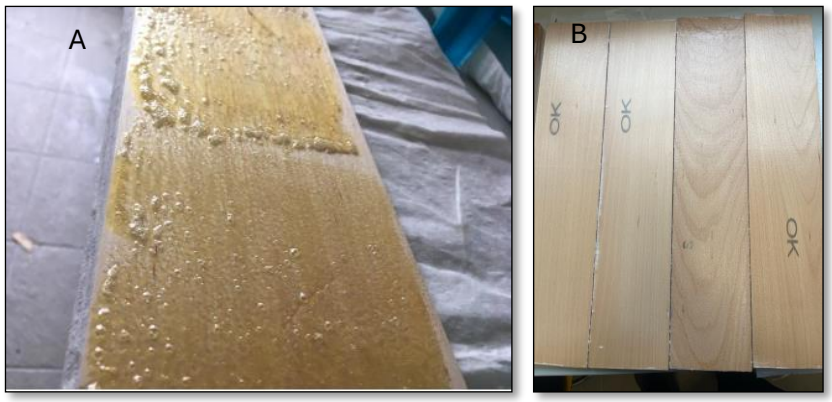

Figure 2.7 A: Bubbles occurring on the surface of wood B: The wood surface by the selectivity of the application adhesive amount

After drying, disk-like samples were prepared using a drilling machine with a 100 mm diameter crown saw, as shown in Fig. 2.8 (FP-13A Asztali Fúrógép, VKM Co., Hungary). Each disk had a thickness of 10 mm, with a grain direction parallel to the specimen's surface.

Figure 2.8 Bench Drilling Machine

The specimens were acclimatized to room temperature and relative humidity before testing, conditioned to 12±0.5% moisture content. The test followed the cup method following ISO 12572:2016 and ASTM E96/E96M:2004 standards, as illustrated in Fig. 3.9. The cup was

manufactured by using aluminum with a thickness of 1.25 mm, with dimensions similar to the standard. Each aluminum cup, impermeable to vapor, was filled with 150 g of silica gel, filling by this up to approximately 65% the cup. The edges of the wood disks were sealed to the cups' edges, using silicone, following the sample preparation guidelines outlined in ISO 13061-2:2014.

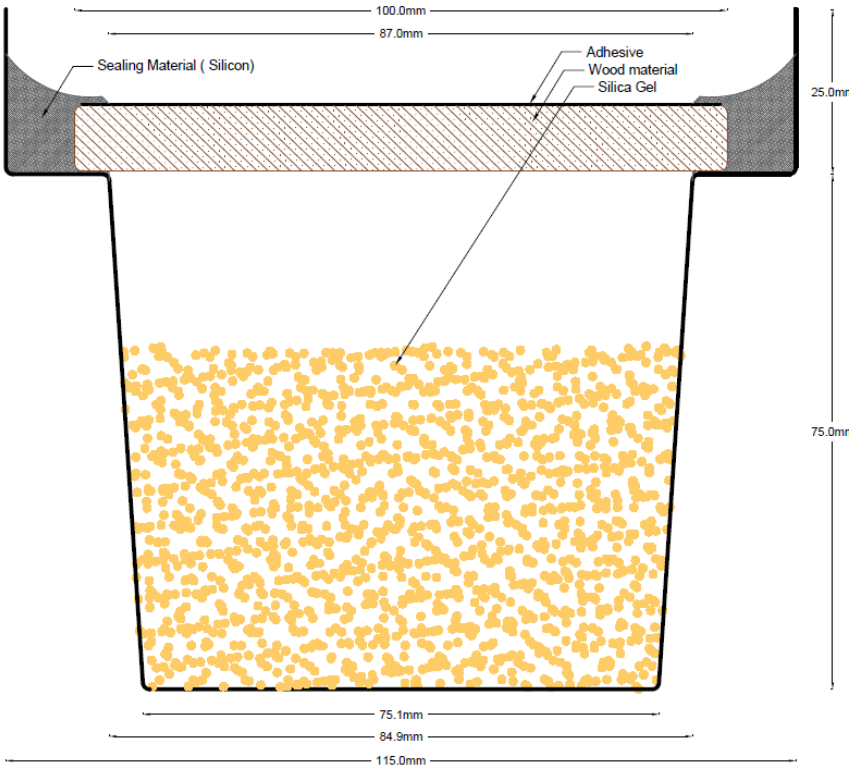

Figure 2.9 Cup setup

In this experiment, as shown in Fig. 2.10, warm-mist humidifiers (a household kettle) (HM-EK-A150SS, Home Ltd.) were used to achieve high humidity levels within the testing chamber. The hot steam was continuously provided by boiling water, the samples were then placed inside the airtight chamber to prevent water vapor loss. This chamber was an insulated refrigerator of 240 litter, out of function, conveniently modified for experimental purposes, as shown in Fig. 2.10. Inside the chamber, a water boiler was continuously generating hot steam of 100°C. The cups were placed top-down on a metallic grid at a 75 cm distance from the steam source. As shown in Fig. 2.11 the metal grid keeping the cups tilted by 15° in order to support the continuous skidding of condensed water precipitation from the surface of the samples.

Temperature and RH inside the chamber were continuously monitored using a Rev Ritter GmbH indoor hygro-thermometer (Model No. 5058037). Throughout the test, RH reached 100% and temperature remained close to 70 °C at the level of the samples, as shown

in Fig. 2.12 the temperature inside the chamber depends on the steam rate (g/min). The 70º C were typical to the kettle used.

Ultrasonic humidifiers could have been also considered as a testing device; however, following reports by (Shamaev et al., 2025a), the decision was made to conduct the tests under warm vapor conditions. These authors noted a drawback of ultrasonic humidifiers: prolonged exposure to ultrasonic waves can increase internal friction in hardwoods such as oak by up to 41% due to microstructural changes, thereby link the increase in damping due to ultrasonics to microstructural changes in the wood's internal channels and structure. The internal structure (e.g., cell walls, channels) of oak is altered, possibly by cavitation, micro jets, or mechanical strain from ultrasonic waves. These changes make the wood's viscoelastic behavior more pronounced. Shamaev suggests that these structural modifications are why damping increases, and the measure of real diffusion is altered (Shamaev et al., 2025b). This was the reason why for the experiments warm mist humidifying technique was used. The experiments followed thus an accelerated diffusion procedure, which was not simulating a real case scenario, but by exposing the samples to similar conditions was suitable to make comparison between the diffusion performance of the different polymer formulations. The resulting diffusion coefficients, however, are independent of whether the real-case scenario or the artificially accelerated procedure was followed. In principle, the diffusion coefficient is an intrinsic material property, meaning that if the material's structure and the thermodynamic conditions (temperature, humidity, pressure) are the same it should not depend on test conditions. The diffusion coefficient in case of wood is suggested not to be considered alone (see thesises in chapter 4).

Figure 2.10 Heating Evaporator Chamber

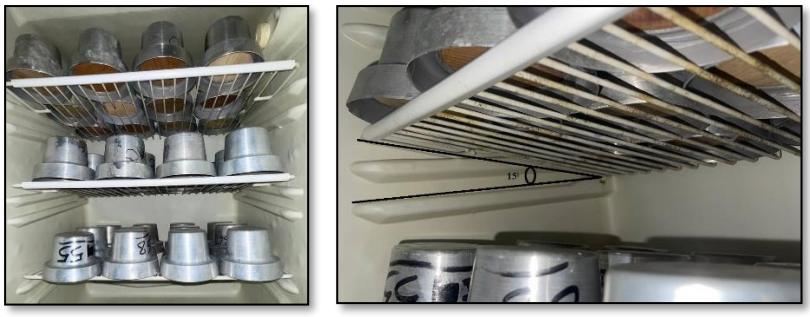

Figure 2.11 Samples tilted by 15°

Figure 2.12 Hydro Thermometer

Number of samples: a total of 315 specimens were prepared under three conditions: natural (uncoated), coated with lasure, coated with commercial adhesive (AJ, AX) and coated with custom-made synthesized resin (S1-S5), as shown in Table 2.2.

Table 2-2 Number of samples per wood species/treatment

	Uncoated	**Lasure**	**AJ**	**AX**	**S1**	**S2**	**S3**	**S4**	**S5**
BW	5	5	5	5	5	5	5	5	5
OW	5	5	5	5	5	5	5	5	5
SW	5	5	5	5	5	5	5	5	5
GPW	5	5	5	5	5	5	5	5	5
SMW	5	5	5	5	5	5	5	5	5
EUW	5	5	5	5	5	5	5	5	5
OPW	5	5	5	5	5	5	5	5	5

Each specimen was numbered and weighed periodically, and 90 samples were introduced into the steaming chamber at a time. Over 20 systematic measurements were taken for each sample across a total test duration of approximately 22,500 minutes (15.6 days), with the measurements for individual samples shifted with the same time interval, according to

Table 2.3 .During each measurement, a sample was quickly removed from the chamber, surface moisture was gently wiped off using a highly absorbent paper towel, and the specimen was weighed within 20 seconds. To minimize environmental disruption, the chamber door was opened for less than 5 seconds each time, with at least 20-minute interval between openings to allow internal conditions to stabilize before the next measurement.

Table 2-3 Time of mass measurement

Time (hours) of mass measurements for uncoated wood, wood Coating with lasure, wood with Commercial adhesive	Time (hours) of mass measurements for wood sample with (S1,S2,S3,S4,S5)
3 , 5 , 13 , 22 , 29 , 40 , 53 , 67 , 72 , 96 , 115 , 139 , 166 , 188 , 194 , 210 , 225 , 240 , 260 , 280 , 300 , 325	3 , 9 , 14 , 19 , 26 , 31 , 37 , 45 , 50 , 62 , 68 , 80 , 90 , 104 , 120 , 144 , 174 , 222 , 240 , 276 , 294 , 342

Figure 2.13 The wood Species cup sample (Coated and Uncoated)

2.2.2. Measuring the water vapor permeability through the adhesive layer:

Moisture diffusion is traditionally evaluated using Fick's first and second laws of diffusion, which can be expressed as,

- First Law steady state:

$$J = -D_{\propto}\frac{\partial \propto}{\partial x} \quad \text{....(Equation 1)}$$

- Second Law transient

$$\frac{\partial \propto}{\partial t} = \frac{\partial}{\partial x}\left(D_{\propto}\frac{\partial \propto}{\partial x}\right) \quad \text{....(Equation 2)}$$

where $D_{\propto}$ is the diffusion coefficient with the parameter $\propto$ refers to the driving potential for moisture diffusion, which in this study is the water-vapor concentration (or partial vapor pressure) gradient (Robert, 2010).

There are two widely spread standards used for the evaluation of water vapor diffusion of anisotropic materials: ISO 12572:2016 and ASTM E95/96M. Both standards characterize the diffusion by the diffusion coefficient, with similar principles:

The water vapor permeability, calculated by equation 3.

$$\delta = Wd \quad \text{kg/(m·s·Pa)} \qquad \text{….(Equation 3)}$$

Water-vapor permeability (δ) is the mass of water vapor that diffuses through a material of unit thickness, per unit area, per unit time, per unit vapor-pressure difference. The parameter d represents the specimen thickness.

where t is the time (in s), G is the mass change rate (in kg), A is the surface area of the specimen (in m^2), Ps is the saturation vapor pressure (in Pa), RH is the relative humidity (unitless), and d is the average thickness of the specimen (in m).

The water vapor permeance W can be calculated by

$$W = \frac{g}{\Delta p} \quad \text{kg/(m}^2\text{·s·Pa)} \qquad \text{….(Equation 4)}$$

The change of vapor pressure (ΔP) can be estimated as a function of temperature (T, °C) by Tetens equation (Tetens, 1930)

$$p = 610.5\, e^{\left(\frac{17.27\,T}{T+237.3}\right)} \qquad \text{....(Equation 5)}$$

$$\Delta p = (Ps * RH2) - (Pa * RH1) \qquad \text{… (Equation 6)}$$

The water vapor flow rate: g, can be calculated by

$$g = \frac{G}{A}\ \text{(kg/s. m}^2\text{)} \qquad \text{….(Equation 7)}$$

Where A is the exposed area (arithmetic mean of the inside and outside surface areas of the disklike samples free of silicone, in m^2). The mass change rate per time was calculated based on the following equation:

$$G = \frac{m_2 - m_1}{t_2 - t_1}\ \text{(kg/s)} \qquad \text{….(Equation 8)}$$

Further to the calculation of the mass change rate, this modelling approach leads to the determination of the transition point "A" between the non-linear (pre-steady) and linear (steady) regions of the diffusion curve.

The segment preceding this transition point was defined being the pre-steady zone, while the linear portion that followed point G was identified being the steady zone as in ASTM E95/96 and ISO 12572/2016. The difference between these two standards is, that in ASTM E95/96 the

mass change rate is defined as the slope of the steady zone of the diffusion curve whilst in ISO 12572/2016 the final value of G is obtained when the mean of the last five successive determinations is within ±5 % of G, indicating that the diffusion reached the steady state. For our measurements G was identified based on ASTM method, using equation 8, but the expectations of ISO were also met.

The diffusion test included five specimens per type, and the average change in mass was calculated for each type. For equation 6, the RH_1 in our case was zero, as the relative humidity above the silica gel inside the cup was zero. For our experiments, RH_2 was 100%, the relative humidity inside the chamber.

The weight measurements for all specimens were recorded at short intervals to ensure consistent measurement conditions.

In some cases, measurements were stopped due to cracking of the disks or damage of the seal as shown in Fig. 2.14

Figure 2.14 Failure in samples

To support the analysis of mass-change behavior over time, Statistica V2025 software was employed to generate the mathematical models of the function. The software was used to identify the trend line that best represented the relationship between mass change and exposure time, automatically selecting the most appropriate function based on goodness-of-fit criteria. This software also enabled the determination of the transition point “A” between the non-linear (pre-steady) and linear (steady) regions of the diffusion curve.

2.2.3. Measuring the strain in the adhesive layer caused by water vapor diffusion

This section describes the methodology employed to evaluate the internal strains that develop in the adhesive layer at the surface of wood samples, as shown in Fig. 2.9. These strains result from water vapor diffusion through the layer. A comparative analysis was conducted using three wood species:

Beech *(Fagus sylvatica):* Selected as the reference species due to its relatively uniform anatomical structure, which facilitates consistent baseline comparisons.

Grey Poplar *(Populus × canescens):* Chosen for its regional availability in Europe and the limited number of existing studies addressing its moisture-related behavior.

Spruce *(Picea abies)*: Included because of its heterogeneous structure, characterized by pronounced growth rings and variable properties across annual layers and is one of the wood species involved in structural bonding.

Although all wood species are inherently non-homogeneous, the selected specimens were intentionally chosen to represent a wide structural and anatomical contrast. The selection was also constrained by the technical capacity of the strain-testing device, which permits testing of only a limited number of samples, as will be detailed later.

To investigate the influence of adhesive type on water diffusion and the resulting internal strain formation, for each wood species, four specimens were prepared with different layers: uncoated wood, wood coated with a lasure, wood coated with a commercial adhesive AJ, and wood coated with S5, a formulation composed of a resin polymer blended with a polyol-type compound (Pure 6000 Triol, Average MW = 6000).

These combinations allowed for a comparative analysis of the internal strains in case of varying diffusion resistance of the samples. To measure the strain within the adhesive layer, a collaboration was established with HBK -Hottinger Brüel & Kjær, specifically at their Gödöllő branch. As part of this collaboration, a workshop and hands-on training were conducted using the Quantum MX1615 device (16-channel data acquisition system), as shown in Fig. 2.15B. This device was operated in conjunction with the CatMan Easy v5.6 software for data logging and analysis. The system was connected to high-precision pressure-resistant strain gauges (YOUMILE 350 Ω), enabling accurate strain measurement at the adhesive interface. The same specimen configuration shown in Fig. 2.9 (aluminum cup) was used to evaluate the strain behavior. Wood samples were prepared following the same procedure as in the water vapor diffusion tests, using the same application amounts (150 g/m^2) of adhesive, lasure, and S5 custom-made synthetic resin.

A strain gauge was affixed to the wood surface either directly or on the coated layer, depending on the case, as shown in Fig. 2.15A, set at a parallel angle with the wood grain to test the strain perpendicular to the grain. The strain gauge was connected via wires to the measurement device, and the system, using a computerized program, was balanced to ensure an initial zero-strain reading. Subsequently, the aluminum cup was opened from the bottom (Fig. 2.15C), and boiling water was introduced into the cavity. This setup was intended to accelerate water vapor diffusion, as elevated MC are directly correlated with increased diffusion rates, thereby intensifying the strain response in the system. Testing under boiling

water conditions subjects the specimens to more aggressive environmental exposure, making it an effective approach for revealing the strain induced by the diffusion-blocking effect of the adhesive.

The test was conducted continuously for 100 hours. At the beginning of the test, hot water was added to each specimen simultaneously, and all samples were left to cool naturally under the same conditions. This approach ensured uniform thermal exposure across all specimens. Strain values were recorded over time to analyze the diffusion-induced mechanical response.

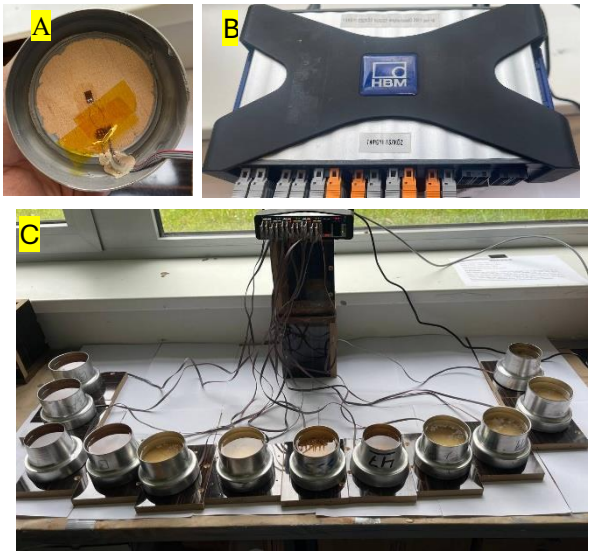

Figure 2.15 A: Strain Gauge glued on wood surface, B: The strain measuring device, C: Sample preparation for the test

3. Results and discussion

3.1. Water vapor diffusion and modelling

The results are presented and analyzed separately for each wood species, as their behavior depends on the specific species.

According to ASTM E96/95, the water vapor flow rate is recommended to be calculated under the same conditions as those specified in ISO 12572:2016. According to both standards, the material's diffusion coefficient is typically calculated under steady-state conditions, based on the slope of the portion where the curve of diffusion straightens.

For each wood species, a function of the generalized form shown below was identified following the experiments to best fit the observed diffusion trend:

$$\Delta m = b_1 * \tanh(b_0 * t) \quad [g] \qquad \ldots (Equation\ 9)$$

where :

b_0,b_1 : coefficients depend on both wood species, MW of the adhesive, coating material type

t : time in hours

The diffusion process consisted of an initial pre-steady stage, symbolized by point "A (x_A; y_A)" transitioning into a steady zone, which provided the basis for deriving curve slopes and quantifying both diffusion coefficients, vapor flow rates and the measure of diffusion hindering.

The lowercase letter (s) denotes results obtained in the steady-state zone, whereas (p) denotes results obtained in the pre-steady zone; thus, identical sample designations like SMW, SMW_{AJ}, SMW_{AX}, SMW_L, SMW_{S1}–SMW_{S5} are labeled with s or p solely to distinguish the evaluation stage of diffusion.

For clarity regarding the abbreviations used to designate wood species, adhesives, coating systems, and molecular-weight classifications, the reader is referred to **Appendix III**: List of Abbreviations.

3.1.1. Water vapor diffusion of beech wood (BW) (*Fagus sylvatica l.)*

The water vapor diffusion of beech wood samples was found to follow **a function of the generalized form**:

$$\Delta m = b_1 * \tanh(b_0 * t) \quad [g] \qquad \ldots (Equation\ 9)$$

where :b_0,b_1 :coefficients depend on the MW of the adhesive and coating material (Table 3-1)

t : time in hours

All the functions of water vapor diffusion of BW were characterized by having both a pre-steady and steady zone, enabling the calculation of the slope of the curves, identification of the transition point "A", calculation of the permeability coefficient and the water vapor flow rate, along with identification of the measure of diffusion resistance.

3.1.1.1. Evaluation of water vapor diffusion for BW samples in the steady zone

As shown in Fig. 3.1 and 3.2, the steady-state diffusion behavior of water vapor both through the BW_{NS} and the adhesive coated BW_{AJS} samples begins only after several days of exposure. Once the permeability process stabilizes, the curves become linear, allowing for accurate calculation of the water vapor flow rate G and the permeability coefficient δ. The permeability behavior of BW_{NS} and BW_{AJS} according to the result as showed in Table 3.1, BW_{NS} was different. Whilst BW_{NS} had a permeability coefficient of 3.82×10^{-14} kg/(Pa·m·s) with a water vapor flow rate G = 0.00303 g/h, the BW_{AJS} showed a significant difference, with a more than around 12-time lower permeability coefficient $\delta = 0.31 \times 10^{-14}$ kg/(Pa·m·s) and G=0.000244 g/h.A one-way ANOVA revealed a statistically significant difference in the water vapor permeability coefficient δ between BW_{NS} and BW_{AJS} ($F(1, 8) \approx 392$, $p < 0.027$), confirming the pronounced vapor-blocking effect of the commercial adhesive layer. This comparison reveals a substantial difference in vapor permeability behavior of the natural beech wood and the beech samples treated with commercial adhesive. The differences in y-coordinate, representing the mass change at the A point, were 10 times lower in favour of BW_{AJS} compared to BW_{NS}. This leads to the conclusion that the commercial adhesive has a strong water vapor diffusion hindering effect.

Table 3-1 Water vapor permeability of beech wood (BW)

Sample	b_1	b_0	x_A(h)	y_A(g)	G (g/h.)	W * 10^{-12} kg/(m²·s·Pa)	δ *10^{-14} kg/(m·s·Pa)
BW_{NS}	9.766500	0.006965	262.8	9.2769	0.003029	3.816391	3.816391
BW_{NP}					0.035300	44.46985	44.46985
BW_{AJS}	0.988300	0.008988	203.8	0.9389	0.000244	0.307742	0.307742
BW_{AJP}					0.004607	5.803594	5.803594
BW_{AXS}	0.798176	0.007490	244.6	0.7583	0.000231	0.291098	0.291098
BW_{AXP}					0.003100	3.905422	3.905422
BW_{LS}	3.503060	0.006734	272.0	3.3279	0.001119	1.410279	1.410279
BW_{LP}					0.012235	15.41297	15.41297
BW_{S5S}	4.903300	0.009700	188.8	4.6579	0.001142	1.438627	1.438627
BW_{S5P}					0.024671	31.08002	31.08002
BW_{S4S}	3.284220	0.009460	193.6	3.1199	0.000780	0.982195	0.982195
BW_{S4P}					0.016115	20.3014	20.3014
BW_{S3S}	2.325140	0.009440	194.0	2.2087	0.000553	0.696614	0.696614

BW_{S3P}					0.011386	14.34307	14.34307
BW_{S2S}	1.513900	0.009160	199.9	1.4381	0.000369	0.464686	0.464686
BW_{S2P}					0.007194	9.062894	9.062894
BW_{S1S}	0.918614	0.009040	202.6	0.8726	0.000226	0.284807	0.284807
BW_{S1P}					0.004307	5.426188	5.426188

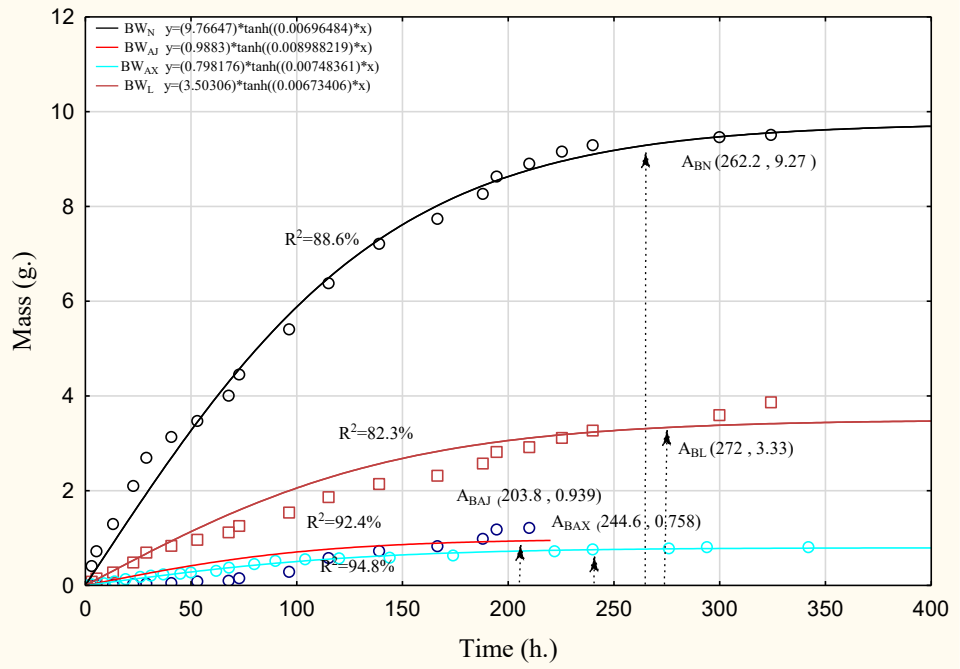

Figure 3.1 The mass change over time for BW_N, BW_L, BW_{AJ}, and BW_{AX}

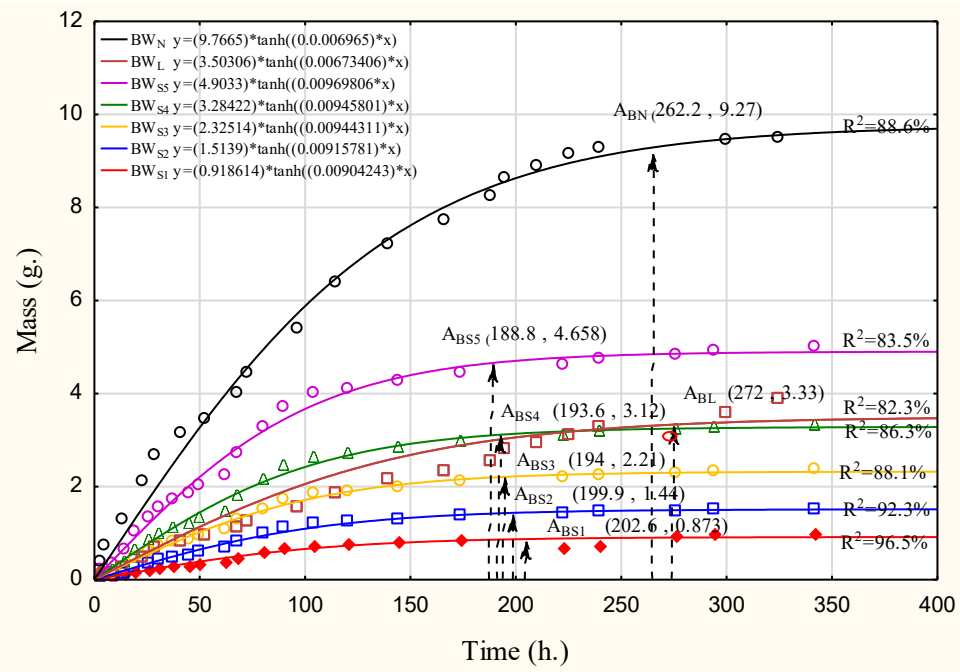

Figure 3.2 The mass change over time for BW_N, BW_L, BW_{S1}, PW_{S2}, BW_{S3}, BW_{S4}, and BW_{S5}

The parameter G = 0.001119 g/h and the parameter δ = 1.41 × 10^{-14} kg/(m·s·Pa), of BW_{LS} samples is approximately 2.7 times lower than that of BW_{NS} and about 4.5 times higher than that of BW_{AJS}. The transition point "A" for BW_{LS} samples was reached after 272 hours (x-coardinate), with a mass change, reflected by the y-coordinate equal to 3.27 g, compared to BW_{NS} samples, which reached their transition point after 262.8 hours with a mass change of 9.3 g. This indicates a broadly similar steady-state time for the diffusion process relative to the BW_{NS}, albeit with a substantially lower total mass change. The higher vapor permeability observed in BW_{LS} compared to BW_{AJS} suggests that the lasure layer permits partial vapor permeability, likely facilitated by its layer's capillary structure.

As shown in Fig. 3.2 and Table 3-1, the beech wood samples coated with custom-made synthesized polymer S1–S5 exhibited diverse steady-state permeability behaviors, largely depending on the average molecular weight of the applied polyol mixtures. In general, beech wood with the commercial adhesive BW_{AXS} and beech wood with the lower MW custom-made synthesized polymers, such as S1, S2, and S3 demonstrated a reduced and significant difference in water vapor diffusion compared to the lasure-coated samples BW_{LS}.

For instance, BW_{LS} recorded G = 0.001119 g/h and δ = 1.41 × 10^{-14} kg/(m·s·Pa). In contrast, BW_{S1S} showed G = 0.000226 g/h and δ = 0.285 × 10^{-14} kg/(m·s·Pa), representing a statistically significant difference, with values nearly five times lower than BW_{LS}. The BW_{S2S} samples exhibited G = 0.000369 g/h and δ = 0.465 ×10^{-14} kg/(m·s·Pa), approximately three times lower than the lasure coated samples A one-way ANOVA revealed a statistically significant difference in the water vapor permeability coefficient δ among BW_{LS}, BW_{S1S}, BW_{S2S}, BW_{S3S}, and BW_{AXS} ($F(4, 20) \approx 68.5$, $p < 0.031$), confirming that the polymer-modified and adhesive-coated systems exhibited substantially lower permeability compared to the lasure-coated specimens. The BW_{S3S} showed G = 0.000553 g/h and δ = 0.697 × 10^{-14} kg/(m·s·Pa), roughly two times lower, while BW_{AXS} displayed G = 0.000231 g/h and δ = 0.291 × 10^{-14} kg/(m·s·Pa), again about five times lower values than those of BW_{LS}.

Among the experimentally custom-made synthesized polymers, S4 and S5 stood out for their permeability performance, as the steady-state behavior of these high–molecular-weight formulations closely matched that of the lasure coating. BW_{S4S} recorded G = 0.000780 g/h and δ = 0.982 × 10^{-14} kg/(m·s·Pa), values within the same order of magnitude as BW_{LS}, indicating moderate permeability. BW_{S5S}, with an even higher molecular weight, achieved G=0.001142 g/h and δ =1.44 × 10^{-14} kg/(m·s·Pa), values almost identical to BW_{LS}.

These findings demonstrate that, by carefully tuning the MW of polyol-based adhesives, it is possible to design polymer formulations that achieve semi-vapor permeability

similar to lasures, offering a balance between water vapor permeability and liquid water penetration.

3.1.1.2. Evaluation of water vapor diffusion for BW in the pre-steady zone

The term pre-steady zone refers to the initial period preceding the establishment of steady-state water vapor diffusion. This phase is particularly critical for understanding the early-stage diffusion behavior of wood and adhesive-coated systems, as it reflects the immediate interaction between vapor molecules and the material structure before stabilization occurs.

To evaluate the diffusion-hindering effect of the adhesive, attention was focused on the pre-steady zone, where a significant difference can be observed between specimens covered with an adhesive layer and those without. Monitoring this zone allows the detection of the adhesive's role in impeding water vapor diffusion across the bonded layers, as shown in Fig. 3.1, 3.2.

After defining the function of water vapor diffusion and identifying correctly the transition point "A" the y coordinates of the mass change in the pre-steady zone are suitable to express the water vapor hindering or promoting ability of an adhesive (coating) layer.

The y-coordinate of the transition point "A" for the structural adhesive bonded samples is equal with y_{ABAJ}= 0.939 g whilst the y-coordinate of point "A" for natural samples is equal with y_{ABN}= 9.27 g. The y-coordinate of the two sample types indicates that the mass change of the adhesive-coated samples is around 10 times lower than that of the natural BW_N, leading to the conclusion that the adhesive applied in the indicated amount causes a 10-fold mass increase, hindering water vapor diffusion

While the general recommendation of the mentioned standards is suitable for characterizing diffusion in the steady zone, the pre-steady zone was found suitable for describing the diffusion blocking effect of the adhesive, based on the current results.

As shown in Fig. 3.2 and Table 3.2 for BW_{NP}, the mass change in the pre-steady zone was rapid, indicating unimpeded vapor diffusion through the porous wood matrix. In this region, the water vapor flow rate—calculated from the slope of the linear regression drawn from the origin to the transition point—was 0.0353 g/h, resulting in a permeability coefficient of $\delta = 4.46 \times 10^{-13}$ kg/(m·s·Pa).

The samples coated with an adhesive layer manifested a considerably lower mass increase exposed to similar environmental conditions, the vapor diffusion was pronouncedly

hindered, and for BW_{AJP}, the value of the water vapor flow rate G = 0.004607 g/h was the lowest among all beech samples, with a very low permeability of $\delta = 5.804 \times 10^{-14}$ kg/(m·s·Pa).

Raises the question of whether the G value of the pre-steady zone is suitable for expressing the blocking effect of the adhesive. Since G, by definition, is the slope of the linear in the steady zone, it cannot be interpreted in the pre-steady zone. It was assumed that the mass change up to the transition point "A" adequately reflects the degree of blockage, expressed by the value of the y-coordinate of point A.

Before reaching the steady-state zone, all specimens exhibited a non-linear water vapor flow rate. The water vapor flow rate during the pre-steady zone of uncoated BW_{NP} was 0.0353 g/h, resulting permeability of $\delta = 4.46 \times 10^{-13}$ kg/(m·s·Pa), representing the highest observed value across all beech samples. This confirms high intrinsic diffusion of BW_{NP} and also reflects the absence of any barrier layer. In contrast, adhesive-coated BW_{AJP} exhibited a low value of G = 0.004607 g/h. The significant difference in mass increase illustrates the strong blocking effect of the commercial adhesive, which considerably hinders water vapor permeability during the early exposure stages.

Lasure coated samples showed lower mass increase than the uncoated samples but higher than the commercial adhesive-coated ones. BW_{LP} recorded 45% difference compared to uncoated BW_{NP} with G value, but still substantially higher than adhesive-coated BW_{AJP}, confirming that the lasure layer allows partial water vapor diffusion without fully obstructing vapor flow. Among the adhesive-treated samples, a trend was observed wherein higher MW formulations led to increased vapor permeability in the pre-steady zone. For instance: BW_{S5P} samples coated with 6000 MW S_5 exhibited mass change over time G = 0.024671 g/h, BW_{S4P} samples coated with 5000 MW S_4 exhibited mass change over time G = 0.016115 g/h, and BW_{S3P} samples coated with 4000 S_3 MW exhibited mass change over time G = 0.011386 g/h which a difference close to the BW_{NP}, indicating minimal blocking effect. The commercial adhesive formulation BW_{AXP} and the low MW custom-made synthesized polymers like BW_{S1P}, BW_{S2P}, offered the highest vapor permeability resistance in the pre-steady phase, close to the performance of the commercial adhesive. **By this it was proven in the pre-steady zone also that the vapor blocking or promoting behavior of an adhesive can be adjusted by adjusting its molecular weight**. The results emphasize the necessity of targeted action in formulating adhesives, especially for structural applications. In contrast, adhesives with MW close to the one of the lasures allow for convenient vapor diffusion.

The MW polyol formulation S4 and S5 allowed moderate permeability. This provided partial permeability while maintaining noticeable restrictions relative to the lasure coated

samples, thus in case of BW wood the most convenient MW of the selected polyols would be series S4 and S5 from point of view of diffusion.

The pre-steady zone is particularly critical in assessing the short-term vapor permeability and the blocking effect of adhesive,- or lasure-coated materials. While traditional standards like ISO 12572 and ASTM E96 are primarily designed to evaluate permeability under steady-state conditions, the pre-steady phase reveals crucial differences in how various coatings respond to supporting water vapor diffusion.

3.1.2. Water vapor diffusion of oak wood (OW) *(Quercus spp.)*

The water vapor diffusion of oak wood samples was found to follow **a function of the generalized form**:

$$\Delta m = b_1 * \tanh(b_0 * t) \qquad [g] \qquad \ldots (Equation\ 9)$$

where :

where :b_0,b_1 :coefficients depend on the MW of the adhesive and coating material (Table 3-2)

t : time in hours

All water vapor diffusion curves for OW exhibited a distinct pre-steady stage followed by a steady-state region, which allowed determining the curve slope, locating the A-transition point, and calculating both the diffusion coefficient and vapor flow rate.

3.1.2.1. Evaluation of water vapor diffusion for OW in the steady zone

The diffusion parameters of OW are summarized in Table 3.2 and were calculated based on the hyperbolic tangent equation presented in Figures 3.3–3.4. The results reveal a significant difference in permeability between OW_{NS} and OW_{AJS}. The uncoated specimens exhibited a permeability coefficient of $\delta = 3.45 \times 10^{-14}$ kg/(m·s·Pa) and a vapor flow rate of G = 0.002737 g/h. In contrast, the adhesive-coated samples demonstrated substantially lower values, with $\delta = 0.258 \times 10^{-14}$ kg/(m·s·Pa) and G = 0.000205 g/h. Both parameters were reduced by approximately 13.3-fold compared to OW_{NS}, indicating a strong vapor-blocking effect of the structural adhesive. A one-way ANOVA revealed a statistically significant difference in the water vapor permeability coefficient δ between OW_{NS} and OW_{AJS} ($F(1, 8) \approx 412$, $p < 0.081$), confirming that the approximately 13-fold reduction observed in the adhesive-coated specimens represents a true and statistically validated vapor diffusion hindering effect of the structural adhesive layer. The transition point "A" was identified on the diffusion curve, where its x-coordinate represents the time required to reach the steady-state zone, for OW_N, the steady state was attained within x-coordinate of A_{ON}=223.1 h, whereas for OW_{AJ} it occurred earlier

A_{OAJ}= 142.4 h . These results indicate that the mass increase of adhesive-coated samples was moderate, albeit at a substantially lower mass-change rate compared to the uncoated specimens, this comparison clearly demonstrates a pronounced contrast in vapor permeability performance between OW_{NS} and OW_{AJS}, confirming that the commercial adhesive blocking water vapor permeability while accelerating the time to reach the permeability steady state at a much lower mass exchange rate.

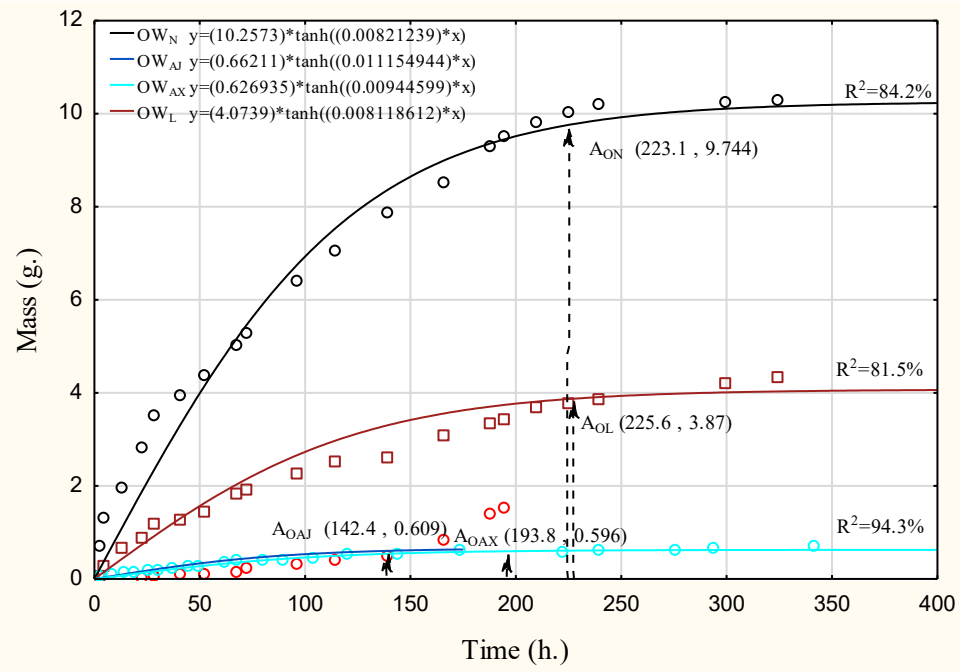

Figure 3.3 The mass change over time for OW_N, OW_L, OW_{AJ}, and OW_{AX}

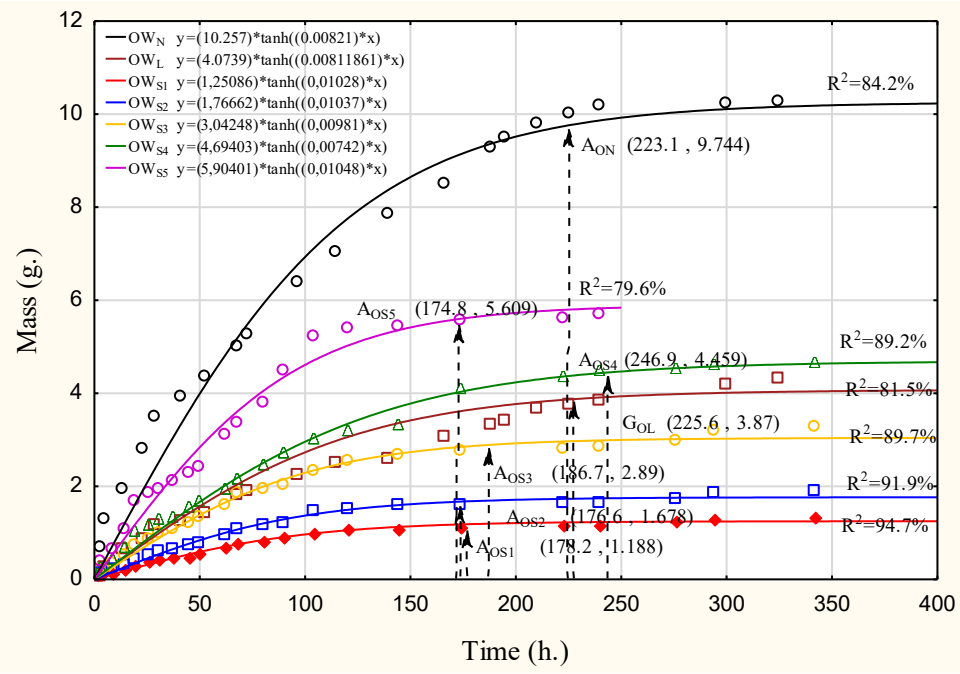

Figure 3.4The mass change over time for OW_L, OW_N, OW_{S1}, OW_{S2}, OW_{S3}, OW_{S4}, and OW_{S5}

Table 3-2 Water vapor permeability of oak wood (OW)

Sample	b_0	b_1	x_A(h)	y_A (g)	G (g/h)	W * 10^{-12} kg/(m²·s·Pa)	δ *10^{-14} kg/(m·s·Pa)
OW_{NS}	0.008210	10.257300	223.1	9.744	0.002737	3.448301	3.448301
OW_{NP}					0.043677	55.02262	55.02262
OW_{AJS}	0.011155	0.662110	142.4	0.609	0.000205	0.258456	0.258456
OW_{AJP}					0.004277	5.388366	5.388366
OW_{AXS}	0.009450	0.626935	193.8	0.596	0.000149	0.187662	0.187662
OW_{AXP}					0.003073	3.87138	3.87138
OW_{LS}	0.008119	4.073900	225.6	3.870	0.001098	1.383216	1.383216
OW_{LP}					0.017155	21.611	21.611
OW_{S5S}	0.010480	5.904010	174.8	5.609	0.001299	1.635862	1.635862
OW_{S5P}					0.032087	40.42264	40.42264
OW_{S4S}	0.007420	4.694030	246.9	4.459	0.001371	1.726800	1.726800
OW_{S4P}					0.018062	22.75349	22.75349
OW_{S3S}	0.009810	3.042480	186.7	2.890	0.000702	0.884871	0.884871
OW_{S3P}					0.015481	19.50229	19.50229
OW_{S2S}	0.010370	1.766620	176.6	1.678	0.000392	0.493560	0.493560
OW_{S2P}					0.009503	11.97144	11.97144
OW_{S1S}	0.010280	1.250860	178.2	1.188	0.000279	0.351339	0.351339
OW_{S1P}					0.006669	8.400782	8.400782

For OW_{LS}, the water vapor flow rate G = 0.001098 g/h and a permeability coefficient δ = 1.383 × 10^{-14} kg/(m·s·Pa) with a mass change, reflected by the y-coordinate at the transition point "A" =3.91 g within x-coordinate = 225.6 h , comparing with OW_{NS} having the permeability and water vapor flow rate more than around 2.5 time and mass change at point A = 10.26 g within 223.1 h On the other hand the OW_{LS} having permeability and water vapor flow rate more than around 5.35 times compared with OW_{AJS}.

The water vapor permeability behavior observed in OW_{LS} compared to OW_{AJS} and OW_{NS} suggests that the lasure layer allows partial vapor permeability, not blocking the water vapor permeability, most likely facilitated by improved permeability due to its capillary structure.

As shown in Fig. 3.4 and Table 3.2, OW_{AXS} and 2000 MW S_1 and 3000 MW S_2, with lower MW custom-made synthesized polymers, demonstrated reduced vapor permeability compared to the OW_{LS}. For instance, OW_{LS} recorded G = 0.001098 g/h and δ = 1.383 × 10^{-14} kg/(m·s·Pa). In contrast OW_{S1S} with 2000 MW showed G = 0.000279 g/h and δ = 0.351 × 10^{-14} kg/(m·s·Pa), approximately 3.94 times lower than OW_{LS}, whilst OW_{S2S} with 3000 MW exhibited G = 0.000392 g/h and δ = 0.494 × 10^{-14} kg/(m·s·Pa), around 2.8 times lower, and OW_{AXS} showed G = 0.000149 g/h and δ = 0.188 × 10^{-14} kg/(m·s·Pa), more than around 7 times lower than the OW_{LS} control samples coated with lasure.

The OW_{S3S}, OW_{S4S}, and OW_{S5S} samples stood out as high MW formulations whose steady-state behavior was relatively close to that of the OW_{LS}. The OW_{S3S} samples recorded G

= 0.000702 g/h and δ = 0.885 × 10^{-14} kg/(m·s·Pa), showing moderate vapor permeability, albeit slightly lower than OW_{LS} samples. The OW_{S4S} samples achieved G = 0.001371 g/h and δ = 1.727 × 10^{-14} kg/(m·s·Pa), while OW_{S5S} recorded G = 0.001299 g/h and δ = 1.636 × 10^{-14} kg/(m·s·Pa) both very close to the permeability of OW_{LS} samples A one-way ANOVA revealed a statistically significant difference in the water vapor permeability coefficient δ among OW_{LS}, OW_{S3S}, OW_{S4S}, and OW_{S5S} ($F(3, 16) \approx 24.6$, $p < 0.052$), indicating that although the high molecular weight formulations approached the permeability behavior of OW_{LS}, measurable statistical differences remained among the tested surface conditions.

Overall, the steady-state data for OW confirm that the lower MW custom-made synthesized polymers like S1 act as strong vapor barriers. Also, the intermediate formulations, like S_2 provide partial permeability, whilst higher MW systems S_3, S_4, and S_5 closely match the semi-vapor permeable behavior of lasures. This highlights the potential for molecular weight adjustment to fine-tune the vapor diffusion properties of structural adhesives for optimized performance in OW products bonded in layer.

3.1.2.2.Evaluation of water vapor diffusion for OW in the pre-steady zone

The assessment of water vapor diffusion through OW highlights distinct differences between natural, adhesive-coated, and lasure-coated specimens, particularly in the pre-steady state region. This stage proved especially informative for identifying the extent to which adhesives restrict vapor diffusion.

For OW_{NP}, the y-coordinate represented the mass change, at the transition point is equal = 9.744 g, whereas the mass change of adhesive-coated samples OW_{AJP} showed only 0.61g. This nearly fifteenfold reduction illustrates the strong blocking action of the adhesive layer. The water vapor permeability for OW_{NP} was δ = 5.502 × 10^{-}13 kg/(m·s·Pa) with G=0.043677 g/h, compared to δ = 5.3883 × 10^{-14} kg/(m·s·Pa) and G = 0.004277 g/h for OW_{AJP}. Such a sharp contrast confirms the adhesive's dominant vapor-barrier effect under identical conditions in OW. OW_{LP} specimens presented partial permeability through the lasure with δ = 2.1611 × 10^{-}13 kg/(m·s·Pa) and G = 0.017155 g/h. This means the water vapor permeability with OW_{LP} is less than around 40% of the permeability in OW_{NP} and four times that of the permeability in OW_{AJP}. This behavior supports the role of lasure as a semi-permeable coating that balances diffusion and blocking.

Changes in the MW of a custom-made synthesized polymer can affect water vapor diffusion through oak wood sample assemblies, as shown in Fig. 3.4, demonstrating that MW

governs the vapor permeability. High molecular-weight systems exhibited closely comparable water-vapor diffusion characteristics. The Oak samples coated with custom made polymer with 6000 MW, 5000 MW, and 4000 MW (OW_{S5P}, OW_{S4P}, and OW_{S3P}) demonstrated permeability coefficients δ of 4.042264×10^{-13}, 2.27535×10^{-13}, and 1.950229×10^{-13} kg/(m·s·Pa), respectively. Correspondingly, their water vapor flow rates G were 0.032087, 0.018062, and 0.015481 g/h these values were relatively close to one another within the high-MW series, indicating a converging diffusion behavior at elevated molecular weights. Moreover, their permeability and vapor flow-rate values closely approached and in some cases slightly exceeded those of the lasure-coated samples. This trend suggests that increasing molecular weight enables improved control over water-vapor diffusion, allowing the adhesive system to achieve a semi-permeable yet regulated transport behavior.

In contrast to OW_{AJP}, which exhibited failure after 175 h due to excessive vapor blockage and the resulting strain accumulation, the OW_{S5P} series representing the closest behavior to lasure coatings also showed failure at 255 h. However, in this case, the failure was triggered by excessive water vapor penetration into the wood, leading to cracking caused by the internal strain and by the differences in strains on the two faces of wood species. This dual outcome highlights a critical principle: neither excessive vapor blocking nor excessive vapor transmission ensures long-term stability. Instead, a balance must be achieved between the molecular weight of the adhesive and the degree of vapor diffusion it permits. Both increased and decreased molecular weight can compromise structural integrity, underscoring the necessity of carefully tuning adhesive formulations to maintain durability in bonded wood systems.

An adhesive material with a medium MW, like OW_{S2P}, $\delta = 1.1971 \times 10^{-}13$ kg/(m·s·Pa), and G = 0.0095 g/h , showed reduced permeability. By contrast, the lowest MW adhesives, OW_{S1P} with $\delta = 0.84 \times 10^{-}13$, G = 0.00667g/h and OW_{AXP} with $\delta = 0.387 \times 10^{-}13$ kg/(m·s·Pa), and G = 0.00307 g/h, provided the strongest vapor-blocking capacity, nearly replicating the performance of OW_{AJP}.

The MW polyol formulation S4 and S5 allowed moderate permeability. This provided partial permeability while maintaining noticeable restrictions relative to the lasure coated samples, thus in case of OW wood the most convenient MW of the selected polyols would be series S4 and S5 from point of view of diffusion.

The steady- and pre-steady diffusion parameters G and δ clearly differentiate between natural, lasure-coated, and adhesive-bonded systems; however, their slope-based formulation inherently limits their capacity to fully quantify the real blocking efficiency of the adhesive

layers. Since permeability is calculated as a mass change per unit time, a large mass increase over a long period may numerically resemble a small mass increase over a shorter period, leading to comparable rate values despite fundamentally different diffusion behaviors. This effect becomes evident when comparing the steady-to-pre-steady ratios of the uncoated OW_N and OW_L, while the steady-state δ and G values indicate a 13-fold reduction for OW_{AJS} relative to OW_{NS}, the absolute accumulated mass at the transition point "A" reveals a more pronounced physical contrast. At x_A = 223.1 h, OW_{NS} reached y_A = 9.7 g, whereas OW_{AJS} stabilized at only ≈ 0.609 g (xA ≈ 142.4 h), representing an absolute difference of more than 9 g. This substantial gap directly reflects the adhesive's vapor-blocking capacity in a way that slope-derived parameters alone cannot fully express. Therefore, for oak systems, unlike slope-based parameters, the y_A coordinate at point "A" representing the cumulative mass change at the diffusion transition, serves as a more physically meaningful and sensitive indicator of adhesive-induced diffusion blocking

3.1.3. Water vapor diffusion of spruce wood (SW) *(Picea abies)*

The water vapor diffusion of spruce wood samples was found to follow **a function of the generalized form**:

$$\Delta m = b_1 * \tanh(b_0 * t) \qquad [g] \qquad \ldots (Equation\ 9)$$

where :

where :b_0,b_1 :coefficients depend on the MW of the adhesive and coating material (Table 3-3)

t : time in hours

The diffusion behavior of the SW samples exhibited two distinct phases pre-steady-state and steady-state thereby enabling accurate determination of curve slopes, identification of the transition point "A," and quantitative evaluation of both the water vapor permeability coefficient and the water vapor flow rate.

3.1.3.1.Evaluation of water vapor diffusion for SW in the steady zone

The steady-state zone of water vapor diffusion for SW was evaluated according to ISO 12572, as shown in Fig. 3.5, 4.6.

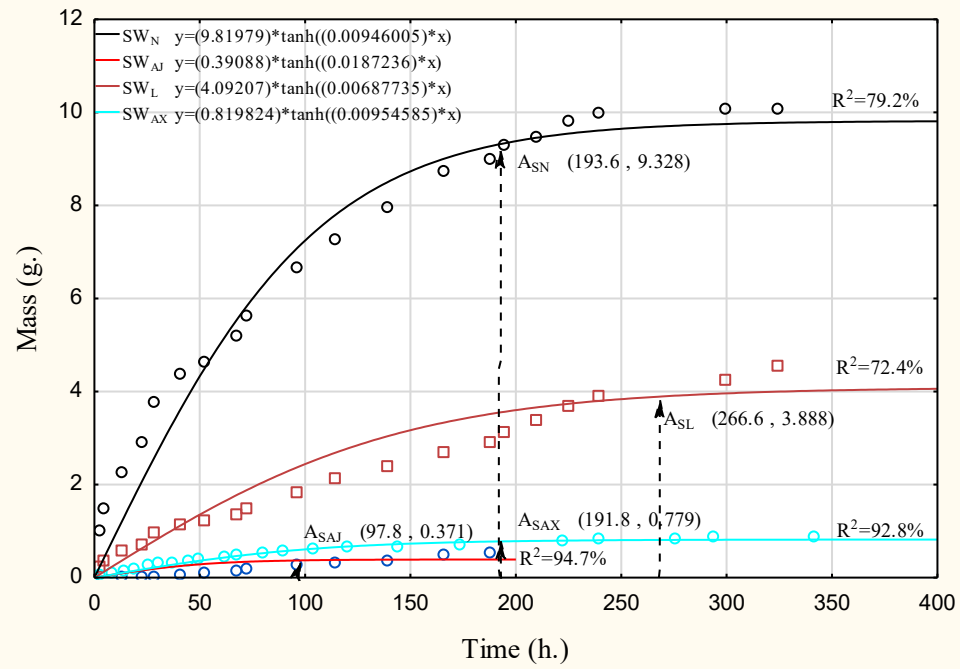

Figure 3.5 The mass change over time for SW_N, SW_L, SW_{AJ}, and SW_{AX}

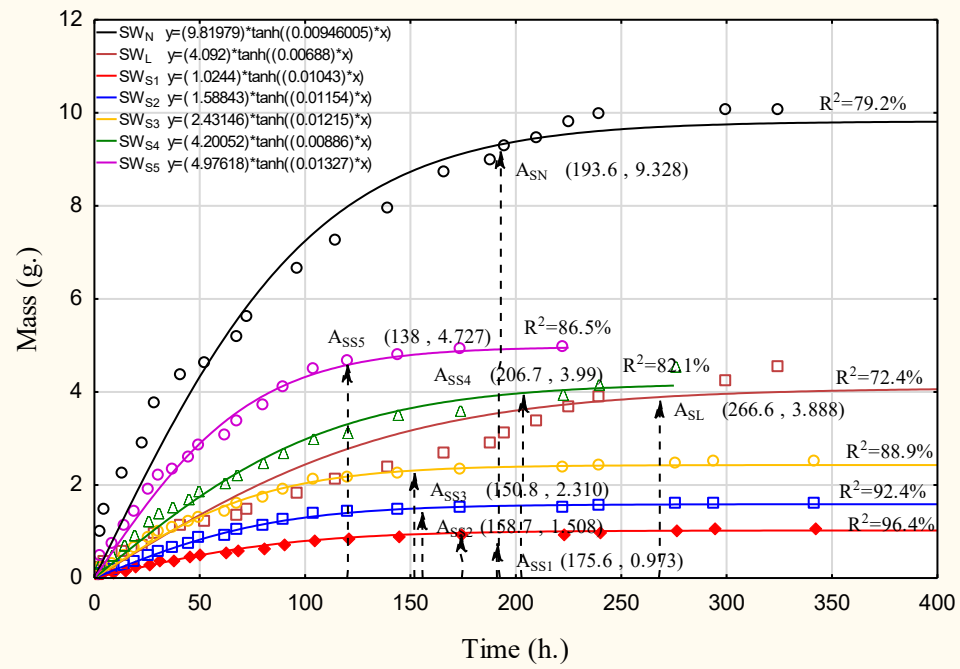

Figure 3.6 The mass change over time for SW_L, SW_{S1}, SW_{S2}, SW_{S3}, SW_{S4}, and SW_{S5}

The water vapor diffusion parameters of SW_{NS} as shown in Table 3.3 were: δ = 2.94×10−14 kg/(m·s·Pa) and G = 0.002331 g/h, compared with SW_{AJS} having water vapor permeability δ=0.082×10−14 kg/(m·s·Pa) and water vapor flow rate equal to G = 0.000065 g/h, reveals a significant difference in permeability behavior between SW_{NS} and SW_{AJS}, leading to the conclusion that the commercial adhesive strongly blocks water vapor diffusion and behaves as a barrier, blocking diffusion to an extent around 97%. An one-way ANOVA

performed on the δ values (n = 5 per group) revealed a statistically significant difference between SW_{NS} and SW_{AJS} ($F(1, 8) \approx 510$, $p < 0.065$), confirming the pronounced vapor-blocking performance of the commercial adhesive layer. Since uncoated samples reached the transition point earlier than the lasure coated one, it can be stated that the transition point alone is not suitable to reflect the water vapor hindering effect.

Table 3-3 Water vapor permeability of spruce wood (SW)

Sample	b_0	b_1	x_A (h)	y_A (g)	G (g/h)	W * 10^{-12} kg/(m²·s·Pa)	δ *10^{-14} kg/(m·s·Pa)
SW_{NS}	0.009460	9.819790	193.6	9.328	0.002331	2.936754	2.936754
SW_{NP}					0.048184	60.70101	60.70101
SW_{AJS}	0.018720	0.391000	97.8	0.371	0.000065	0.081568	0.081568
SW_{AJP}					0.003797	4.782999	4.782999
SW_{AXS}	0.009550	0.819824	191.8	0.779	0.000193	0.243303	0.243303
SW_{AXP}					0.004061	5.115423	5.115423
SW_{LS}	0.006880	4.092000	266.6	3.888	0.001278	1.609708	1.609708
SW_{LP}					0.014585	18.37371	18.37371
SW_{S5S}	0.013270	4.976180	138.0	4.727	0.000950	1.196383	1.196383
SW_{S5P}					0.034254	43.15264	43.15264
SW_{S4S}	0.008860	4.200520	206.7	3.990	0.001051	1.324208	1.324208
SW_{S4P}					0.019305	24.31966	24.31966
SW_{S3S}	0.012150	2.431460	150.8	2.310	0.000486	0.612578	0.612578
SW_{S3P}					0.015318	19.29741	19.29741
SW_{S2S}	0.011540	1.588430	158.7	1.509	0.000328	0.413326	0.413326
SW_{S2P}					0.009508	11.97809	11.97809
SW_{S1S}	0.010430	1.024370	175.6	0.973	0.000226	0.284956	0.284956
SW_{S1P}					0.005542	6.981259	6.981259

The steady-state water vapor diffusion behavior of the lasure-coated spruce samples SW_{LS} demonstrated moderate permeability relative to the uncoated and adhesive-bonded systems. SW_{LS} exhibited a water vapor flow rate of G = 0.001278 g/h and a permeability coefficient of $\delta = 1.609708 \times 10^{-14}$ kg/(m·s·Pa). These values are approximately 1.8 times lower than those of the SW_{NS} and about 19 times higher than those of SW_{AJS} samples.

The steady-state regime for SW_{LS} was reached after 266.6 h, corresponding to the x-coordinate of the transition point "A", with an y_A mass change of 3.88 g. In comparison, SW_{NS} reached its transition point earlier, at 193.6 h, with a substantially higher mass accumulation of 9.32 g. This indicates that SW_{LS} required a longer exposure time to stabilize, while exhibiting a lower total vapor uptake than the uncoated reference. Compared with SW_{AJS}, however, SW_{LS} clearly allowed partial vapor diffusion. This behavior can be attributed to the manufacturing characteristics of the lasure layer, likely influenced by its capillary surface structure, which moderates but does not fully block vapor transport.

Regarding the custom-made polymer systems, SW_{S1S}, SW_{S2S}, and SW_{AXS} demonstrated the lowest steady-state permeability, approaching the vapor-blocking performance of SW_{AJS}. Specifically, SW_{S1S} exhibited $\delta = 0.285 \times 10^{-14}$ kg/(m·s·Pa) and G = 0.000226 g/h; SW_{S2S} showed $\delta = 0.413 \times 10^{-14}$ kg/(m·s·Pa) and G = 0.000328 g/h; and SW_{AXS} recorded $\delta = 0.243 \times 10^{-14}$ kg/(m·s·Pa) with G = 0.000193 g/h. When compared with SW_{NS} $\delta = 2.94 \times 10^{-14}$ kg/(m·s·Pa), G = 0.00233 g/h, these systems reduced permeability by approximately 7–12 times, confirming their strong vapor-barrier efficiency. Although SW_{AJS} remained the most effective vapor barrier overall, SW_{AXS} and the lower molecular weight systems like S1and S2 exhibited comparable blocking behavior.

The SW_{S3S} displayed intermediate permeability $\delta = 0.613 \times 10^{-14}$ kg/(m·s·Pa), G = 0.000486 g/h, approximately 4.8 times lower than SW_{NS}, yet higher than S1 and S2, indicating partial vapor transport. In contrast, the higher molecular weight formulations SW_{S4S} and SW_{S5S} exhibited permeability behavior similar to the lasure-coated samples. SW_{S4S} recorded $\delta = 1.324 \times 10^{-14}$ kg/(m·s·Pa) with G = 0.00105 g/h, while SW_{S5S} showed $\delta = 1.196 \times 10^{-14}$ kg/(m·s·Pa) and G = 0.00095 g/h. These values confirm that increasing molecular weight shifts the system from strong vapor blocking toward semi-permeable behavior comparable to lasure coatings.

3.1.3.2.Evaluation of water vapor diffusion for SW in the pre-steady zone

As shown in Fig. 3.5 and Fig. 3.6, the y-coordinate of transition point "A" representing the mass change of the uncoated sample was A_{SN} = 9.32 g at 193.6 h (x-coordinate). Before the transition point in the pre-steady zone, SW_{NP} exhibited a water vapor permeability of $\delta = 6.070 \times 10^{-13}$ kg/(m·s·Pa) with a water vapor flow rate of G = 0.048184 g/h. In comparison, the adhesive-coated SW_{AJP} $\delta = 0.4783 \times 10^{-13}$ kg/(m·s·Pa), G = 0.003797 g/h showed a reduction of more than around 90% in its permeability relative to SW_{NP}. The mass change at A_{SAJ} was only 0.371 g within 97.8 h, representing a value more than around 25 times lower than the mass change at the A point of the SW_{NP}

The SW species coated with lasure SW_{LP} having the mass change at the transition point A_{SL}=3.88 g. within =266.6 h, showed lower mass change increment than the SW_{NP} and higher than the SW_{AJP}, The water vapor permeability for SW_{LP} was $\delta = 1.837 * 10^{-13}$ kg/(m·s·Pa) being 30% lower compared with SW_{NP} and around 3.7 times more than SW_{AJP}, confirming that the lasure layer allows partial water vapor diffusion without fully obstructing vapor flow.

On the other hand, the SW coated with different MW custom-made synthesized polymers S1–S5 exhibited diverse behavior in the pre-steady zone depending on the average

MW of the polyol mixture. Generally, 2000 MW S1, 3000 MW S2, 4000 MW S3, 5000 MW S4, 6000 MW S5, and SW_{AXP}, demonstrated reduced water vapor permeability compared to the lasure-coated sample SW_{LP}.

The low MW polyols like S1, S2 and the AX adhesive showed reduction in water vapor water vapor permeability about 62%,- 35%,- and 72% respectively. Compared with SW_{LP}, the mass change at point A decreased by approximately 75%, 61.2%, and 80% relative to A_{SL}. The corresponding times were 175.6 h, 158.7 h, and 191.8 h, respectively, compared to 266.6 h for ASL. This indicates that the behavior of the transition point between the pre-steady state and steady state may differ from the trends observed for permeability and flow rate. The moderate molecular weight MW polyol S3 exhibited a water vapor permeability of $\delta = 1.932 \times 10^{-13}$ kg/(m·s·Pa) and a vapor flow rate of G = 0.015318 g/h. The mass change at the transition point A_{SS3} was 2.31 g, reached after 150.8 h This corresponds to a water vapor permeability approximately 5% higher than that of SW_{LP}, while the time required to reach the transition point was about 43.4% shorter.

When comparing SW_{S4P}, SW_{S5P}, and SW_{LP}, the average water vapor permeability increased by 24.4% and 57.4%, respectively, relative to SW_{PL}, which showed a reduction of 22.4% and 48.2% in the time required to reach the 'A' point compared with A_{SL}, however, both SW_{S4P} and SW_{S5P} exhibited cracking, caused by uneven strain distribution along the adhesive layer. Cracking facilitated excessive vapor penetration, and this is the reason why both measurements and evaluation of results were stopped at this point. In the same time the high water uptake of the silica gel after cracking proved that the silica gel was far from saturation.

Consequently, while the higher molecular weight in S4 and S5 promoted greater permeability, it simultaneously induced cracking, compromising performance. By contrast, SW_{S3P} represented the most suitable adhesive system with SW, providing a balanced molecular weight, that combined adequate permeability capacity with equilibrate diffusion process, achieving a stable water vapor diffusion behavior comparable to lasure coatings **Intermediate MW polyol formulation S3 allowed moderate permeability. This provided partial permeability while maintaining noticeable restrictions relative to the lasure coated samples, thus in case of SW wood the most convenient MW of the selected polyols would be series S3 from point of view of diffusion.**

According to ASTM E96, water vapor permeability is determined from the steady-state slope of the mass–time curve, where diffusion parameters as G and δ, are calculated based on the linear rate of mass change. While this method clearly differentiates between SW_{NS} and

SW_{AJS} showing nearly 97% reduction in δ it does not fully represent the actual vapor-blocking performance observed in spruce. The cumulative mass at the transition point "A" provides a more physically meaningful contrast: SW_{NS} reached y_A = 9.328 g at 193.6 h, whereas SW_{AJS} reached only 0.371 g at 97.8 h, indicating a difference of almost 9 g in absorbed moisture. This substantial disparity more clearly reflects the adhesive's blocking efficiency than slope-based parameters alone. Therefore, although ASTM E96 relies on steady-state slope evaluation, the y_A coordinate at point "A" offers a more sensitive indicator for assessing real vapor blocking or transmission behavior in bonded SW systems.

3.1.4. Water vapor diffusion of grey poplar (GPW) *(Populus canescens)*

The water vapor diffusion of grey poplar wood samples was found to follow a function of the generalized form:

$$\Delta m = b_1 * \tanh(b_0 * t) \qquad [g] \qquad \ldots (Equation\ 9)$$

where :

b0,b1 : coefficients depend on the MW of the adhesive and coating material type (Table 3-4)

t : time in hours

Grey poplar was evaluated also as a possible substitute to spruce and other coniferous species in engineering applications. It was also a question whether water vapor diffusion has similar characteristic like the other species investigated, especially spruce, demonstrating two distinct regions of diffusion: pre steady zone and steady zone. Across all measurements GPW behaved similar to other wood species and demonstrated the two distinct zones, enabling the determination of the transition point 'A'.

3.1.4.1.Evaluation of water vapor diffusion for GPW in the steady zone

As shown in Fig. 3.7 and 3.8, the comparison between GPW_{NS} and GPW_{AJS} demonstrates a substantial reduction in water vapor diffusion. The steady-state water vapor diffusion analysis for GPW resulted that GPW_{NS} exhibited a water vapor permeability of δ = 3.69×10^{-14} kg/(m·s·Pa) with a mass-change rate of G = 0.002928 g/h, whereas GPW_{AJS} showed significant difference, with δ = 0.318×10^{-14} kg/(m·s·Pa) and G = 0.000253 g/h. This represents an approximate 11.6-fold decrease in both permeability and vapor flow rate relative to GPW_{NS}. Furthermore, the transition from the pre-steady to steady zone occurred at 209.6 h for GPW_{NS}, compared with 145.1 h for GPW_{AJS}. Although GPW_{AJS} eventually reached a steady-state condition but the mass change at transition point remained lower than that of A_{GPNS}. These findings confirm the strong vapor-barrier behavior introduced by the adhesive

layer and highlight its pronounced effect on limiting water vapor diffusion.A one-way ANOVA performed on the δ values (n = 5 per group) confirmed that the difference between GPW_{NS} and GPW_{AJS} was statistically significant ($F(1, 8) \approx 427$, $p < 0.075$), verifying the strong vapor diffusion hindering effect of the commercial

To investigate the behaviour of grey poplar wood samples coated with lasure and to compare them with uncoated samples and samples coated with a commercial adhesive, the permeability values for GPW_{LS} were calculated according to Table 3.4. The water vapor permeability was $\delta = 2.847 \times 10^{-14}$ kg/(m·s·Pa), with a vapor flow rate of G = 0.002260 g/h. This permeability is approximately 1.29 times lower than that of GPW_{NS} and about 8.95 times higher than that of GPW_{AJS}.

Furthermore, the mass change indicated by the y-coordinate at point "A" A_{GPLS} reached 6.64 g after 291.7 h, compared with 11.58 g after 209.6 h for GPW_{NS}.

These results show that GPW_{LS} required a longer duration to achieve steady-state permeability than GPW_{NS}, while also exhibiting a lower mass change from water vapor over the same period. Compared with GPW_{AJS}, the GPW_{LS} permitted partial water vapor permeability, a behavior likely influenced by its capillary surface structure and manufacturing characteristics. However, its vapor diffusion capacity remained slightly lower than that of GPW_{NS}, reflecting the moderating effect of the lasure coating layer.

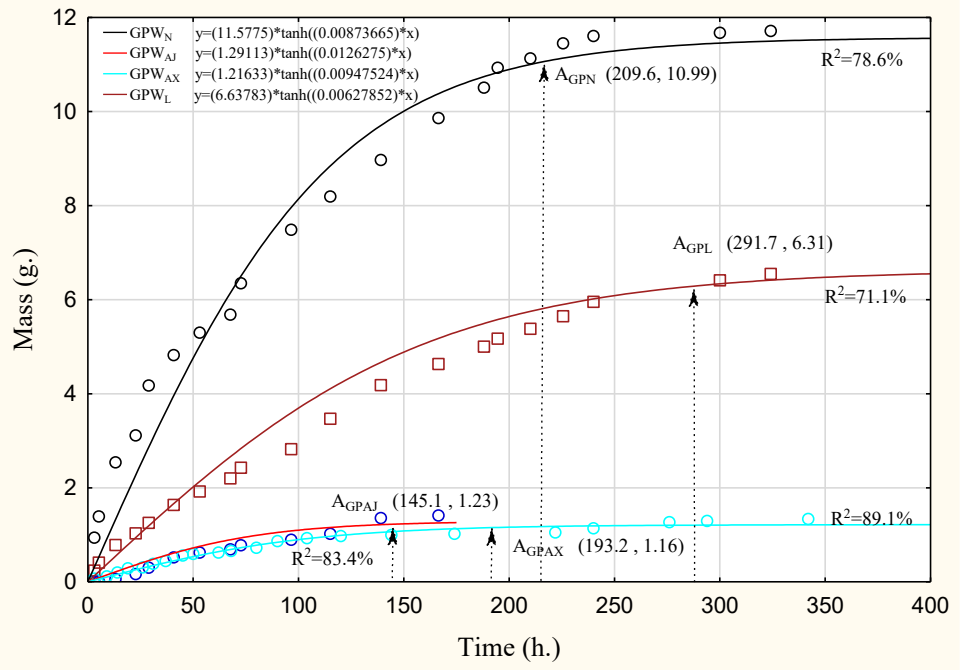

Figure 3.7 presents the mass change over time for GPW_N, GPW_L, GPW_{AJ}, and GPW_{AX}

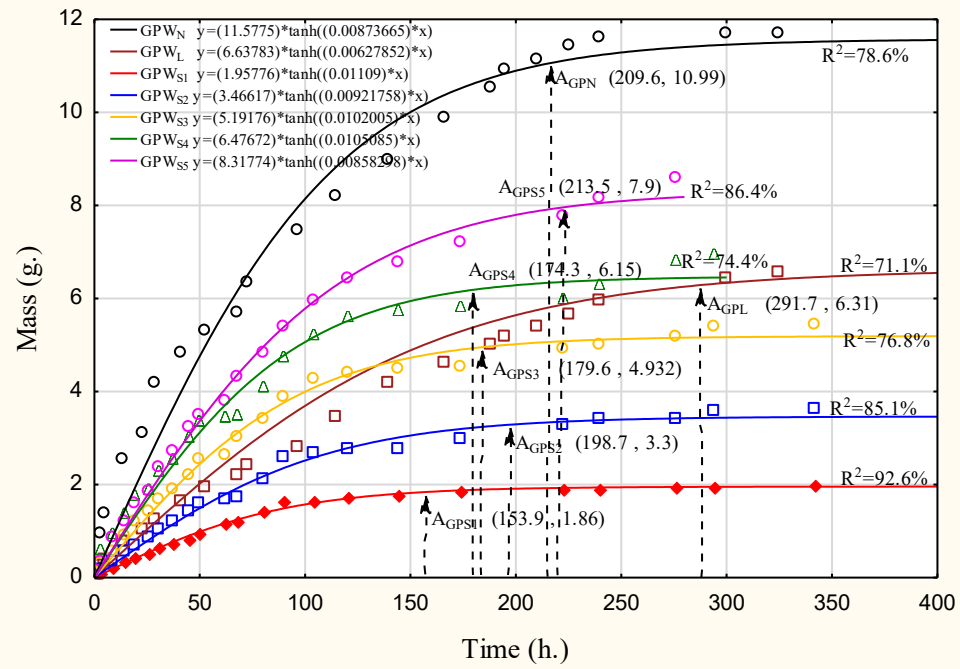

Figure 3.8 The mass change over time for GPW_L, GPW_{S1}, GPW_{S2}, GPW_{S3}, GPW_{S4}, and GPW_{S5}

Table 3-4 Water vapor permeability of grey-poplar wood (GPW)

Sample	b_0	b_1	x_A(h)	Ya (g)	G (g/h)	W * 10^{-12} kg/(m^2·s·Pa)	δ *10^{-14} kg/(m·s·Pa)
GPW_{NS}	0.008740	11.577500	209.6	10.999	0.002928	3.688464	3.688464
GPW_{NP}					0.052475	66.10626	66.10626
GPW_{AJS}	0.012628	1.291130	145.1	1.226	0.000253	0.318236	0.318236
GPW_{AJP}					0.008454	10.64969	10.64969
GPW_{AXS}	0.009480	1.216330	193.2	1.155	0.000288	0.363122	0.363122
GPW_{AXP}					0.005981	7.53437	7.53437
GPW_{LS}	0.006279	6.637830	291.7	6.306	0.002260	2.847070	2.847070
GPW_{LP}					0.021620	27.2361	27.2361
GPW_{S5S}	0.008580	8.317740	213.5	7.902	0.002137	2.691683	2.691683
GPW_{S5P}					0.037011	46.62547	46.62547
GPW_{S4S}	0.010510	6.476720	174.3	6.153	0.001422	1.791001	1.791001
GPW_{S4P}					0.035301	44.47094	44.47094
GPW_{S3S}	0.010200	5.191760	179.6	4.932	0.001164	1.466394	1.466394
GPW_{S3P}					0.027462	34.59617	34.59617
GPW_{S2S}	0.009220	3.466170	198.7	3.293	0.000839	1.056953	1.056953
GPW_{S2P}					0.016572	20.87738	20.87738
GPW_{S1S}	0.011900	1.957760	153.9	1.860	0.000397	0.499973	0.499973
GPW_{S1P}					0.012084	15.22362	15.22362

On the other hand, the behavior of diffusion process through the GPW samples coated with custom-made synthesized polymers samples S1–S5, exhibited notable variation in steady-state water vapor diffusion, strongly influenced by the average MW of the applied polyol mixtures.

Lower MW polyols, such as 2000 MW GPW_{S1S}, 3000 MW GPW_{S2S}, and GPW_{AXS}, statically significant reduced water vapor permeability compared to GPW_{LS}. For instance, GPW_{S1S} recorded G = 0.000397 g/h and δ = 0.500 × 10^{-14} kg/(m·s·Pa) ~5.7 times lower than GPW_{LS} , GPW_{S2S} exhibited G = 0.000839 g/h and δ = 1.057 × 10^{-14} kg/(m·s·Pa) ~2.7 times lower, while GPW_{AXS}, at G = 0.000288 g/h and δ = 0.363 × 10^{-14} kg/(m·s·Pa), was only marginally higher than GPW_{AJS}, indicating similar vapor-blocking capacity. By contrast, higher MW formulations, such as GPW_{S4S} and GPW_{S5S}, approached the laser's semi-diffusion performance, GPW_{S4S} showed G = 0.001422 g/h and δ = 1.791 × 10^{-14} kg/(m·s·Pa), with the x-coordinate of the transition point equal 174.3 h and a the y-coordinate equal 6.48 g, indicating earlier stabilization but lower total mass change than GPW_{LS}. A one-way ANOVA performed on the δ values (n = 5 per group) revealed a statistically significant difference among the tested formulations ($F(5, 24) \approx 52.3$, $p < 0.009$). For GPW_{S5S} recorded G = 0.002137 g/h and δ = 2.692 × 10^{-14} kg/(m·s·Pa), closely matching GPW_{LS} values, with a similar stabilization time of 213.5 h but a higher mass change reflected by the y-coordinate of 8.32 g, suggesting slightly greater vapor diffusion. Overall, the GPW results confirm the trend observed in other wood species, like low MW adhesives S1, act as strong vapor barriers, closely approaching the blocking of a vapor permeability of commercial adhesives like GPW_{AJS}. Intermediate MW systems like S2 and S3 provide partial vapor permeability. High MW systems like S_4 and S_5 allow vapor permeability comparable to GPW_{LS}, with S5 in particular exhibiting nearly identical δ values and stabilization behavior.

3.1.4.2.Evaluation of water vapor diffusion for GPW in the pre-steady zone

The pre-steady diffusion behavior of grey poplar wood GPW, illustrated in Fig. 3.7 and 3.8, was evaluated using the parameters summarized in Table 3.4. Analysis of this region enables a clear assessment of the adhesive layer's role in restricting water vapor transport. For GPW_{NP},the mass change at the transition point was y_A = 10.9 g within 209.6 h, with a calculated permeability of δ = 6.61 × 10^{-13} kg/(m·s·Pa) and a vapor flow rate of G = 0.052475 g/h.

In contrast, GPW_{AJP} exhibited a substantially lower mass accumulation at the transition point, y_A = 1.2 g within 145.1 h, with δ = 1.060626 × 10^{-13} kg/(m·s·Pa) and G = 0.008454 g/h The y-coordinate of the transition point for the adhesive-coated sample is therefore approximately nine times lower than that of the uncoated reference, clearly demonstrating the strong diffusion-hindering effect of the adhesive layer, the permeability of GPW_{AJP} decreased by more than 84% compared with GPW_{NP}, confirming that the applied adhesive significantly

restricts water vapor transport during the pre-steady phase and acts as an effective vapor barrier in the early stage of exposure.A one-way ANOVA performed on the pre-steady permeability coefficients δ (n = 5 per group) revealed a statistically significant difference among GPW_{NP}, GPW_{LP}, and GPW_{AJP} ($F(2, 12) \approx 58.4$, $p < 0.015$). Post hoc Tukey analysis confirmed that GPW_{AJP} exhibited significantly lower permeability than both GPW_{NP} and GPW_{LP}. For GPW_{LP}, the mass change represented by the y-coordinate of the transition point was $y_A = 6.306$ g, reached after 291.7 h This value is clearly lower than that of the GPW_{NP}, which exhibited $y_A = 10.9$ g at 209.6 h, yet substantially higher than the GPW_{AJP}, where $y_A = 1.2$ g at 145.1 h.

The corresponding water vapor permeability of GPW_{LP} was $\delta = 2.723 \times 10^{-13}$ kg/(m·s·Pa), representing approximately 60% of the permeability of GPW_{NP} and about 2.5 times higher than that of GPW_{AJP}. These findings confirm that the lasure layer moderates vapor transport: it reduces overall vapor uptake compared with uncoated wood yet still permits partial water vapor diffusion without completely blocking vapor flow.

In contrast, GPW coated with custom-made synthesized polymers of varying molecular weights S1–S5 exhibited a distinctly MW-dependent diffusion behavior, particularly in the pre-steady-state zone. The analysis of these structural adhesive systems demonstrates that the average molecular weight of the applied polyol mixture strongly influences early-stage vapor transport. Overall, all S1–S5 series showed reduced water vapor diffusion compared with the GPW_{LP}, with the degree of reduction governed by the respective molecular weight of the formulation.

The AX commercial adhesive and low MW adhesive resins, such as S1, caused reductions in water vapor permeability of approximately 72% and 44%, respectively, compared with GPW_{LP}. Similarly, the mass change at point A decreased by about 71% and 82% relative to A_{GPL}, with corresponding times of 193.2 h and 153.9 h, compared with 291.7 h for A_{GPL}. These differences indicate that the behaviour of the transition point between the pre-steady state and steady state can differ from the trends observed in permeability and flow rate. S2 and S3 exhibited a moderate effect compared with GPW_{LP}. Their properties were as follows: GPW_{S2P} had $\delta = 2.087 \times 10^{-13}$ kg/(m·s·Pa) with G = 0.016572 g/h, and GPW_{S3P} had $\delta = 3.46 \times 10^{-13}$ kg/(m·s·Pa) with G = 0.027462 g/h. The mass changes at the transition point were AGPS2 = 3.29 g after 198.7 h and $A_{GPS3} = 4.932$ g after 179.6 h. Compared with GPW coated with lasure, the water vapor permeability of GPW_{S2P} and GPW_{S3P} was within approximately ±25% of GPW_{LP}. The mass changes of A_{GPS2} and A_{GPS3} were 47% and 22% lower, respectively, than that of A_{GPL}, indicating moderately reduced vapor transport.

When comparing GPW_{S4P} and GPW_{S5P} with GPW_{LP}, the average water vapor permeability increased by 63% and 71%, respectively, relative to GPW_{LP}. However, both GPW_{S4P} and GP_{S5P} exhibited cracking, caused by uneven strain distribution along the adhesive layer. Cracking facilitated excessive vapor penetration and this is the reason why both measurements and evaluation were stopped at this point for the cracked samples. Consequently, while the higher molecular weight in S_4 and S_5 promoted greater diffusion, it simultaneously induced cracking. **Intermediate MW polyol formulation S4 allowed moderate permeability. This provided partial permeability while maintaining noticeable restrictions relative to the lasure coated samples, thus in case of GPW wood the most convenient MW of the selected polyols would be series S4 from point of view of diffusion.**

By contrast, GPW_{S2P} and GPW_{S3P} represented the most suitable adhesive systems, providing a balanced molecular weight that combined adequate diffusion capacity with resistance to cracking, achieving a stable behavior close to the one of lasure coatings.

3.1.5. Water vapor diffusion of Smaragdfa® (SMW)*(×Paulownia Clone in vitro 112)*

The water vapor diffusion of Smaragdfa wood samples was found to follow a function of the generalized form:

$$\Delta m = b_1 * \tanh(b_0 * t) \qquad [g] \qquad \ldots (Equation\ 9)$$

where :

b0,b1 : coefficients depend on the MW of the adhesive and coating material type (Table 3-5)

t : time in hours

The diffusion process consisted of an initial pre-steady stage, transitioning into a steady zone for SMW, which provided the basis for deriving curve slopes, identifying the A point, and quantifying both diffusion coefficients and vapor flow rates.

3.1.5.1.Evaluation of water vapor diffusion for SMW in the steady zone

According to ASTM E96/95 and ISO 12572 the diffusion coefficients parameters are calculated depending to the slope of the curve line shown in Figs. 3.9 and 3.10.

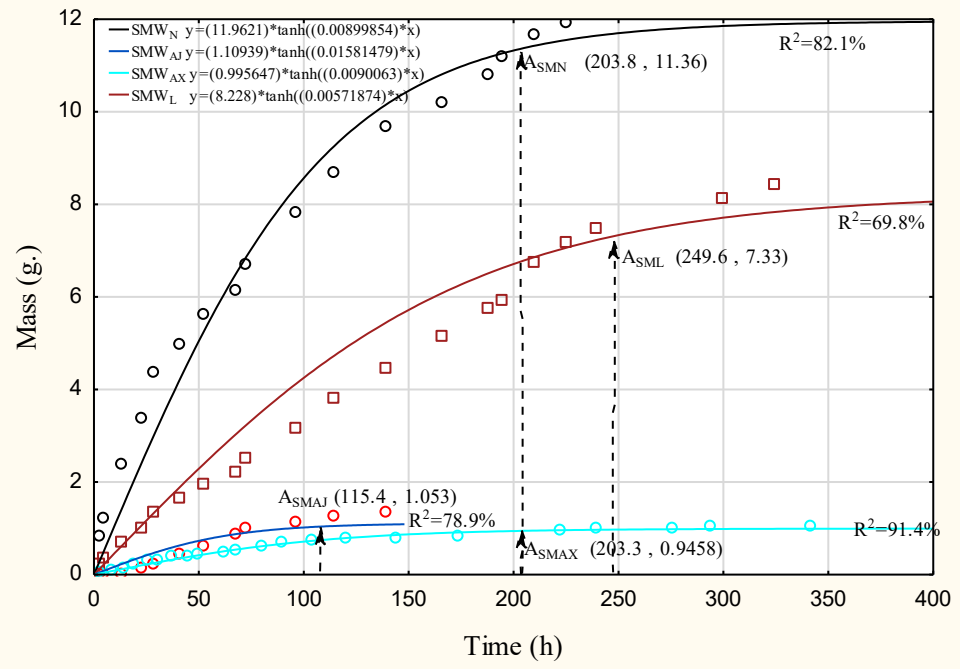

Figure 3.9 The mass change over time for SMW_N, SMW_L, SMW_{AJ} and SMW_{AX}

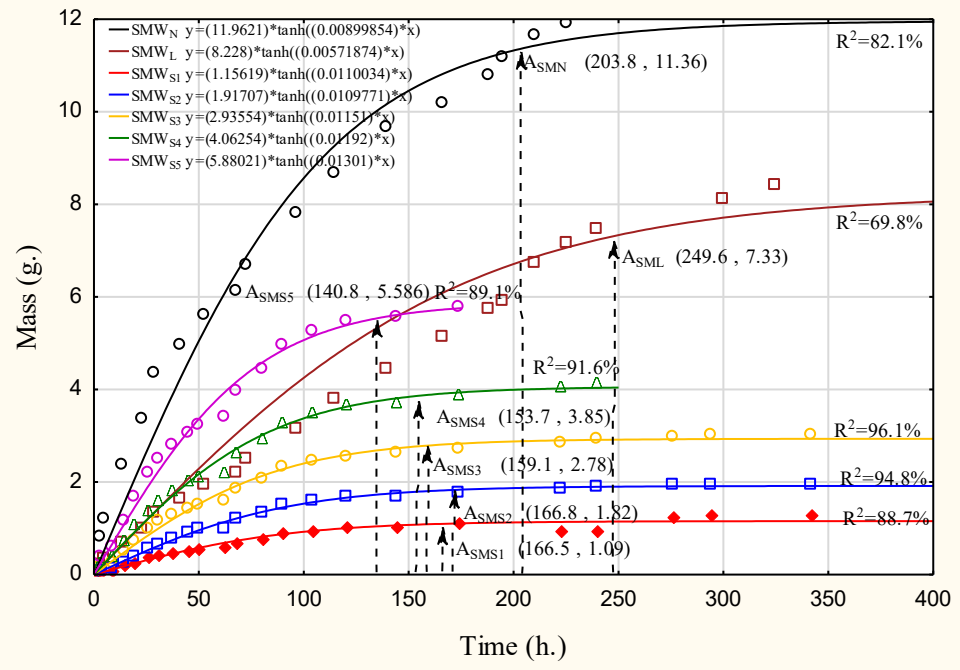

Figure 3.10 The mass change over time for SMW_L, SMW_{S1}, SMW_{S2}, SMW_{S3}, SMW_{S4}, and SMW_{S5},

According to Table 3-5., in the steady zone, SMW shows a water vapor permeability of $\delta = 3.721956 \times 10^{-14}$ kg/(m·s·Pa) and a water vapor flow rate of G = 0.002954 g/h, whereas SMW_{AJS} exhibits a much lower water vapor permeability of $\delta = 0.248 \times 10^{-14}$ kg/(m·s·Pa) and a flow rate of G = 0.000197 g/h. For both SMWs and SMW_{AJs}, a clear difference, of

approximately 15-fold can be observed in the water vapor permeability δ and water-vapor flow rate G. A one-way ANOVA performed on the steady-state permeability coefficients δ (n = 5 per group) revealed a statistically significant difference between SMW and SMW_{AJS} ($F(1, 8) \approx 397$, $p < 0.061$), confirming the pronounced vapor-blocking effect of the commercial adhesive in the steady-state diffusion regime. .

Table 3-5 Water vapor permeability of smaragdfa (SMW)

Sample	**b_1**	**b_0**	x_A(h)	y_A(g)	**G (g/h.)**	**W * 10^{-12} kg/(m^2·s·Pa)**	**δ *10^{-14} kg/(m·s·Pa)**
SMW_{NS}	11.962100	0.008990	203.8	11.364	0.002954	3.721956	3.721956
SMW_{NP}					0.055763	70.24797	70.24797
SMW_{AJS}	1.109390	0.015815	115.4	1.0531	0.000197	0.248756	0.248756
SMW_{AJP}					0.009126	11.49712	11.49712
SMW_{AXS}	0.995647	0.009010	203.3	0.9458	0.000246	0.309423	0.309423
SMW_{AXP}					0.004653	5.861104	5.861104
SMW_{LS}	8.228000	0.005719	249.6	7.3323	0.004840	6.096917	6.096917
SMW_{LP}					0.029376	37.00682	37.00682
SMW_{S5S}	5.880210	0.013010	140.8	5.5862	0.001133	1.427151	1.427151
SMW_{S5P}					0.039675	49.981	49.981
SMW_{S4S}	4.062540	0.011920	153.7	3.8595	0.000822	1.035292	1.035292
SMW_{S4P}					0.025111	31.63383	31.63383
SMW_{S3S}	2.935540	0.011510	159.1	2.7886	0.000607	0.765289	0.765289
SMW_{S3P}					0.017527	22.08042	22.08042
SMW_{S2S}	1.917070	0.010980	166.8	1.8211	0.000409	0.514957	0.514957
SMW_{S2P}					0.010918	13.75439	13.75439
SMW_{S1S}	1.156190	0.011000	166.5	1.0983	0.000246	0.310181	0.310181
SMW_{S1P}					0.006597	8.310287	8.310287

The mass change of SMW_S at transition point "A" in the steady zone was = 1.05 g within 115.4 h but for the SMW_{AJS} mass change was recorded = 11.4 g within 203.8 h at the same point. This comparison reveals a substantial difference in vapor diffusion behavior of the natural Smaragdfa® and the adhesive coated samples. This leads to the conclusion that the commercial adhesive has a strong hindrance on water-vapor diffusion.

The water vapor flow rate G = 0.004840 g/h and water vapor permeability $\delta = 6.097 \times 10^{-14}$ kg/(m·s·Pa) for the SMW_{LS} samples was approximately 1.64 times higher than that of SMW_N and about 24.5 times higher than that of SMW_{AJS}. The transition point for SMW_{LS} was reached after 249.6 hours of testing, with a mass change of 7.33 g, compared to SMW_{NS}, which reached its transition point after 203.8 h with a mass change of 11.364 g, and SMW_{AJS}, which reached the transition point after 115.4 hours with only 1.053 g. This indicates a broadly similar steady-state time for the diffusion process relative to the SMW_{NS}, albeit with a substantially lower total mass gain. The higher vapor diffusion observed in SMW_{LS} compared to SMW_{AJS}

suggests that the lasure layer permits partial vapor diffusion, likely facilitated by its layer's capillary structure induced by it molecular weight. Similarly, the molecular weight of the custom-made synthesized polymers also can be formulated to keep the permeability under control, as shown below.

• Low-MW polyols, like S1 and S2, together with AX , produced the most pronounced vapor resistance with a water vapor permeability δ =0.309×10−14 kg/(m·s·Pa), whilst SMW_{S1S} and SMW_{S2S} achieving 0.31 and 0.514×10−14 kg/(m·s·Pa) respectively. Corresponding vapor flow rates were below 0.0004 g/h, and stabilization occurred early 153.9h and respectively 198.7 h, pointing to an almost continuous vapor barrier comparable to that of the AJ, being δ = 0.249 × 10−14 kg/(m·s·Pa)..

• **Intermediate MW polyol formulation S3 allowed moderate permeability: δ=0.765×10^{-14}, G = 0.0006 g/h, with a transition point at 159.1 h and a mass uptake of 5.19 g. This group provided partial permeability while maintaining noticeable restrictions relative to the lasure coated samples, thus in case of Smaragdfa® wood the most convenient MW of the selected polyols would be series S3 from point of view of diffusion.**

• High-MW polyol formulations like S4 and S5 displayed permeability approaching those of the lasure layer SMW_{LS}. The SMW_{S4S} stabilized at 153.7 h with G=0.00082 g/h and δ=1.03×10−14, whereas SMW_{S5S} recorded G=0.00113 g/h and δ=1.42×10−14, reaching the steady state at 140.8 h. When analyzed against SMW_{LS} (δ=6.09×10−14, G=0.0048 g/h), these data confirm that S1, S2, and AX have a barrier behavior similar to SMW_{AJS} for water vapor diffusion. In the same time S4 and S5 have similar layer properties like SMW_{LS} , of allowing the water vapor diffusion through the adhesive layer. Polyol S3 had special well equilibrated behavior, between partially hindering water diffusion whilst allowing a convenient water vapor diffusion through the adhesive layer This tiered behavior underscores how the MW of the polyol matrix conveniently controls micro-porosity and, consequently, vapor transmission through the adhesive layer.

3.1.5.2. Evaluation of water vapor diffusion for SMW in the pre-steady zone

For SMW_{NP}, the diffusion process consisted of an initial pre-steady stage lasting till point A_{SMN}, at 203.8 h, with a corresponding mass change of 11.36 g. In this phase, the water vapor permeability was δ = 7.02 × 10^{-13} kg/(m·s·Pa), and G = 0.055763 g/h. In contrast, the SMW_{AJP} reached the transition point to the steady zone earlier, at A_{SMAJ} = 115.4 h, with a mass change of 1.05 g. The G and δ values were: G = 0.009126 g/h and δ = 1.149 × 10^{-13} kg/(m·s·Pa),

representing an 84% reduction in permeability capacity relative to SMW_{NP}. A one-way ANOVA performed on the pre-steady permeability coefficients δ (n = 5 per group) revealed a statistically significant difference between SMW_{NP} and SMW_{AJP} ($F(1, 8) \approx 95.6$, $p < 0.081$), confirming the pronounced diffusion-hindering effect of the adhesive layer during the early stage of exposure. This earlier stabilization, despite lower permeability, reflects the restricted diffusion pathways within the adhesive layer. Due to the limited number of effective capillary channels, vapor diffusion reached its maximum capacity rapidly; beyond this point, no further increase occurred, leading to a quicker transition into steady state.

For SMW_{LS}, the transition point occurred at A_{SML} = 249.6 h, with a mass change of 7.33 g. The water vapor permeability and water vapor flow rate were $\delta = 3.70 \times 10^{-13}$ kg/(m·s·Pa) and G = 0.029376 g/h, respectively. Compared with SMW_{NP}, the mass change at point A_{SML}, being its y_A coordinate was about 1.5 times lower, whereas the mass change at A_{SMAJ} was less than 15% of A_{SML}. These results confirm that lasure coatings allow partial vapor transmission, reducing but not completely blocking diffusion. On the other hand, the SMW coated with a different MW adhesive formulation exhibited distinct water vapor diffusion behaviors, particularly in the pre-steady-state zone. As shown in Fig. 3.10 and Table 3.5, the sample treated with adhesive resin with different MW S1-S5, exhibited variable diffusion patterns depending on the average MW of the resin. In general, S1 with 2000 MW, S2 with 3000 MW, S3 with 4000 MW, S4 with 5000 MW, S5 with 6000 MW, and AX adhesive type showed reduced vapor diffusion compared with the uncoated sample SMW_{NP}. The low-MW systems, such as SMW_{S1P} with $\delta = 0.831 \times 10^{-13}$, and G = 0.006597 g/h and SM_{AXP} with $\delta = 0.586 \times 10^{-13}$, and G = 0.00465 g/h, demonstrated strong vapor-blocking capacity compared with SM_{NP}. The water vapor permeability of SMW_{S1P} and SMW_{AXP} were reduced by approximately 78% and 84%, respectively, relative to SMW_{LP}. Their mass changes at A point were also significantly lower: SMW_{S1P} reached only about 15% of the mass change of SMW_{LP}, while SMW_{AXP} was about 13%.

In comparison with SMW_{AJP}, both SMW_{S1P} and SMW_{AXP} showed vapor permeability by approximately 27% and 49% lower respectively. Intermediate MW formulations exhibited moderate permeability. For example, SMW_{S2P} with $\delta = 1.375 \times 10^{-13}$, and G = 0.010918 g/h, A_{SMS2} =166.8 h with mass change 1.821 g and SMW_{S3P} $\delta = 2.208 \times 10^{-13}$, G = 0.017527 g/h, A_{SMS3} =159.1 h with mass change = 2.788 g at displayed permeability properties representing about 63–40% of SMW_{LP}.

Their mass change values at the A point were reduced by 63–74% compared with SMW_{LP}, confirming partial but controlled vapor transmission. By contrast, the higher MW

systems, such as SMW_{S4P} $\delta = 3.163 \times 10^{-13}$, G = 0.025111 g/h, A_{SMS4}= 153.7 h with mass change = 3.859 g and SMW_{S5P} $\delta = 4.998 \times 10^{-13}$, G = 0.039675 g/h, A_{SMS5} = 140.8 h with mass change 5.586 g, showed a significant increase in permeability capacity relative to SMW_{LP}. Specifically, SMW_{S5P} exhibited ~35% higher permeability, whereas SMW_{S4P} was about 14% lower than the water vapor permeability of SMW_{LP}. However, both SMW_{S4p} and SMW_{S5p} developed cracking during testing, attributed to strain concentrations along the adhesive layer. Overall, low-MW systems like S1 acted as strong vapor barriers comparable to SMW_{AJP} and SMW_{AXP} while high-MW systems like S4, S5 allowed excessive permeability. The intermediate formulations like S2, S3, however, proved the most suitable for SMW_{AJ}, offering a balanced molecular weight that a diffusion capacity near to lasure.

Intermediate MW polyol formulation S3 allowed moderate permeability. This provided partial permeability while maintaining noticeable restrictions relative to the lasure coated samples, thus in case of SMW wood the most convenient MW of the selected polyols would be series S3 from point of view of diffusion

Although the steady- and pre-steady diffusion parameters, G and δ indicate differences between coated and uncoated samples, their slope-based nature limits their ability to fully reflect the actual blocking efficiency of the adhesive layers. Since permeability is calculated as a mass change per unit time, a large mass increase over a long period may numerically resemble a small mass increase over a shorter period, leading to comparable rate values despite fundamentally different diffusion behaviors. This effect becomes evident when comparing the steady-to-pre-steady ratios of the uncoated SMW and SMW_L, which appear proportionally similar, although their total accumulated masses differ substantially. For example, at the transition point A, the y_A coordinate of SMW_{NS} reached 11.36 g, whereas SMW_{AJS} reached only 1.05 g and SMW_{AXS} 0.95 g, corresponding to an absolute difference of approximately 10.3–10.4 g. Such a large disparity directly reflects the strong vapor-blocking action of the adhesive layer. In contrast, when evaluating the late-stage slope between 350–400 h (Δm/50 h), the calculated rate values for S1–S5 and AX become relatively close, which does not proportionally represent their markedly different accumulated mass levels. This confirms that slope-derived parameters alone cannot adequately describe the hindering or promoting effect of adhesive systems. Therefore, the y_A coordinate of point A, representing the total mass uptake at the diffusion transition, provides a more physically meaningful and sensitive indicator for assessing adhesive-induced diffusion blocking, in case of SMW also.

3.1.6. Water vapor diffusion of eucalyptus (EUW) *(Eucalyptus camaldulensis)*

The water vapor diffusion of eucalyptus wood samples was found to follow a function of the generalized form:

$$\Delta m = b_1 * \tanh(b_0 * t) \qquad [g] \qquad \ldots (Equation\ 9)$$

where :

b0,b1 : coefficients depend on the MW of the adhesive and coating material type (Table 3-6)

t : time in hours

The water vapor permeability behavior in EUW, similar to that of another wood species, displayed two consecutive regions: a pre-steady segment and a steady zone, allowing determination of the slope of the mass change, the transition point, the water vapor flow rate, and other diffusion parameters.

3.1.6.1. Evaluation of water vapor diffusion for EUW in the steady zone

As presented at Fig 3.11, 3.12 and according to ASTM E96/95 and ISO 12572 the a direct comparison between EUW_{NS} and EUW_{AJS} in the steady-state zone highlights the hindering effect of commercial adhesive. The water vapor permeability were $\delta = 2.623191 \times 10^{-14}$ kg/(m·s·Pa) for EUW_{NS} and $\delta = 0.325575 \times 10^{-14}$ kg/(m·s·Pa) for EUW_{AJS}. Likewise, the water vapor flow rate for EUW_{NS} was eight times higher than that of EUW_{AJS}. This indicates that, although the adhesive-coated sample EUW_{AJS} reached steady state earlier at 150.8 h with a lower mass-change rate, the uncoated EUW_{NS} required 211 h to stabilize. These results confirm the adhesive layer's strong vapor-barrier effect.

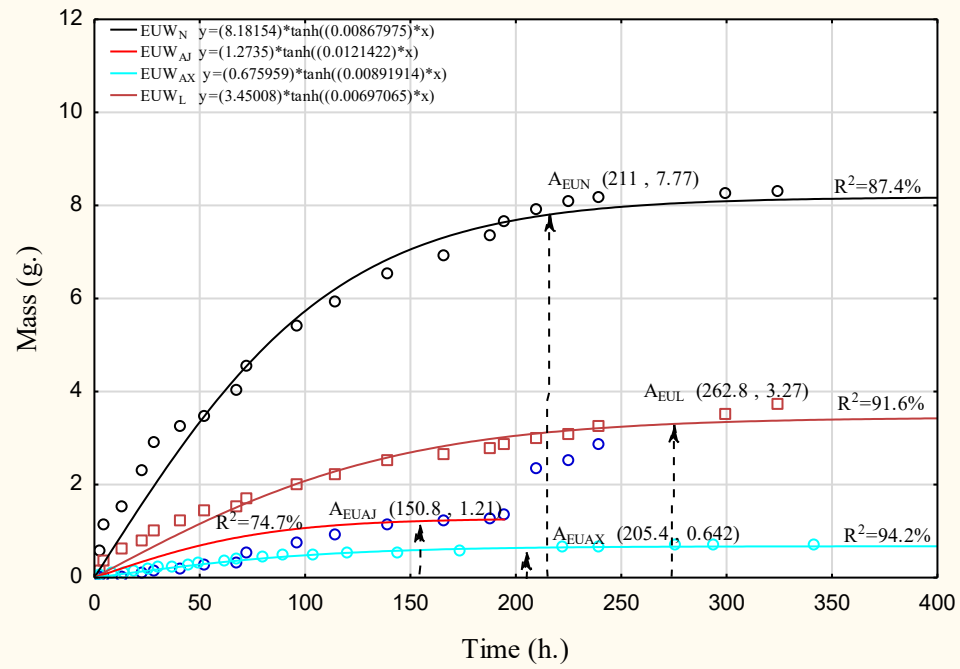

Figure 3.11 The mass change over time for EUW_N, EUWL, EUW_{AJ} and EUW_{AX}

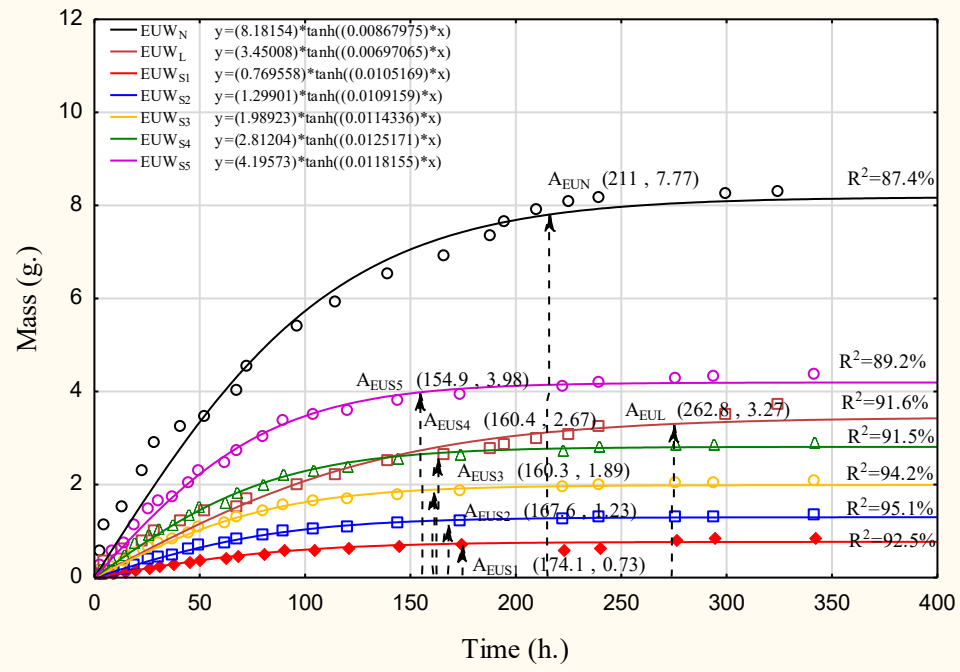

Figure 3.12 The mass change over time for EUW_L, EUW_{S1}, EUW_{S2}, EUW_{S3}, EUW_{S4}, and EUW_{S5}

Although EUW_{AJS} ultimately achieved steady-state conditions according to the standards, its mass-change reflected by the y-coordinate of transition point remained lower than that of EUW_{NS}. This comparison clearly demonstrates the adhesive material's blocking effect on vapor diffusion.

Unlike the adhesive layer, the lasure coating permits partial water vapor permeability, for EUW_{LS}, the water vapor permeability was δ= 1.345056 × 10^{-14} kg/(m·s·Pa), with G = 0.001068 g/h. The x-coordinate of transition point "A" was equal with 262.8 h. This value represents approximately half the water vapor permeability of EUW_{NS} and more than four times the water vapor permeability of EUW_{AJS}. Furthermore, EUW_{LS} required a longer period to reach steady-state diffusion compared to both EUW_{NS} and EUW_{AJS}. These results indicate that, while lasure coating slows down the stabilization process, it still allows partial vapor diffusion, leading to a lower mass increase by water vapor at the same time compared to the uncoated sample.

Table 3-6 Water vapor permeability of eucalyptus (EUW)

Sample	b0	b1	x_A(h)	y_A (g)	G (g/h.)	W * 10^{-12} kg/(m^2·s·Pa)	δ *10^{-14} kg/(m·s·Pa)
EUW_{NS}	0.008680	8.181540	211.0	7.772	0.002082	2.623191	2.623191
EUW_{NP}					0.036835	46.40372	46.40372
EUW_{AJS}	0.012100	1.273500	150.8	1.209	0.000258	0.325575	0.325575
EUW_{AJP}					0.008017	10.09933	10.09933
EUW_{AXS}	0.008920	0.675959	205.4	0.642	0.000168	0.211670	0.211670
EUW_{AXP}					0.003127	3.93868	3.93868
EUW_{LS}	0.006970	3.450080	262.8	3.278	0.001068	1.345056	1.345056
EUW_{LP}					0.012472	15.71139	15.71139
EUW_{S5S}	0.011820	4.195730	154.9	3.986	0.000855	1.076704	1.076704
EUW_{S5P}					0.025730	32.41389	32.41389
EUW_{S4S}	0.011420	2.812040	160.4	2.671	0.000584	0.736089	0.736089
EUW_{S4P}					0.016655	20.98119	20.98119
EUW_{S3S}	0.011430	1.989230	160.3	1.889	0.000413	0.520039	0.520039
EUW_{S3P}					0.011789	14.852	14.852
EUW_{S2S}	0.010920	1.299010	167.7	1.234	0.000278	0.350305	0.350305
EUW_{S2P}					0.007358	9.26981	9.26981
EUW_{S1S}	0.010520	0.769558	174.1	0.731	0.000169	0.212783	0.212783
EUW_{S1P}					0.004199	5.289871	5.289871

The different MW custom-made synthesized polymers with EUW samples S1-S5 revealed distinct differences in steady-state water vapor diffusion, strongly influenced by the molecular characteristics of the applied polyol systems.

Low-permeability adhesives EUW_{S1S} δ = 0.213 × 10^{-14} kg/(m·s·Pa), G = 0.000169 g/h and EUW_{AXS} δ = 0.212 × 10^{-14}, G = 0.000168 g/h, demonstrated pronounced vapor-blocking behavior. Their values approached those of EUW_{AJS} δ = 0.326 × 10^{-14}, G = 0.000258 g/h, confirming a strong similarity to the commercial adhesive's barrier capacity.

Intermediate-permeability adhesives, such as EUW_{S2S} with δ = 0.350 × 10^{-14}, and G = 0.000278 g/h, and EUW_{S3S} with δ = 0.520 × 10^{-14}, and G = 0.000413 g/h, allowed partial diffusion, with stabilization occurring between 160 and 168 h. These values remained lower than those of EUW_{LS} δ = 1.345 × 10^{-14}, G = 0.001068 g/h, and the transition point at 262.8 h

but demonstrated a clear semi-permeable effect. On the other hand, the EUW_{S4S} with $\delta = 0.736 \times 10^{-14}$, G = 0.000584 g/h and EUW_{S5S} had $\delta = 1.077 \times 10^{-14}$, G = 0.000855 g/h showed diffusion behavior approaching the lasure-coated sample EUW_{LS}. In particular, EUW_{S5S} displayed values nearly identical to EUW_{LS}, with a stabilization time of 154.9 h compared to 262.8 h for lasure, suggesting efficient but earlier equilibrium. A one-way ANOVA performed on the steady-state permeability coefficients δ (n = 5 per group) revealed a statistically significant difference among the EUW coated material ($F(6, 28) \approx 47.2$, $p < 0.001$). Overall, the EUW series confirmed the same trend observed in other species: Low-diffusion systems like S1 and EUW_{AXS} act as strong vapor barriers, comparable to EUW_{AJS}.

Intermediate MW formulation like S2 and S3: provide controlled partial diffusion. Higher MW polyols with hugher diffusion, like S4, S5: closely replicate the semi-permeable behavior of EUW_{LS}, with S5 in particular showing nearly equivalent δ and G values but stabilizing earlier. These results underline that adhesive molecular design significantly governs the diffusion pathway, determining whether the system behaves as a vapor-blocking, semi-permeable, or diffusion-permitting barrier.

3.1.6.2.Evaluation of water vapor diffusion for EUW in the pre-steady zone

For EUW_{NP}, the water vapor permeability and flow rate reached $\delta = 4.64 \times 10^{-13}$ kg/(m·s·Pa) and G = 0.036835 g/h, respectively, representing the baseline vapor diffusion capacity of this wood species. The mass change at point G_{EUN} was 7.772 g. within 211 h. In contrast, the commercial adhesive-coated EUW_{AJP} sample exhibited a markedly reduced diffusion performance, with $\delta = 1.01 \times 10^{-13}$ kg/(m·s·Pa) and G = 0.008017 g/h. This corresponds to nearly an 80% reduction in permeability to EUW_{NP}. The earlier stabilization at point A_{EUAJ} = 150.8 h and the mass change at this point = 1.21 g of EUW_{AJP} confirms that the adhesive layer significantly restricted the number of effective diffusion pathways, resulting in rapid saturation and premature diffusion into the steady zone. Such behavior mirrors the strong vapor-blocking capacity observed for commercial adhesive-coated samples compared with EUW_{NP}.

The EUW_{LP} demonstrated partial water vapor diffusion behavior. Its water vapor permeability and flow rate were $\delta = 1.57 \times 10^{-13}$ kg/(m·s·Pa) and G = 0.012472 g/h, respectively. Relative to EUW_{NP}, diffusion was reduced by approximately 66%, indicating that the lasure coatings, which allow vapor diffusion, permit partial diffusion through the micro-porous structure of the film, and it is affected by the type of wood species. This partial diffusion

delayed the transition time from pre-steady to steady zone compared to EUW_{AJP}, extending the pre-steady state and allowing gradual vapor diffusion. These results confirm that the EUW_{NP} represents the natural baseline of high vapor diffusion through the coating materials, and EUW_{AJP} strongly restricts vapor diffusion, producing rapid stabilization but at the cost of strain accumulation at the adhesive wood interface. Beyond the commercial adhesive and lasure coatings, the diffusion behavior of EUW coated with structural adhesives of different polyol molecular weights Series 1–5, exhibited distinct performance patterns within the pre-steady zone.

The low-MW systems EUW_{S1P} and EUW_{AXP} showed the strongest vapor-blocking effects. For EUW_{S1P}, the water vapor water vapor permeability and flow rate were $\delta = 0.529 \times 10^{-13}$ kg/(m·s·Pa) and G = 0.004199 g/h, corresponding to an ~66% reduction compared with EUW_{LP}. For EUW_{AXP}, δ and G dropped further to 0.394×10^{-13} kg/(m·s·Pa) and 0.003127 g/h, representing about a 75% reduction relative to EUW_{LP}. The mass change represented by y-coordinate of transition point reflected this blocking effect, with $A_{EUS1} = 0.73$ g at x-coordinate was 174.1 h and $A_{EUAX} = 0.64$ g at x-coordinate was 205.4 h. These results confirm that MW has a direct influence on the blocking capacity of adhesives.

The intermediate MW formulations EUW_{S2P} and EUW_{S3P} allowed moderate vapor permeability. EUW_{S2P} recorded $\delta = 0.927 \times 10^{-13}$ and G = 0.007358 g/h, corresponding to about a 41% reduction compared with EUW_{LP}. EUW_{S3P} displayed $\delta = 1.49 \times 10^{-13}$ and G = 0.011789 g/h, with a reduction of only ~5% relative to EUW_{LP}. The mass change was $A_{EUS2} = 1.234$ g at 167.7 h and $A_{EUS3} = 1.889$ g at 160.3 h. These results suggest that adhesives with MW in this range – which is close to the lasure, used as controil samples - provide stable systems without cracking, maintaining a controlled diffusion pathway that avoids excessive blocking while preserving structural stability.

The higher MW systems like EUW_{S4P} and EUW_{S5P} exhibited a marked increase in permeability compared to the lower MW adhesives. EUW_{S4P} reached $\delta = 2.10 \times 10^{-13}$ and G = 0.016655 g/h, representing only a 55% reduction relative to EUW_{NP}. EUW_{S5P} further increased to $\delta = 3.24 \times 10^{-13}$ and G = 0.025730 g/h, corresponding to just a 30% reduction compared with EUW_{NP}. **The MW polyol formulations S4 and S5 allowed moderate permeability. This provided partial permeability while maintaining noticeable restrictions relative to the lasure coated samples, thus in case of EUW wood the most convenient MW of the selected polyols would be series S4, S5 from point of view of diffusion.** While this higher diffusion may seem beneficial, both EUW_{S4P} and EUW_{S5P} developed micro-cracks during testing. These cracks acted as secondary capillary channels, accelerating vapor penetration and causing

irregular shifts within the pre-steady zone, thereby compromising their reliability as protective coatings.

3.1.7. Water vapor diffusion of oil palm wood (OPW) *(Elaeis guineensis)*

The water vapor diffusion of oil palm wood samples was found to follow a function of the generalized form:

$$\Delta m = b_1 * \tanh(b_0 * t) \qquad [g] \qquad \ldots (Equation\ 9)$$

where :

b0,b1 : coefficients depend on the MW of the adhesive and coating material type (Table 3-7)

t : time in hours

The diffusion parameters for OPW, the slope of the mass change curves, and the water vapor flow rate were determined in a process consisting of two zones: an initial pre-steady and a steady-state zone.

3.1.7.1.Evaluation of water vapor diffusion for OPW in the steady zone

As shown in Table 3.7 and Fig. 3.13 and 3.14 , the steady-state of diffusion emerges only after several days. After reaching the steady-state zone, both diffusion curves became linear, and the water vapor flow rate G could be calculated accurately.

During the steady-state zone, the OPW_{NS} had a water vapor permeability of $\delta = 2.67 \times 10^{-14}$ kg/(Pa·m·s) with a water vapor flow rate G = 0.00212 g/h, while OPW_{AJ} had a water vapor permeability of $\delta = 2.53 \times 10^{-14}$ kg/(Pa·m·s) with a water vapor flow rate G = 0.00201 g/h. It can be noticed that the slope of the two functions in the steady state zone is close to similar, leading to conclusion that both sample types have similar water vapor diffusion behavior. However, this would be a false interpretation of the situation, as in similar exposure conditions, the OPW_{AJS} demonstrated a significantly lower mass change, leading to the conclusion that the adhesive had a considerable water vapor blocking effect, associated with internal strains. The evaluation of G, the water vapor flow rate of the OPW_{AJS} and OPW_{NS} samples led to generalized conclusion that the slope of the steady state zone G is not suitable to express the water vapor blocking effect of an adhesive, since G resulted rather similar, although the adhesive hindered the mass increase so strong that the accumulated strains resulted in the cracking of the custom-made synthesized polymers sample after 102 hours.

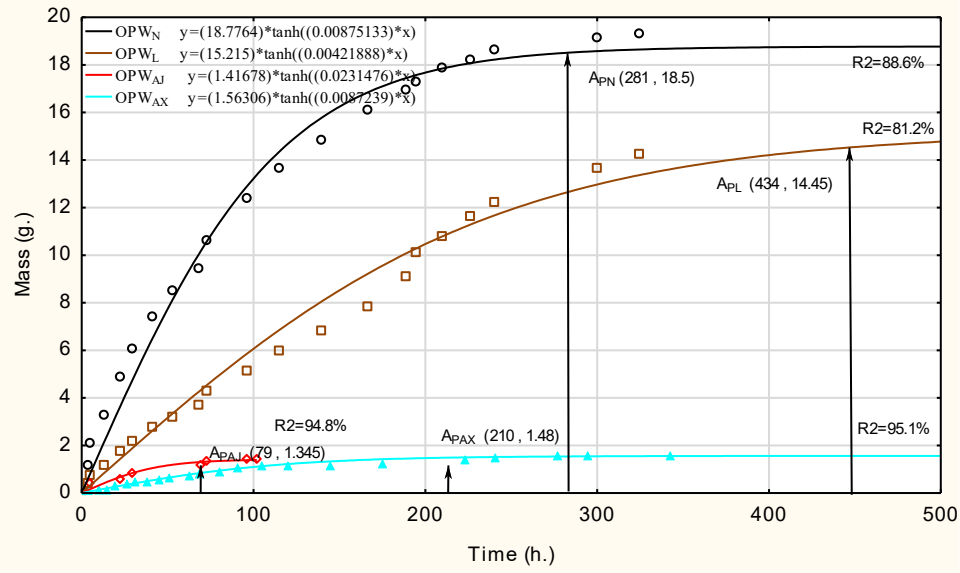

Figure 3.13 The mass change over time for OPW_N, OPW_L, OPW_{AJ}, and OPW_{AX}

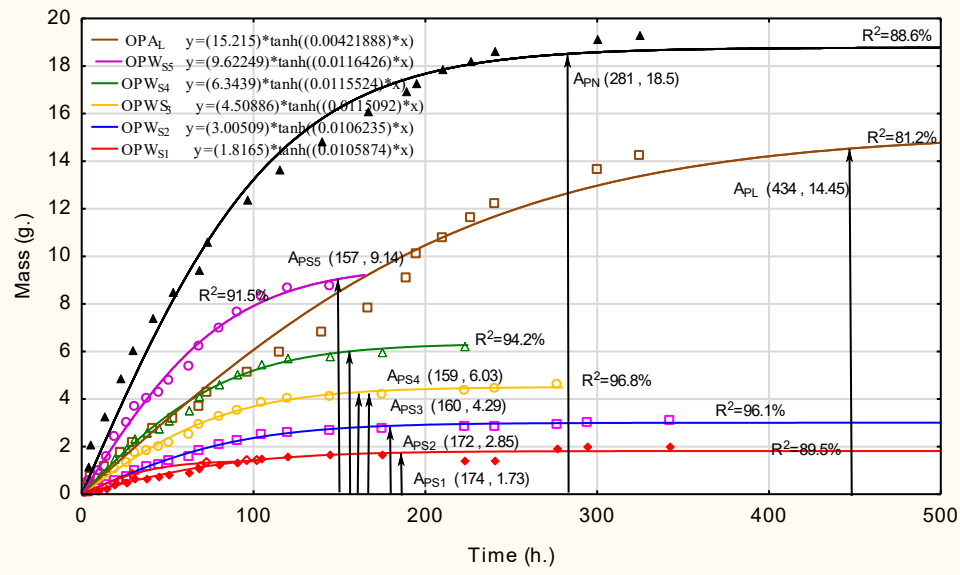

Figure 3.14 The mass change over time for OPW_L, OPW_{S1}, OPW_{S2}, OPW_{S3}, OPW_{S4}, and OPW_{S5}

Table 3-7 Water vapor permeability of oil palm wood (OPW)

Sample	b_1	b_0	x_A(h)	y_A (g)	G (g/h.)	W * 10^{-12} kg/(m²·s·Pa)	δ *10^{-14} kg/(m·s·Pa)
OPW_{NS}	18.7764	0.00875133	281	18.50	0.002127	2.679	2.68
OPW_{NP}					0.065850	82.937	82.94
OPW_{AJS}	1.41678	0.0231476	79	1.345	0.002012	2.535	2.53
OPW_{AJP}					0.017032	21.451	21.45
OPW_{AXS}	1.56306	0.008724	210	1.484	0.000446	0.562	0.56
OPW_{AXP}					0.007071	8.906	8.91
OPW_{LS}	15.215	0.0042188	434	14.45	0.004858	6.119	6.12
OPW_{LP}					0.033302	41.943	41.94
OPW_{S5S}	9.6225	0.011643	157	9.137	0.007784	9.804	9.80
OPW_{S5P}					0.058202	73.305	73.31
OPW_{S4S}	6.3439	0.0115524	159	6.029	0.003703	4.664	4.66
OPW_{S4P}					0.037923	47.764	47.76
OPW_{S3S}	4.50886	0.0115092	160	4.287	0.001614	2.033	2.03
OPW_{S3P}					0.026798	33.752	33.75
OPW_{S2S}	3.00509	0.0106235	172	2.853	0.000736	0.928	0.93
OPW_{S2P}					0.016590	20.895	20.90
OPW_{S1S}	1.8165	0.0105874	174	1.727	0.000436	0.550	0.55
OPW_{S1P}					0.009928	12.504	12.50

On the other hand, OPW_{LS} showed a much higher water vapor flow rate G = 0.004858 g/h and a water vapor permeability of $\delta = 6.12 \times 10^{-14}$ kg/(m·s·Pa), which is more than around 2.3 times higher than that of OPW_N and over 2.4 times higher than OPW_{AJ}. The x-coordinate of transition point for OPW_{LS} was reached after 434 hours, indicating delayed stabilization of the diffusion process. An increased vapor diffusion in case of lasure coated samples versus uncoated ones indicate that the lasure layer even promotes diffusion, probably by its capillary structure. The results confirm that the lasure coating acted as a field of capillaries in top of the natural wood, improving permeability by its capillary forces.

As shown in Fig. 3.14 and Table 3.7, the structural adhesive-coated samples (Series 1–5) exhibited diverse behavior in the steady zone depending on the average molecular weight of the polyol mixture. Generally, lower molecular weight adhesives, such as Series 1 (2000 MW), 2 with 3000 MW, 3 with 4000 MW, 4 with 5000 MW) and AX, demonstrated reduced water vapor permeability compared to the lasure-coated sample OPW_{LS}. Between the experimental adhesives, there was one polyol mixture: S_5, which had a higher, but close to the lasure vapor permeability. OPW_{S5S} showed $\delta = 9.80 \times 10^{-14}$ kg/(m·s·Pa) and G = 0.00778 g/h. This result proves that by adjusting their molecular weight, both theoretically and practically it is possible to find such polymer formulations which have similar water vapor permeability properties like the favorable lasures. There was no significant difference in the water vapor permeability of the uncoated, adhesive-coated, and samples coated with polyol mixture S_3, whilst their mass increase by the time of reaching the steady zone was significantly different based upon t-test.

This leads to the conclusion that the water vapor permeability in the steady zone (as recommended by the standards) is not suitable to express the diffusion blocking effect of the adhesive. These results underscore a clear trend: as the average molecular weight of the polyol mixture is lower than the lasure's or when more impermeable commercial adhesive formulations are used, the coating becomes more effective at blocking water vapor diffusion. These findings illustrate a clear inverse relationship between vapor resistance and the average molecular weight of the tested resins. Lower molecular weights provide better vapor blocking, but at the cost of mechanical strain buildup and premature cracking. Conversely, higher molecular weight systems allow more vapor permeability, reduce internal strain, and perform similarly to semi-vapor permeability coatings like lasure. These results lead to the conclusion that the molecular structure of the structural wood adhesives would need to be adjusted to water vapor permeability.

3.1.7.2.Evaluation of water vapor diffusion for OPW in the pre-steady zone

In order to evaluate the permeability hindering effect of the adhesive attention was accorded to the pre-steady zone, where a significant difference can be observed between specimens containing an adhesive layer and those without. Monitoring this zone, allows the detection of the adhesive's role in impeding water vapor permeability across the bonded layers. The mass change coordinate of the adhesive bonded samples in point A_{PAJ} is equal to Y_{GAJ}= 1.35 g whilst the mass change coordinate of the natural samples in point A_{PN} is equal to Y_{GN}= 18.5 g. The y coordinate of the two sample types indicates that the mass change of the adhesive samples is 13 times lower than the one of the OPW_N, leading to the conclusion that the adhesive applied in the indicated amount causes a 13 time mass increase hindering of the water vapor permeability. After defining the function of water vapor permeability and correctly identifying the transition point "A" the y coordinates of the mass change in the pre-steady zone are suitable to express the water vapor hindering or promoting ability of an adhesive (coating) layer. Whilst the general recommendation of the mentioned standards is suitable for the characterization of the permeability in the steady zone, for the description of the permeability blocking effect of the adhesive, the pre-steady zone was found suitable, based on the current results. As shown in Fig. 3.13 for OPW_{NP}, the mass gain in the pre-steady zone was rapid, indicating unimpeded vapor permeability through the porous wood matrix. In this zone, the water vapor flow rate (calculated based on the slope of the linear drawn from the origin to the transition point) is equal to G 0.06585 g/h, resulting in a water vapor permeability of $\delta = 8.29 \times 10^{-13}$ kg/(Pa·m·s). The samples coated with an adhesive layer manifested a considerably lower mass increase

when exposed to similar environmental conditions; the vapor permeability was significantly hindered. The water vapor flow rate G = 0.01703 g/h and the water vapor permeability $\delta = 2.14 \times 10^{-13}$ kg/(Pa·m·s).

Raises the question whether the G value of the pre-steady zone is suitable to express the blocking effect of the adhesive. Since G, by definition, is the slope of the linear in the steady zone, it can not be interpreted in the pre-steady zone. It was assumed that the mass change till the transition point "A" fairly expresses the blockage by the Y coordinate of point "A" Before reaching the steady-state zone, all specimens exhibited a non-linear water vapor flow rate.

The water vapor flow rate during the pre-steady zone of uncoated OPW_{NP} was G = 0.06585 g/h with water vapor permeability $\delta = 8.29 \times 10^{-13}$ kg/(m·s·Pa) , representing the highest observed value across all samples. This confirms the absence of any barrier layer and the high intrinsic permeability of OPW_{NP}. In contrast, adhesive-coated OPW_{AP} had a lower value of G = 0.002012 g/h. This high difference in the mass increase illustrates the strong blocking effect of the commercial adhesive, which hinders water vapor permeability during early exposure stages. Laser-coated samples showed lower mass increase than the uncoated samples, but higher than the commercial adhesive-coated ones. OPW_{LP} recorded a mass change over time 3.87g a 49.4% difference compared to uncoated OPW_{NP}, but still substantially higher than OPW_{AJP}, confirming that the lasure layer allows partial water vapor permeability without fully obstructing vapor flow. Among the adhesive treated samples, a trend was observed wherein higher molecular weight formulations led to increased vapor permeability, in the pre-steady zone. For instance: OPW_{S5P} samples coated with 6000 MW exhibited water vapor flow rate G = 0.05820 g/h, a difference of only 11.6% compared to OPW_{NP}, indicating minimal blocking effect.

The formulation with the lowest molecular weight OPW_{S1P} (2000 MW) offered the highest vapor permeability resistance in the pre-steady phase, close to the performance of the commercial adhesive. By this it was proven in the pre-steady zone also that the vapor blocking or promoting behavior of an adhesive can be adjusted by adjusting its molecular weight. From a mechanical performance perspective, samples that exhibited low G and δ values in the pre-steady zone such as OPW_{AJS}, OPW_{S1P}, and OPW_{S2P} also experienced early cracking or delamination, with failures occurring at 102 h, 170 h, and 215 h, respectively.

This correlation suggests that strong early blocking effects can result in strain accumulation due to trapped moisture gradients, ultimately compromising structural integrity. In contrast, coatings with higher pre-steady y coordinates (e.g., OPW_{S5P} and OPW_{LP}), delayed failure occurred, or cracking was completely avoided during the test duration, indicating that a moderate vapor transmission (similar to lasures) might be more favorable, in early stages, may

help dissipate internal strains, improving long-term performance. The results emphasize the necessity of targeted action in formulating adhesives (especially for structural applications). While adhesives with molecular weight lower than the one of the lasures) block water vapor permeability, their use may lead to early mechanical failure due to strain buildup. In contrast, adhesives with molecular weight close to the one of the lasures allow for convenient vapor permeability, thus reducing internal strains. The pre-steady zone is particularly critical in assessing the short-term vapor permeability and the blocking effect of adhesive or lasure-coated materials. While traditional standards like ISO 12572 and ASTM E96 are primarily designed to evaluate permeability under steady-state conditions, the pre-steady phase reveals crucial differences in how various coatings respond to initial exposure

3.2. Influence of wood density and adhesive molecular weight on water vapor diffusion

Water vapor diffusion was comprehensively assessed across all investigated wood species by comparing each coated configuration with its corresponding untreated reference sample, thereby enabling a quantitative evaluation of the vapor-blocking efficiency imparted by the different coating adhesive systems. Fig 3.15 and 3.16 illustrate the ratios of water vapor permeability δ_n of uncoated specimens to the corresponding permeabilities of coated systems δS1–δS5, δAJ, δAX, and δL for BW, OW, SW, GPW, SMW, EUW, and OPW. These comparative ratios are presented for both the steady-state and pre-steady zones, enabling a comprehensive assessment of how each adhesive formulation modifies vapor transport behavior under stabilized and early-stage diffusion conditions.

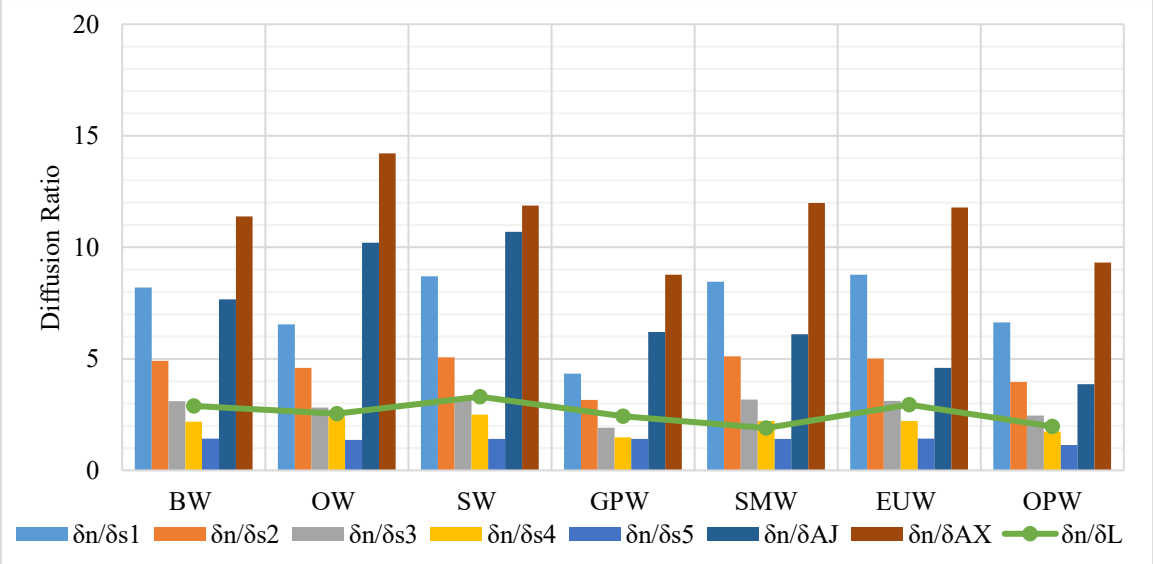

Figure 3.15 Water vapor permeability ratios of uncoated and differently coated wood materials in the pre--steady zone

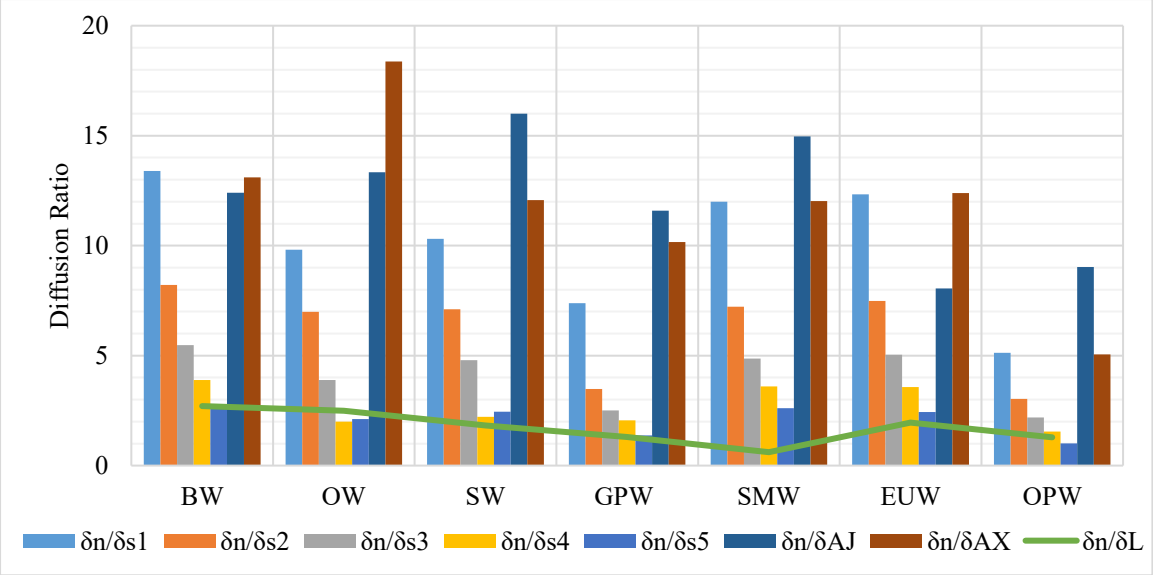

Figure 3.16 Water vapor permeability ratios of uncoated and differently coated wood materials in the steady zone

1- Uncoated wood

As shown in Fig. 3.15 and 3.16, the water vapor permeability values obtained in the pre-steady state exhibit a substantially wider variation between wood species compared with those measured under steady-state conditions. Whereas the steady-state permeabilities of uncoated wood species fall within a relatively narrow and comparable range between 2.62 × 10^{-14} kg/(m·s·Pa) and 3.81 × 10^{-14} kg/(m·s·Pa), the pre-steady permeability coefficients show pronounced differences, extending from 44.46 × 10^{-12} kg/(m²·s·Pa) to 82.94 × 10^{-12} kg/(m²·s·Pa). This wider spread is directly linked to wood density: low-density species like OPW and SMW, with 301.1 kg/m^3 and 379.4 kg/m^3 respectively, exhibited the highest pre-steady-state permeability values, whereas high-density species like BW with 759.9 kg/m^3 and EUW with 952.18 kg/m^3, showed lower steady-state permeability. By doing Pearsons correlation, resulted: $r = -0.933$, $R^2 = 0.871$, $p = 0.002$, a strong and statistically significant negative correlation between wood density and **pre-steady-state** permeability, confirming that lower-density species exhibit substantially higher initial permeability coefficients. While EUW displays a modest departure from the fitted regression line, the overall trend remains robust and statistically significant. The mass change, represented by the y-coordinate of the transition point "A", follows the same trend, further confirming that the pre-steady zone reflects the rapid initial response of the material to water vapor exposure. This phase provides an early and sensitive indication of diffusion behavior, clearly demonstrating the influence of wood density on mass uptake in uncoated wood species.

Unlike pre-steady-state permeability, no significant Pearsons correlation was observed between wood density and **steady-state permeability** ($r = -0.114$, $R^2 = 0.013$, $p = 0.808$), indicating that steady-state vapor transport is essentially independent of density. The correlation is **very weak and negative. Only ~1.3% of the variability in steady-state permeability is explained by density. The relationship is not statistically significant, meaning steady-state permeability is largely independent of wood density.**

When both diffusion zones are evaluated together, it becomes evident that although different wood species exhibit similar behavior under steady-state conditions, the pre-steady region reveals the actual impact of density and anatomical structure on early-stage vapor transport. Consequently, the pre-steady analysis delivers critical insight into diffusion mechanisms that cannot be fully captured by steady-state permeability values alone.

Based on diffusion tests performed on uncoated wood samples from seven wood species, the conclusion was deduced, that **density strongly affects pre-steady diffusion, but not the steady-state permeability behaviour**.

Table 3-8 permeability/mass change within uncoated wood samples

	Density Kg/m^3	δ (steady state) $\times10^{-14}$ kg/(m·s·Pa)	δ (pre-steady zone) $\times10^{-14}$ kg/(m·s·Pa)	Mass change at transition point (g)
OPW	301.1	2.68	82.94	18.5
SMW	379.4	3.72	70.24	11.36
GPW	449.3	3.68	66.10	10.99
SW	511.4	2.93	60.70	9.32
OW	682.1	3.44	55.02	9.74
BW	759.9	3.81	44.46	9.27
EUW	952.18	2.62	46.40	7.77

2- Wood coated with lasure

The wood samples coated with lasure exhibited semi-permeable behavior across all investigated wood species, as illustrated in Fig. 3.15 and 3.16. In each case, the vapor permeability of the lasure-coated specimens remained proportionally related to that of the corresponding uncoated reference, indicating moderated but not fully restricted water vapor diffusion. The wide variation in wood density (301.1–952.18 kg/m^3) makes the steady-state water vapor permeabilities range from 1.34–6.12 $\times10^{-14}$ kg/(m·s·Pa), while the pre-steady-state values range between 15.71–41.94 $\times10^{-14}$ kg/(m·s·Pa) as shown in Table 3.9. These results confirm that lasure partially permits water-vapor permeability compared with the uncoated one. Low-density species OPWand SMW showed the highest δ values and the greatest mass change, due to their structure and larger accessible pore volume, compared with other wood species

used in both zones (pre-steady and steady zones). In contrast, high-density woods like EUW, BW, and OW exhibited lower δ values and minimal mass change, conforming the density effect and the wood internal porosity. The water vapor permeability and the mass change showed an inverse relationship with sample density, and a clear dependence on the structural properties of each wood species.

Table 3-9 Permeability/mass change within lasure coated wood samples

	Density Kg/m^3	δ (steady state) $\times10^{-14}$ kg/(m·s·Pa)	δ (pre-steady zone) $\times10^{-14}$ kg/(m·s·Pa)	Mass change at transition point (g)
OPW	301.1	6.12	41.94	14.45
SMW	379.4	6.09	37.00	7.33
GPW	449.3	2.84	27.23	6.30
SW	511.4	1.60	18.37	3.88
OW	682.1	1.38	21.61	3.87
BW	759.9	1.41	15.41	3.32
EUW	952.18	1.34	15.71	3.27

3- Wood coated with commercial adhesive

The permeability behavior of wood coated with commercial adhesives AJ and AX reveals clear density-dependent patterns as shown in Fig.3.15, 3.16 for example in case of BW and OW. The steady-state water vapor permeabilities remain relatively low between 0.08–0.36 $\times10^{-14}$ kg/(m·s·Pa) for all species as presented in Table 3.10.

Similar to other wood species the mass change at the transition point "A", shows a strong inverse relationship with density: lower-density woods e.g., OPW at 301.1 kg/m³ and SMW at 379.4 kg/m³ exhibited noticeably higher mass change 1.34–1.48 g, whereas denser species such as EUW (952.18 kg/m³) recorded the lowest mass changes (0.59–0.64 g).

A moderate negative correlation was observed between wood density and pre-steady-state permeability across all adhesive coated samples, both with the commercial structural adhesive AJ and the custom made AX, with $r = -0.492$, $R^2 = 0.242$, and $p = 0.074$, suggesting that higher-density species tend to exhibit lower initial permeability. Although not statistically significant at the 0.05 level, the trend indicates that wood density still influences pre-steady vapor diffusion even in the presence of the commercial structural adhesive coatings. The correlation is **moderately negative**, suggesting that higher-density species tend to have lower pre-steady permeability even when coated. R^2 shows that approximately **24% of the variability** in pre-steady permeability is explained by wood density.

These contrasts highlight that permeability behavior cannot be predicted solely from density or wood species type; instead, it emerges from the interaction between wood anatomy,

adhesive permeability, and molecular structure of the adhesive. Consequently, each wood species must be evaluated independently and compared with other adhesive or coating materials, to accurately calculate the difference in permeability within the same wood with different conditions (uncoated / coated)

Table 3-10 Permeability/mass change within wood sample with AJ and AX adhesive

	Density Kg/m^3	δ (steady state) $\times10^{-14}$ kg/(m·s·Pa)	δ (pre-steady zone) $\times10^{-14}$ kg/(m·s·Pa)	Mass change at transition point (g)
SW_{AJ}	511.4	0.08	4.78	0.37
OW_{AX}	682.1	0.18	3.87	0.59
OW_{AJ}	682.1	0.25	5.38	0.60
EUW_{AX}	952.18	0.21	3.93	0.64
BW_{AX}	759.9	0.29	3.90	0.75
SW_{AX}	511.4	0.24	5.11	0.77
BW_{AJ}	759.9	0.31	5.80	0.93
SMW_{AX}	379.4	0.31	5.86	0.94
SMW_{AJ}	379.4	0.24	11.49	1.05
GPW_{AX}	449.3	0.36	7.53	1.15
EUW_{AJ}	952.18	0.32	10.09	1.20
GPW_{AJ}	449.3	0.32	10.64	1.22
OPW_{AJ}	301.1	2.53	21.45	1.34
OPW_{AX}	301.1	0.56	8.91	1.48

4- Wood with custom-made synthesized polymer

A consistent pattern becomes apparent when comparing the permeability behavior in the pre-steady Fig. 3.15; Table 3.11 and steady-state Fig. 3.16; Table 3.12 zones for the investigated wood species coated with custom-made synthesized polymers S1–S5. Despite the systematic control of adhesive formulations, the resulting permeability performance varied significantly among the different wood species. This clearly indicates that the intrinsic characteristics of the wood, particularly density, anatomical structure, and porosity play a decisive role in governing overall vapor transport behavior. Therefore, the final permeability of the adhesive–wood system is not determined solely by the adhesive itself, but rather by the interaction between the adhesive properties and the specific structural features of each wood species. In both the pre-steady and steady-state zones, the water vapor permeability consistently reflected the structural characteristics of the wood. Dense and anatomically compact species, such as EUW (952.18 kg/m³), exhibited the lowest permeability values, whereas highly porous, low-density species, such as OPW (301.1 kg/m³), consistently showed

the highest vapor permeability. Mass change showed an inverse relationship with density: low-density woods accumulated the highest mass change, whereas high-density woods exhibited the lowest mass change even when water vapor permeability were comparable. Within each wood species, water vapor permeability among different MW adhesive systems remained relatively close, yet mass-change values diverged significantly. This again reflects the strong role of density and wood structure properties storage capacity, where lower-density woods consistently absorbed more moisture despite comparable δ values.

Although the steady- and pre-steady diffusion parameters G and δ indicate differences between coated and uncoated samples, their slope-based nature limits their ability to fully reflect the actual blocking efficiency of the adhesive layers. Since permeability is calculated as a mass change per unit time, a large mass increase over a long period may numerically resemble a small mass increase over a shorter period, leading to comparable rate values despite fundamentally different diffusion behaviors. This effect becomes evident when comparing the steady-to-pre-steady ratios of the uncoated and samples coated with lasure, which appear proportionally similar, although their total accumulated masses differ substantially. For example, at the transition point A, the y_A coordinate of SMW_N reached 11.36 g, whereas SMW_{AJS} reached only 1.05 g and SMW_{AXS} 0.95 g, corresponding to an absolute difference of approximately 10.3–10.4 g. Such a large disparity directly reflects the effective vapor-blocking action of the adhesive layer. In contrast, when evaluating the late-stage slope between 350–400 h (Δm/50 h), the calculated rate values for S1–S5 and AX become relatively close, which does not proportionally represent their markedly different accumulated mass levels. This confirms that slope-derived parameters alone cannot adequately describe the hindering or promoting effect of adhesive systems. Therefore, the y_A coordinate of point A, representing the total mass uptake at the diffusion transition, provides a more physically meaningful and sensitive indicator for assessing adhesive-induced diffusion blocking effect.

Table 3-11 Permeability/mass change within a wood sample with a custom-made synthesized polymer at pre steady zone

No.	Type	Density Kg/m^3	δ ×10^{-14} kg/(m·s·Pa)	Mass change at transition point (g)
1	EUW_{S1}	952.18	5.29	0.73
2	BW_{S1}	759.9	5.43	0.87
3	SW_{S1}	511.4	6.98	0.97
4	SMW_{S1}	379.4	8.31	1.10
5	OW_{S1}	682.1	8.40	1.19
6	BW_{S2}	759.9	9.06	1.44
7	EUW_{S2}	952.18	9.27	1.23
8	OW_{S2}	682.1	11.97	1.68

9	SW_{S2}	511.4	11.98	1.51
10	OPW_{S1}	301.1	12.50	1.73
11	SMW_{S2}	379.4	13.75	1.82
12	BW_{S3}	759.9	14.34	2.21
13	EUW_{S3}	952.18	14.85	1.89
14	GPW_{S1}	449.3	15.22	1.86
15	SW_{S3}	511.4	19.30	2.31
16	OW_{S3}	682.1	19.50	2.89
17	BW_{S4}	759.9	20.30	3.12
18	GPW_{S2}	449.3	20.88	3.29
19	OPW_{S2}	301.1	20.90	2.85
20	EUW_{S4}	952.18	20.98	2.67
21	SMW_{S3}	379.4	22.08	2.79
22	OW_{S4}	682.1	22.75	4.46
23	SW_{S4}	511.4	24.32	3.99
24	BW_{S5}	759.9	31.08	4.66
25	SMW_{S4}	379.4	31.63	3.86
26	EUW_{S5}	952.18	32.41	3.99
27	OPW_{S3}	301.1	33.75	4.29
28	GPW_{S3}	449.3	34.60	4.93
29	OW_{S5}	682.1	40.42	5.61
30	SW_{S5}	511.4	43.15	4.73
31	GPW_{S4}	449.3	44.47	6.15
32	GPW_{S5}	449.3	46.63	7.90
33	OPW_{S4}	301.1	47.76	6.03
34	SMW_{S5}	379.4	49.98	5.59
35	OPW_{S5}	301.1	73.31	9.14

Table 3-12 Permeability/mass change within a wood sample with a custom-made synthesized polymer at a steady state zone

No.	Type	Density Kg/m^3	δ $\times 10^{-14}$ kg/(m·s·Pa)	Mass change at transition point (g)
1	EUW_{S1}	952.18	0.21	0.73
2	BW_{S1}	759.9	0.28	0.87
3	BW_{AJ}	759.9	0.31	0.94
4	SW_{S1}	511.4	0.28	0.97
5	OW_{S1}	682.1	0.35	1.19
6	EUW_{S2}	952.18	0.35	1.23
7	BW_{S2}	759.9	0.46	1.44
8	SW_{S2}	511.4	0.41	1.51
9	OW_{S2}	682.1	0.49	1.68
10	OPW_{S1}	301.1	0.55	1.73
11	SMW_{S2}	379.4	0.51	1.82
12	GPW_{S1}	449.3	0.50	1.86
13	EUW_{S3}	952.18	0.52	1.89
14	BW_{S3}	759.9	0.70	2.21
15	SW_{S3}	511.4	0.61	2.31
16	EUW_{S4}	952.18	0.74	2.67
17	SMW_{S3S}	379.4	0.77	2.79
18	OPW_{S2}	301.1	0.93	2.85
19	OW_{S3}	682.1	0.88	2.89
20	BW_{S4}	759.9	0.98	3.12

21	GPW_{S2}	449.3	1.06	3.29
22	SMW_{S4}	379.4	1.04	3.86
23	EUW_{S5}	952.18	1.08	3.99
24	SW_{S4}	511.4	1.32	3.99
25	OPW_{S3}	301.1	2.03	4.29
26	OW_{S4}	682.1	1.73	4.46
27	BW_{S5}	759.9	1.44	4.66
28	SW_{S5}	511.4	1.20	4.73
29	GPW_{S3}	449.3	1.47	4.93
30	SMW_{S5}	379.4	1.43	5.59
31	OW_{S5}	682.1	1.64	5.61
32	OPW_{S4}	301.1	4.66	6.03
33	GPW_{S4}	449.3	1.79	6.15
34	GPW_{S5}	449.3	2.69	7.90
35	OPW_{S5}	301.1	9.80	9.14

Overall conclusion: Based on diffusion tests conducted on uncoated, lasure-coated, and high MW, custom made polyol-coated samples from seven wood species, it was concluded that wood density strongly influences pre-steady-state diffusion, but has little effect on steady-state permeability. Consequently, correlations between density and permeability indicate that the pre-steady zone is the most suitable region for evaluating water vapor diffusion behaviour of adhesives—particularly their barrier or blocking effect—while the steady-state portion of the mass change curve is less informative in this regard.

3.3. Measuring strain behavior

internal strains created by water vapor diffusion through wood surfaces with and without adhesive were evaluated in an accelerated experiment.

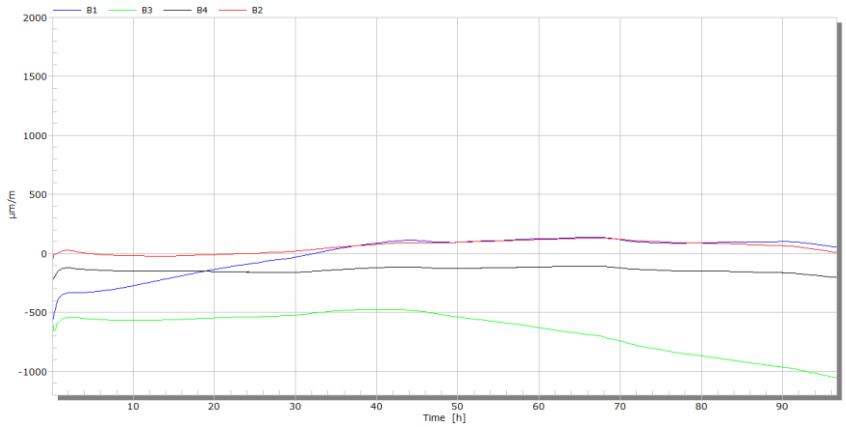

Figure 3.17 Strain caused by water vapor permeability through BW coated with lasure and with/without adhesive

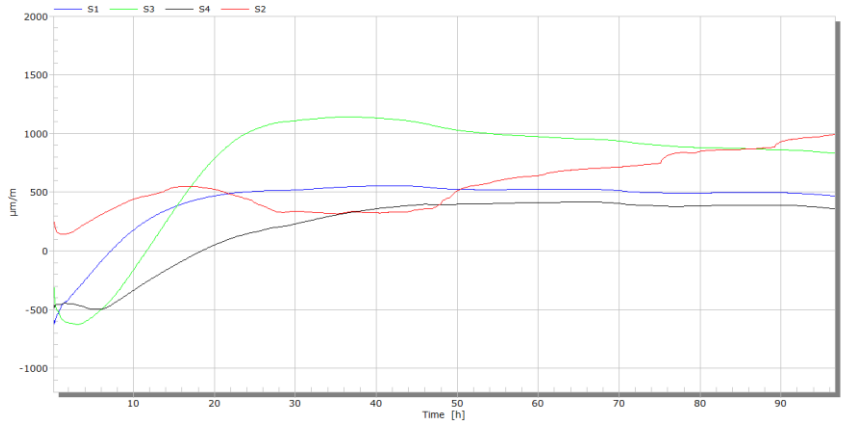

Figure 3.18 Strain caused by water vapor diffusion through SW coated with lasure and with/without adhesive

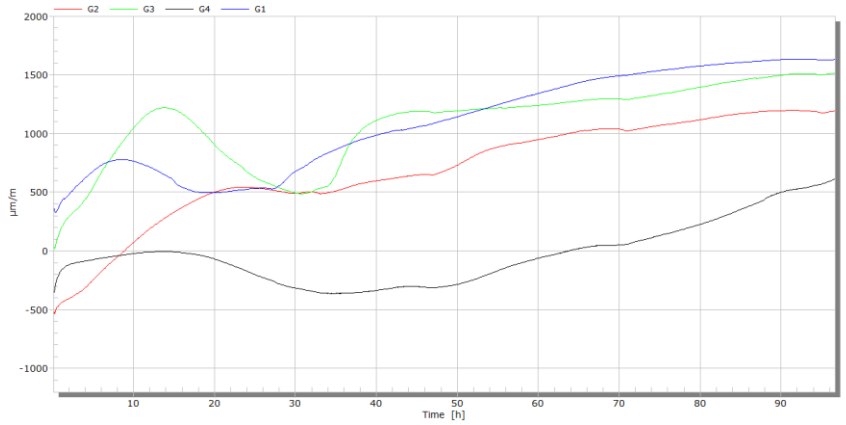

Figure 3.19 Strain caused by water vapor diffusion through GPW coated with lasure and with/without adhesive

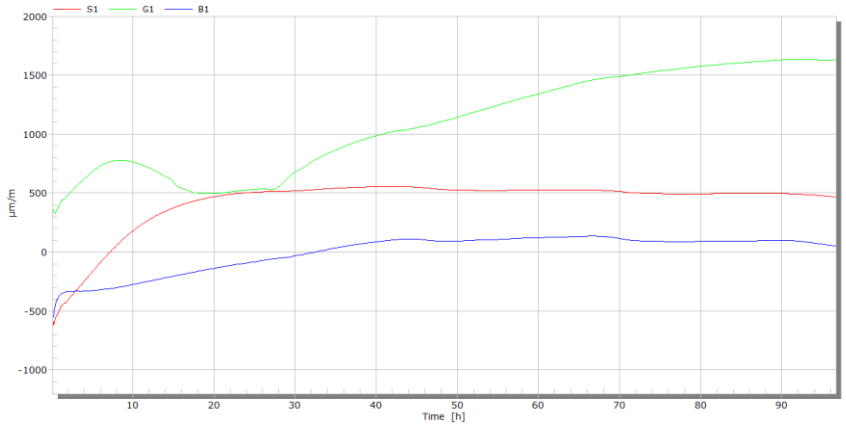

Figure 3.20 Strain caused by water vapor diffusion through BW, SW, and GPW

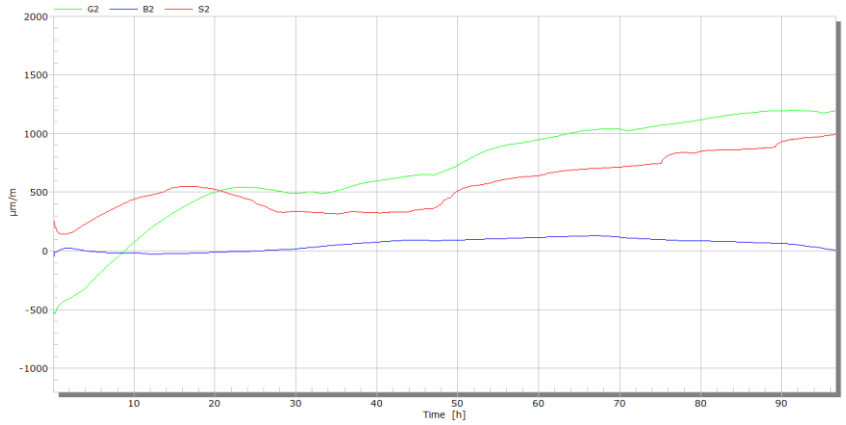

Figure 3.21 Strain caused by water vapr diffusion through BW, SW, and GPW coated with lasure

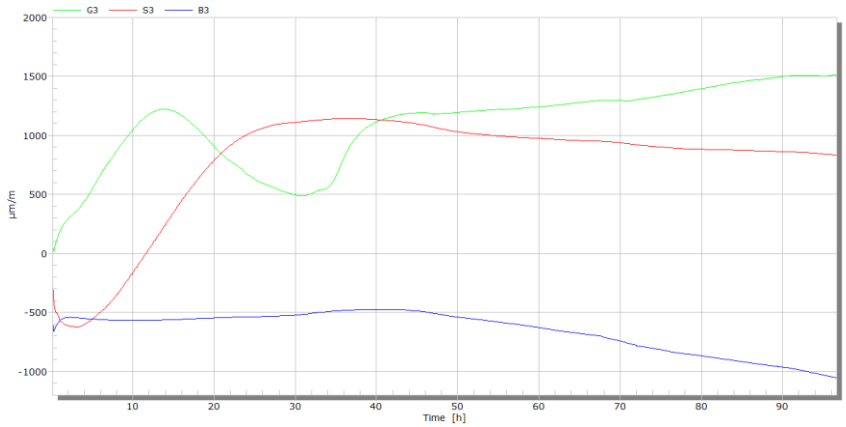

Figure 3.22 Strain caused by water vapor diffusion through BW, SW, and GPW with adhesive

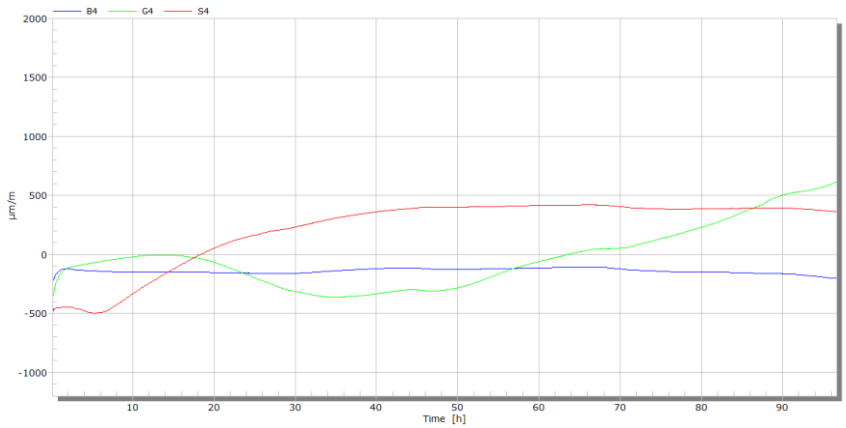

Figure 3.23 Strain caused by water vapor diffusion through BW, SW, and GPW with S5 adhesive formulation

3.3.1. Evaluation of strain of uncoated samples:

Grey Poplar (g1): strain rises sharply to ~700 µm/m at ~12 h, then after a dip continues climbing to ~1,650–1,700 µm/m by 90–95 h. This reflects its low density and high porosity,

which allow fast water uptake and deep moisture diffusion, leading to the highest long-term strains.

Spruce (s1): increases quickly from –600 to ~550 µm/m within 30 h, then stabilizes at a plateau (~500–550 µm/m). Its anatomic structure enables rapid early diffusion but limited total diffusion capacity keeps the final strain moderate.

Beech (b1): shows the slowest and smallest response: from –400 to ~140 µm/m, peaking around 65–70 h, then relaxing slightly (~50 µm/m at 95 h). Its dense, fine structure slows vapor diffusion, resulting in lower overall stress.

Grey poplar develops the largest and most prolonged strains, spruce responds quickly but levels off, and beech remains the least affected . g1 ≫ s1 > b1 in peak strain. This matches the diffusion picture: highly porous, low-density GPW takes up more moisture (large welling/shrinkage), while denser BW equalizes faster through thickness and develops smaller gradients stress.

A strong negative correlation was observed with Pearsons between wood density and maximum strain of **uncoated samples** during moisture diffusion ($r = -0.822$), indicating that lower-density species like Grey Poplar experience higher and faster strains, whereas higher-density species such as Beech exhibit lower and slower strain responses. **$r = -0.822$** showes a strong negative correlation. Higher-density woods like beech, show lower maximum strain; lower-density woods like grey poplar show higher strain. This reflects the influence of anatomical structure on water uptake and diffusion dynamics.

3.3.2. Evaluation of strain of lasure coated samples:

As shown in Fig. 4.17,4.18,4.19, and 4.21 when coated with lasure grey poplar (g2) showed a smooth and continuous increase, reaching ~1,150–1,200 µm/m at 90–95 h. Spruce (s2) followed a similar trend but at a lower level (~950–1,000 µm/m), with a small step at ~70–75 h indicating a two-phase diffusion process. Beech (b2), in contrast, displayed only a minor response, peaking at ~150–180 µm/m around 65–70 h and stabilizing near ~100 µm/m.

Overall, the hierarchy is clear: g2 ≳ s2 ≫ b2. Grey Poplar still shows the largest strains, Spruce intermediate, and Beech minimal. Importantly, all lasure-coated samples display smoother and more stable strain curves than their uncoated counterparts, without sharp drops or irregularities. This stability aligns with the role of lasure as a vapor-open coating. It does not fully block diffusion but reduces liquid water sorption and slows gradient development. As a result, strains build gradually and remain within moderate levels, avoiding the abrupt strain

peaks seen in uncoated wood. Lower-density wood like grey poplar reaches much higher strain than higher-density wood (Beech) when coated with lasure.

For lasure-coated samples, maximum strain exhibited a nearly perfect negative Pearsons correlation with wood density r ≈ −1.00, indicating that lower-density species such as grey poplar develop substantially higher strains compared with higher-density species like beech. Spruce showed intermediate behaviour, consistent with its density, reflecting the strong influence of wood anatomical structure on moisture-induced strain even under coating.

3.3.3. Evaluation of strain of adhesive coated samples:

As shown in Fig. 4.17,4.18,4.19, and 4.22 for wood coated with structural adhesive AJ

Grey poplar (g3) showed a steep early rise, reaching ~1,150–1,250 µm/m at 12–15 h, before dropping sharply to ~350 µm/m at ~28 h, a clear sign of crack formation. Afterwards, strain increased again to ~1,500–1,600 µm/m by 90–95 h. Spruce (s3) reached a peak of ~1,100–1,200 µm/m at 18–22 h, followed by a gradual decline to ~850–900 µm/m. This peak-and-relief profile also indicates crack-induced permeability, where initial blocking drives high strains that later relax once micro-cracks form. Beech (b3) behaved differently, showing a continuous negative drift from ~–400 to ~–1,100 µm/m. This reflects a tension-dominated response: the adhesive strongly restricted diffusion, inducing shrinkage, and subsequent micro-damage maintained a restrained, tension-biased trajectory without the typical swelling peak.

AJ adhesive generated the steepest initial ramps and largest peaks, confirming its strong vapor-blocking effect. In Beech, the adhesive response was dominated by restrained tension rather than swelling.

For samples coated with the structural adhesive AJ, maximum strain exhibited an almost perfect negative Pearsons correlation with wood density (r ≈ −0.998). Lower-density species, such as grey poplar, experienced high positive strains, whereas higher-density beech showed strong negative strains, reflecting differing moisture-induced deformation and crack formation behaviours. Spruce displayed intermediate responses consistent with its density, emphasizing the role of wood anatomical structure in strain development under adhesive treatment.

As shown in Fig. 4.17,4.18,4.19, and 4.23 For wood coated with custom made polyol Series 5, grey poplar (g4) first showed a negative phase (~–600 µm/m at ~35 h) before shifting to a delayed rise, reaching ~650–700 µm/m by 90–95 h. Spruce (s4) followed a similar pattern, rising from ~–500 to ~400–500 µm/m by ~50–60 h, then stabilizing; in extended runs, late

cracking was observed after ~225–275 h. Beech (b4) remained the most stable, fluctuating only around –300 ± 50 μm/m throughout 0–95 h without any cracks.

Both S5 and lasure coatings produced smoother, more gradual strain development compared with AJ. S5 allowed controlled diffusion that avoided the sharp peaks and abrupt strain drops typical of adhesive cracking of AJ.

For wood coated with the custom polyol S5, maximum strain showed an almost perfect negative Pearsons correlation with wood density, as $r \approx -1.00$. Lower-density species show higher positive strain, whereas higher-density species remain relatively stable or negative. Grey poplar developed the highest positive strains, spruce exhibited moderate strain, and beech remained nearly stable with minor negative strains, highlighting the influence of density on diffusion-controlled strain even under smoother, crack-free coatings. Trend indicates that S5 produces **controlled, gradual diffusion** similar to lasures, without the abrupt peaks seen in AJ-coated samples, but strain still scales inversely with density.

In summary: across all treatments, wood density exhibited a strong and consistent influence on moisture-induced strain. For uncoated samples and all coated systems (lasure, AJ and S5), lower-density species such as grey poplar developed substantially higher strains, while higher-density species such as beech showed much lower or even negative strains. Pearson correlation coefficients for all coatings were strongly negative, from $r \approx -0.82$ to -1.00, demonstrating that the inverse relationship between density and strain holds regardless of coating type.

However, the type of coating strongly influenced the **strain dynamics**: uncoated and AJ-coated samples exhibited abrupt peaks and relief phases indicative of rapid water uptake or crack formation, whereas lasure and S5 coatings produced smoother, more gradual strain profiles.

Across all treatments, wood density was the primary factor controlling moisture-induced strain: lower-density species such as Grey Poplar consistently exhibited higher strains, while higher-density species such as Beech showed lower or even negative strains. Pearson correlations for all coatings were strongly negative ($r \approx -0.82$ to -1.00), confirming that this inverse density–strain relationship holds across species regardless of coating.

Coating type, however, strongly modulated the **magnitude and dynamics** of strain. Samples coated with the commercial structural adhesive AJ displayed the highest and most abrupt strain peaks, reflecting rapid water uptake and crack formation. In contrast, lasure and custom polyol S5 coatings produced smoother, more gradual strain profiles with lower peak magnitudes. Uncoated wood exhibited intermediate behavior.

Overall, while coatings determined the **absolute strain level and temporal profile**, the fundamental trend — that strain decreases with increasing wood density — remained consistent. This highlights that pre-steady-state strain is a sensitive and informative indicator of how wood species respond mechanically to moisture, and that coating type primarily affects the **rate and magnitude** of the response rather than the density-driven trend itself.

4. Conclusion and theses

1- Based on the results, it can be concluded that commercial structural adhesives impede water-vapor diffusion through the adhesive layer in bonded wood, creating a vapor-blocking effect that induces internal strains. Diffusion is hindered approximately five times more compared to lasures.

2- Based on diffusion tests conducted on uncoated, lasure-coated, and high MW, custom made polyol-coated samples from seven wood species, it was concluded that wood density strongly influences pre-steady-state diffusion, but has little effect on steady-state permeability. Consequently, correlations between density and permeability indicate that the pre-steady zone is the most suitable region for evaluating water vapor diffusion behaviour of adhesives—particularly their barrier or blocking effect—while the steady-state portion of the mass change curve is less informative in this regard

3- Based on the results the following exponential relation is valid between the density and the permeability is the steady state zone:

$$\delta_{steady}(\rho) \approx 12.31\, e^{-0.00233\,\rho} \text{x } 10^{-14}$$

and in the pre-steady state zone:

$$\delta_{pre\text{-}steady}(\rho) \approx 65.95\, e^{-0.00151\,\rho} \text{x } 10^{-14}$$

4- Based on the results it was proved that the MW of the adhesive is responsible for blocking or supporting the water vapor diffusion. Low-MW adhesive systems (MW≈2000) restrict diffusion due to their compact polymer structure, whereas high-MW formulations (MW 5000–6000) exhibit wider molecular spacing, allowing greater penetration of water vapor or even liquid water. Therefore, controlling the adhesive molecular weight represents an effective approach for regulating vapor diffusion and vapor-diffusion-induced strains in bonded wood structures.

5- The water vapor diffusion of all the tested different wood species with different MW adhesives can be described by the following generalized hyperbolic tangential equation:

$$\Delta m = b_1 * \tanh(b_0 * t) \qquad [\boldsymbol{g}] \qquad R^2 \geq 70\%$$

the b_0 and b_1 are empirical parameters of the mass change function and are both wood species and adhesive MW specific.

6- The pre-steady diffusion zone revealed significant differences in water-vapor diffusion behavior among different wood species and adhesive molecular-weight systems. In contrast, evaluating diffusion solely under steady-state conditions, as specified by ISO 12572 and ASTM E96, may obscure the true vapor-blocking performance of adhesive layers.

Consequently, identifying the (x, y) coordinates of the A-point (transition point) on the diffusion curve provides a more sensitive and reliable parameter for determining whether an adhesive system hinders or facilitates water-vapor diffusion.

7- while coatings determined the **absolute strain level and temporal profile**, the fundamental trend — that strain decreases with increasing wood density — remained consistent. This highlights that pre-steady-state strain is a sensitive and informative indicator of how wood species respond mechanically to moisture, and that coating type primarily affects the **rate and magnitude** of the response rather than the density-driven trend itself

5. Publications

1- **Zinad, Omar saber** and Csiha, Csilla (2024) Review on water vapor diffusion through wood adhesive layer. Journal of the Korean Wood Science and Technology, 52 (4). pp. 301-318. ISSN 1017-0715 (**Q2**)

2- Csiha, C., Hofmann, T., & **Zinad, O. S**. (2025). Investigation into Adhesion of Coatings and Adhesives of Eucalyptus and Grey Poplar for Building Applications. Forests, 16(2), 287. (**Q1**)

3- **Zinad, Omar saber** and Csiha, Csilla (2025). Investigation of Adhesion Properties of Red Eucalyptus Structural Wood in Relation to Its Chemical Composition . Book of abstract of 8th International Conference on Process Technologies for the Forest and Biobased Products Industries 2025 Conference: Kuchl, Austria 2025.09.18. - 2025.09.19. (Salzburg University of Applied Sciences Design and Green Engineering Department Campus Kuchl) : Salzburg University of Applied Sciences Design and Green Engineering Department Campus Kuchl, pp 39.

4- **Zinad, Omar saber** and Csiha, Csilla (2025). Water Vapor Transport Challenges Across Structural Wood Adhesive Layer. Book of abstract of 8th International Conference on Process Technologies for the Forest and Biobased Products Industries 2025 Conference: Kuchl, Austria 2025.09.18. - 2025.09.19. (Salzburg University of Applied Sciences Design and Green Engineering Department Campus Kuchl) : Salzburg University of Applied Sciences Design and Green Engineering Department Campus Kuchl, pp 38

5- **Zinad, O. S.,** & Csiha, C. (2024). Improving sustainability of mortar by wood-ash and Nano-SiO2. Case studies in chemical and environmental engineering, 9, 100597.(**Q1, D1**)

6- **Zinad, Omar Saber ,** Csiha Csilla , Al-Attar Alya'a Abas. Cost Analysis of Sustainable Concrete Production Using Waste Nanoparticles In: társadalom – gazdaság – természet: szinergiák a fenntartható fejlődésben (nemzetközi tudományos konferencia a magyar tudomány ünnepe alkalmából):KONFERENCIAKÖTET, Conference: Sopron, Hungary 2022.11.03-2022.11.03. Sopron: University of Sopron Press, pp 585-593 (2023)

7- **Zinad Omar Saber** ,Csiha Csilla, Zinad Dhafer, Fahem Al-Mamoori Ali (2024). Ecological and Health Implications of Microplastics in Water: A Short Review In: Csiha Csilla (Csiha Csilla Faanyagok felületkezelése és ragasztása) SOE/ FWECI/ Institute of Applied Sciences (eds.) Wood 4 Sustainability : Processing, Construction, Products and Design 2024 Sopron: University of Sopron Press, Soproni Egyetem Faipari Mérnöki és Kreatívipari Kar, pp 121-130

8- **Zinad Omar Saber** , Csilla Csiha. Study on Moisture Diffusion in Structural Adhesives. (2025), Sopron: University of Sopron Press, Language: English | ISBN: 9789633345412 1

9- **Zinad, Omar saber** and Csiha, Csilla (2025). Evaluation of water vapor diffusion of Empress tree hybrid samples with adhesive. Book of abstract of 14. International Conference on Wood Science and Engineering in the Third Millennium (ICWSE 2025) Conference: Transilvania" University of Brasov (Romania), Faculty of Furniture Design and Wood Engineering, and it will be held between 6-8 November 2025, at the Aula of the "Transilvania" University of Brasov

6. Appendix I

Data Sheet about the different MW of Adhesive provide from BorsodChem Com.

Kedves Csilla!

A csomagban lévő minták külön Nektek készültek, a korábbi XP1166 mintánál egyszerűbb összetételben. Kísérleti minták, még nincs BC-s nevük.

A használt MDI komponens kizárólag monomer-MDI, nem tartalmaz magasabb aromás gyűrűszámú oligomert. Remélem az egyszerűbb szerkezet jobban kiadja a kívánt eredményeket.

2 féle poliolt használtunk: 2000-es MW-ű PPG diolt és 6000-es MW-ű PPG triolt. Ezekből készítettünk 12 – 12 % NCO tartalmú prepolimert (mit alap) azután kikevertük a 3, 4, 5000 MW-ű keverékeket is. A PPG diol estében a prepolimer molekulatömege 2500g/ mol = 2000 POL – 2x250 MDI míg a 6000 triol esetében 6000 + 3x250= 6750g/mol.

Az összes minta tartalmaz szabad monomer MDI-t aminek 250 g/mol a tömege.

Ezek alapján az anyagok csak 2 féle típusú molekulákat tartalmaznak: prepolimer és szabad monomer. Remélem ezzel egyszerűbb lesz számolni. Ha látszik valami eltérés, tendencia akkor részletesebben is áttekinthetjük az anyagokat.

Vevői tapasztaltok alapján valószínű, hogy a monomer MDI behatol a pólusokba és ott is reagál a szabad OH csoportokkal vagy a nedvességgel. A hosszabb láncú molekulák természetesen kevésbé mozgékonyak, jobb eséllyel a felszínen „dúsulnak". Erre nem tudok irodalmat javasolni, de ez azelterjedt elmélet.

A lenti táblázat mutatja a keverési arányokat:

	keverési arányok				
2000-es diol	1	3	1	1	0
6000-es triol	0	1	1	3	1
A poliol komponens átlagos MW-e:	2000	3000	4000	5000	6000
A minta száma (az edényen):	1	2	3	4	5

Ha bármi kérdés felmerül igyekszem válaszolni.

Üdv:

Fekete László

BorsodChem, Gödöllő

7. Appendix II

Jowapur®

Liquid one-component polyurethane adhesive for load-bearing structural wood bonding

681.60

Application:
Jowapur® 681.60 is a joint-filling, fibre-reinforced one-component adhesive based on polyurethane. It cures with wood moisture and/or ambient humidity to create a water-insoluble resin, and is used for manufacturing bonded load-bearing timber structures.

Characteristics/ Directions for Use:
Jowapur® 681.60 was tested by the Materials Testing Institute (MPA, Otto-Graf Institut) of the University of Stuttgart, Germany, and classified according to EN 15425:2017 as follows:

Adhesive Type: **EN 15425 – I – 70 – GP – 0.3 – w**

It has been established that Jowapur® 681.60 can be used for the manufacture of bonded load-bearing timber structures according to EN 14080:2013, EN 15497:2014, and EN 16351:2015 made of spruce, fir, or pine wood. In addition, the MPA Stuttgart has also determined the performance characteristics of the adhesive following EN 15416-4/5.

The manufacture of load-bearing timber structures is subject to the specifications in the applicable national and/or European regulations for the manufacture of the corresponding timber structures (e.g. EN 14080, EN 15497, EN 16351, diverse ETA, etc.). Beyond that, the information indicated on this this Technical Data Sheet is to be observed.

Appearance:	beige to yellowish
Density [g/cm³]:	1.15 (Jowat test method)

Our Application Technology Department and our Application Specialists will provide technical data to assist you in your choice of an appropriate product for your requirements. Please observe the information in the section "Remarks".

General bonding requirements:
The properties (e.g. surface tension, plasticiser content…) and the conditioning of the substrates, as well as the processing conditions (e.g. ambient temperature, humidity…) will influence the processes of joining and bonding. Customer tests under consideration of everyday production conditions are therefore absolutely necessary to define stable process parameters and to ensure that the product is fit for purpose. For best bonding results, the materials to be bonded should be free of dust, oil, and grease, and be dry.

Application parameters:

Maximum assembly time:	60 minutes
Minimum pressing time (flat bonding):	100 minutes
Minimum pressing time (fingerjointing):	as specified in the standard
Minimum curing time (fingerjointing):	100 minutes
Maximum joint thickness allowed:	0.3 mm

All values indicated above refer to a processing temperature of 20 °C, humidity of 65 %, and a wood moisture content of 12 %, as well as a perfectly matching joint. For further information concerning the assembly time and the minimum pressing time, please refer to the processing guidelines on pages 3 – 5 of this Technical Data Sheet.

continued on page 2

Jowat Klebstoffe

Specification:

Viscosity at 20 °C [mPas]: (Brookfield, spindle 5, 20 rpm)	15,500 ± 2,500
Solids content [%]: (Jowat test method)	99 ± 1

Storage/ Transport:
The product should remain stored in properly closed original containers, dry and cool (15 – 25 °C). At no time must the adhesive be exposed to temperatures below +5 °C.
For best-before date, please see container label.
After the elapse of the best-before date, it is essential that you again verify that the product is fit for your intended application.

Disposal:
Cured adhesive can undergo disposal with the domestic waste disposal.

Packaging:
Information about packaging types and units is available upon request.

Remarks:
For further information concerning safety, handling, transport and disposal, please refer to the Safety Data Sheet.
The information on this data sheet is based on test results from our laboratories as well as on reported experience gained in the field by our customers. It can, however, not cover all parameters for each specific application and is therefore not binding upon Jowat, nor should it be relied upon in lieu of your own required testing. The information given in this leaflet does not represent a performance guarantee. Unless otherwise agreed with our customers, the values stated in the section "Specification" shall be regarded as the finally agreed upon product properties. No liability may be derived from the information contained herein nor from the information provided by our free technical advisory service.

continued on page 3

8. Appendix III

List of Abbreviations

EWP - engineered wood products

RH - relative humidity

MC - moisture content

CLT - cross-laminated lumber

PUR - polyurethane

PRF - phenol-resorcinol-formaldehyde

PF - phenol formaldehyde

EPI - emulsion polymer with isocyanate

PVA - polyvinyl acetate

MW - molecular weight

AJ - commercial adhesive JOWAPUR 681-60

AX - adhesive XP 1166

ASTM - American society for testing and materials

ISO - international organization for standardization

MDI - methylene diphenyl diisocyanate

PPG - polypropylene glycol

BW - beech wood

OW - oak wood

SW - spruce

OPW - oil palm wood

EUW - eucalyptus

SMW - Smaragdfa ®

GPW- grey-poplar wood

BW_N - uncoated beech wood

A_{BN} - transition point for uncoated beech wood

BW_{NS} - uncoated beech wood in steady zone

BW_{NP} - uncoated beech wood in pre-steady zone

BW_{AJ} - beech wood coated with commercial adhesive JOWAPUR

A_{BAJ} - transition point for beech wood with commercial adhesive JOWAPUR

BW_{AJS} -beech wood coated with commercial adhesive JOWAPUR in steady zone

BW_{AJP} - beech wood coated with commercial adhesive JOWAPUR in pre-steady zone

BW_{AX} - beech wood coated with adhesive XP 1166

A_{BAX} – transition point for beech wood with adhesive XP 1166

BW_{AXS} - beech wood coated with adhesive XP 1166 in steady zone

BW_{AXP} - beech wood coated with adhesive XP 1166 in pre-steady zone

BW_{L} - beech wood coated with lasure

A_{BL} - transition point for beech wood with lasure

BW_{LS} - beech wood coated with lasure in steady zone

BW_{LP} - beech wood coated with lasure in pre-steady zone

BW_{S1} – beech wood coated with custom-made synthesized resins series 1

A_{BS1} – transition point for beech wood coated with custom-made synthesized resins series 1

BW_{S1S} - beech wood coated with custom-made synthesized resins series 1 in steady zone

BW_{S1P} - beech wood coated with custom-made synthesized resins series 1 in pre-steady zone

BW_{S2} - beech wood coated with custom-made synthesized resins series 2

A_{BS2} - transition point for beech wood coated with custom-made synthesized resins series 2

BW_{S2S} - beech wood coated with custom-made synthesized resins series 2 in steady zone

BW_{S2P} - beech wood coated with custom-made synthesized resins series 2 in pre-steady zone

BW_{S3} - beech wood coated with custom-made synthesized resins series 3

A_{BS3} - transition point for beech wood coated with custom-made synthesized resins series 3

BW_{S3S} - beech wood coated with custom-made synthesized resins series 3 in steady zone

BW_{S3P} - beech wood coated with custom-made synthesized resins series 3 in pre-steady zone

BW_{S4} - beech wood coated with custom-made synthesized resins series 4

A_{BS4} -transition point for beech wood coated with custom-made synthesized resins series 4

BW_{S4S} - beech wood coated with custom-made synthesized resins series 4 in steady zone

BW_{S4P} - beech wood coated with custom-made synthesized resins series 4 in pre-steady zone

BW_{S5} - beech wood coated with custom-made synthesized resins series 5

A_{BS5} -transition point for beech wood coated with custom-made synthesized resins series 5

BW_{S5S} - beech wood coated with custom-made synthesized resins series 5 in steady zone

BW_{S5P} - beech wood coated with custom-made synthesized resins series 5 in pre-steady zone

OW_{N} - uncoated oak wood

A_{ON} - transition point for uncoated oak wood

OW_{NS} - uncoated oak wood in steady zone

OW_{NP} - uncoated oak wood in pre-steady zone

OW_{AJ} – oak wood coated with commercial adhesive JOWAPUR

A_{OAJ} - transition point for oak wood with commercial adhesive JOWAPUR

OW_{AJS} – oak wood coated with commercial adhesive JOWAPUR in steady zone

OW_{AJP} – oak wood coated with commercial adhesive JOWAPUR in pre-steady zone

OW_{AX} – oak wood coated with adhesive XP 1166

A_{OAX} – transition point for oak wood with adhesive XP 1166

OW_{AXS} – oak wood coated with adhesive XP 1166 in steady zone

OW_{AXP} – oak wood coated with adhesive XP 1166 in pre-steady zone

OW_{L} – oak wood coated with lasure

A_{OL} - transition point for oak wood with lasure

OW_{LS} – oak wood coated with lasure in steady zone

OW_{LP} – oak wood coated with lasure in pre-steady zone

OW_{S1} – oak wood coated with custom-made synthesized resins series 1

A_{OS1} – transition point for oak wood coated with custom-made synthesized resins series 1

OW_{S1S} – oak wood coated with custom-made synthesized resins series 1 in steady zone

OW_{S1P} – oak wood coated with custom-made synthesized resins series 1 in pre-steady zone

OW_{S2} – oak wood coated with custom-made synthesized resins series 2

A_{OS2} – transition point for oak wood coated with custom-made synthesized resins series 2

OW_{S2S} – oak wood coated with custom-made synthesized resins series 2 in steady zone

OW_{S2P} – oak wood coated with custom-made synthesized resins series 2 in pre-steady zone

OW_{S3} – oak wood coated with custom-made synthesized resins series 3

A_{OS3} – transition point for oak wood coated with custom-made synthesized resins series 3

OW_{S3S} – oak wood coated with custom-made synthesized resins series 3 in steady zone

OW_{S3P} – oak wood coated with custom-made synthesized resins series 3 in pre-steady zone

OW_{S4} – oak wood coated with custom-made synthesized resins series 4

A_{OS4} - transition point for oak wood coated with custom-made synthesized resins series 4

OW_{S4S} – oak wood coated with custom-made synthesized resins series 4 in steady zone

OW_{S4P} – oak wood coated with custom-made synthesized resins series 4 in pre-steady zone

OW_{S5} – oak wood coated with custom-made synthesized resins series 5

A_{OS5} – transition point for oak wood coated with custom-made synthesized resins series 5

OW_{S5S} – oak wood coated with custom-made synthesized resins series 5 in steady zone

OW_{S5P} - oak wood coated with custom-made synthesized resins series 5 in pre-steady zone

SW_{N} - uncoated spruce wood

A_{SN} - transition point for uncoated spruce wood

SW_{NS} - uncoated spruce wood in steady zone

SW_{NP} - uncoated spruce wood in pre-steady zone

SW_{AJ} – spruce wood coated with commercial adhesive JOWAPUR

A_{SAJ} - transition point for spruce wood with commercial adhesive JOWAPUR

SW_{AJS} – spruce wood coated with commercial adhesive JOWAPUR in steady zone

SW_{AJP} – spruce wood coated with commercial adhesive JOWAPUR in pre-steady zone

SW_{AX} – spruce wood coated with adhesive XP 1166

A_{SAX} – transition point for spruce wood with adhesive XP 1166

SW_{AXS} – spruce wood coated with adhesive XP 1166 in steady zone

SW_{AXP} – spruce wood coated with adhesive XP 1166 in pre-steady zone

SW_{L} – spruce wood coated with lasure

A_{SL} - transition point for spruce wood with lasure

SW_{LS} – spruce wood coated with lasure in steady zone

SW_{LP} – spruce wood coated with lasure in pre-steady zone

SW_{S1} – spruce wood coated with custom-made synthesized resins series 1

A_{SS1} – transition point for spruce wood coated with custom-made synthesized resins series 1

SW_{S1S} – spruce wood coated with custom-made synthesized resins series 1 in steady zone

SW_{S1P} – spruce wood coated with custom-made synthesized resins series 1 in pre-steady zone

SW_{S2} – spruce wood coated with custom-made synthesized resins series 2

A_{SS2} – transition point for spruce wood coated with custom-made synthesized resins series 2

SW_{S2S} – spruce wood coated with custom-made synthesized resins series 2 in steady zone

SW_{S2P} – spruce wood coated with custom-made synthesized resins series 2 in pre-steady zone

SW_{S3} – spruce wood coated with custom-made synthesized resins series 3

A_{SS3} – transition point for spruce wood coated with custom-made synthesized resins series 3

SW_{S3S} – spruce wood coated with custom-made synthesized resins series 3 in steady zone

SW_{S3P} – spruce wood coated with custom-made synthesized resins series 3 in pre-steady zone

SW_{S4} – spruce wood coated with custom-made synthesized resins series 4

A_{SS4} - transition point for spruce wood coated with custom-made synthesized resins series 4

SW_{S4S} – spruce wood coated with custom-made synthesized resins series 4 in steady zone

SW_{S4P} – spruce wood coated with custom-made synthesized resins series 4 in pre-steady zone

SW_{S5} – spruce wood coated with custom-made synthesized resins series 5

A_{SS5} – transition point for spruce wood coated with custom-made synthesized resins series 5

SW_{S5S} – spruce wood coated with custom-made synthesized resins series 5 in steady zone

SW_{S5P} - spruce wood coated with custom-made synthesized resins series 5 in pre-steady zone

GPW_{N} - uncoated grey poplar wood

A_{GPN} - transition point for uncoated grey poplar wood

GPW_{NS} - uncoated grey poplar wood in steady zone

GPW_{NP} - uncoated grey poplar wood in pre-steady zone

GPW_{AJ} – grey poplar wood coated with commercial adhesive JOWAPUR

A_{GPAJ} - transition point for grey poplar wood with commercial adhesive JOWAPUR

GPW_{AJS} – grey poplar wood coated with commercial adhesive JOWAPUR in steady zone

GPW_{AJP} – grey poplar wood coated with commercial adhesive JOWAPUR in pre-steady zone

GPW_{AX} – grey poplar wood coated with adhesive XP 1166

A_{GPAX} – transition point for grey poplar wood with adhesive XP 1166

GPW_{AXS} – grey poplar wood coated with adhesive XP 1166 in steady zone

GPW_{AXP} – grey poplar wood coated with adhesive XP 1166 in pre-steady zone

GPW_{L} – grey poplar wood coated with lasure

A_{GPL} - transition point for grey poplar wood with lasure

GPW_{LS} – grey poplar wood coated with lasure in steady zone

GPW_{LP} – grey poplar wood coated with lasure in pre-steady zone

GPW_{S1} – grey poplar wood coated with custom-made synthesized resins series 1

A_{GPS1} – transition point for grey poplar coated with custom-made synthesized resins series 1

GPW_{S1S} – grey poplar coated with custom-made synthesized resins series 1 in steady zone

GPW_{S1P} – grey poplar coated with custom-made synthesized resins series 1 in pre-steady zone

GPW_{S2} – grey poplar coated with custom-made synthesized resins series 2

A_{GPS2} – transition point for grey poplar with custom-made synthesized resins series 2

GPW_{S2S} – grey poplar coated with custom-made synthesized resins series 2 in steady zone

GPW_{S2P} – grey poplar coated with custom-made synthesized resins series 2 in pre-steady zone

GPW_{S3} – grey poplar coated with custom-made synthesized resins series 3

A_{GPS3} – transition point for grey poplar coated with custom-made synthesized resins series 3

GPW_{S3S} – grey poplar coated with custom-made synthesized resins series 3 in steady zone

GPW_{S3P} – grey poplar coated with custom-made synthesized resins series 3 in pre-steady zone

GPW_{S4} – grey poplar coated with custom-made synthesized resins series 4

A_{GPS4} - transition point for grey poplar coated with custom-made synthesized resins series 4

GPW_{S4S} – grey poplar coated with custom-made synthesized resins series 4 in steady zone

GPW_{S4P} – grey poplar coated with custom-made synthesized resins series 4 in pre-steady zone

GPW_{S5} – grey poplar coated with custom-made synthesized resins series 5

A_{GPS5} – transition point for grey poplar coated with custom-made synthesized resins series 5

GPW_{S5S} – grey poplar coated with custom-made synthesized resins series 5 in steady zone

GPW_{S5P} - grey poplar coated with custom-made synthesized resins series 5 in pre-steady zone

SMW_N - uncoated smaragdfa wood

A_{SMN} - transition point for uncoated smaragdfa wood

SMW_{NS} - uncoated smaragdfa wood in steady zone

SMW_{NP} - uncoated smaragdfa wood in pre-steady zone

SMW_{AJ} – smaragdfa wood coated with commercial adhesive JOWAPUR

A_{SMAJ} - transition point for smaragdfa wood with commercial adhesive JOWAPUR

SMW_{AJS} – smaragdfa wood coated with commercial adhesive JOWAPUR in steady zone

SMW_{AJP} – smaragdfa wood coated with commercial adhesive JOWAPUR in pre-steady zone

SMW_{AX} – smaragdfa wood coated with adhesive XP 1166

A_{SMAX} – transition point for smaragdfa wood with adhesive XP 1166

SMW_{AXS} – smaragdfa wood coated with adhesive XP 1166 in steady zone

SMW_{AXP} – smaragdfa wood coated with adhesive XP 1166 in pre-steady zone

SMW_L – smaragdfa wood coated with lasure

A_{SML} - transition point for smaragdfa wood with lasure

SMW_{LS} – smaragdfa wood coated with lasure in steady zone

SMW_{LP} – smaragdfa wood coated with lasure in pre-steady zone

SMW_{S1} – smaragdfa wood coated with custom-made synthesized resins series 1

A_{SMS1} – transition point for smaragdfa coated with custom-made synthesized resins series 1

SMW_{S1S} – smaragdfa coated with custom-made synthesized resins series 1 in steady zone

SMW_{S1P} – smaragdfa coated with custom-made synthesized resins series 1 in pre-steady zone

SMW_{S2} – smaragdfa coated with custom-made synthesized resins series 2

A_{SMS2} – transition point for smaragdfa with custom-made synthesized resins series 2

SMW_{S2S} – smaragdfa coated with custom-made synthesized resins series 2 in steady zone

SMW_{S2P} – smaragdfa coated with custom-made synthesized resins series 2 in pre-steady zone

SMW_{S3} – smaragdfa coated with custom-made synthesized resins series 3

A_{SMS3} – transition point for smaragdfa coated with custom-made synthesized resins series 3

SMW_{S3S} – smaragdfa coated with custom-made synthesized resins series 3 in steady zone

SMW_{S3P} – smaragdfa coated with custom-made synthesized resins series 3 in pre-steady zone

SMW_{S4} – smaragdfa coated with custom-made synthesized resins series 4

A_{SMS4} - transition point for smaragdfa coated with custom-made synthesized resins series 4

SMW_{S4S} – smaragdfa coated with custom-made synthesized resins series 4 in steady zone

SMW_{S4P} – smaragdfa coated with custom-made synthesized resins series 4 in pre-steady zone

SMW_{S5} – smaragdfa coated with custom-made synthesized resins series 5

A_{SMS5} – transition point for smaragdfa coated with custom-made synthesized resins series 5

SMW_{S5S} – smaragdfa coated with custom-made synthesized resins series 5 in steady zone

SMW_{S5P} – smaragdfa coated with custom-made synthesized resins series 5 in pre-steady zone

EUW_N - uncoated eucalyptus wood

A_{EUN} - transition point for uncoated eucalyptus wood

EUW_{NS} - uncoated eucalyptus wood in steady zone

EUW_{NP} - uncoated eucalyptus wood in pre-steady zone

EUW_{AJ} – eucalyptus wood coated with commercial adhesive JOWAPUR

A_{EUAJ} - transition point for eucalyptus wood with commercial adhesive JOWAPUR

EUW_{AJS} – eucalyptus wood coated with commercial adhesive JOWAPUR in steady zone

EUW_{AJP} – eucalyptus wood coated with commercial adhesive JOWAPUR in pre-steady zone

EUW_{AX} – eucalyptus wood coated with adhesive XP 1166

A_{EUAX} – transition point for eucalyptus wood with adhesive XP 1166

EUW_{AXS} – eucalyptus wood coated with adhesive XP 1166 in steady zone

EUW_{AXP} – eucalyptus wood coated with adhesive XP 1166 in pre-steady zone

EUW_L – eucalyptus wood coated with lasure

A_{EUL} - transition point for eucalyptus wood with lasure

EUW_{LS} – eucalyptus wood coated with lasure in steady zone

EUW_{LP} – eucalyptus wood coated with lasure in pre-steady zone

EUW_{S1} – eucalyptus wood coated with custom-made synthesized resins series 1

A_{EUS1} – transition point for eucalyptus coated with custom-made synthesized resins series 1

EUW_{S1S} – eucalyptus coated with custom-made synthesized resins series 1 in steady zone

EUW_{S1P} – eucalyptus coated with custom-made synthesized resins series 1 in pre-steady zone

EUW_{S2} – eucalyptus coated with custom-made synthesized resins series 2

A_{EUS2} – transition point for eucalyptus with custom-made synthesized resins series 2

EUW_{S2S} – eucalyptus coated with custom-made synthesized resins series 2 in steady zone

EUW_{S2P} – eucalyptus coated with custom-made synthesized resins series 2 in pre-steady zone

EUW_{S3} – eucalyptus coated with custom-made synthesized resins series 3

A_{EUS3} – transition point for eucalyptus coated with custom-made synthesized resins series 3

EUW_{S3S} – eucalyptus coated with custom-made synthesized resins series 3 in steady zone

EUW_{S3P} – eucalyptus coated with custom-made synthesized resins series 3 in pre-steady zone

EUW_{S4} – eucalyptus coated with custom-made synthesized resins series 4

A_{EUS4} - transition point for eucalyptus coated with custom-made synthesized resins series 4

EUW_{S4S} – eucalyptus coated with custom-made synthesized resins series 4 in steady zone

EUW_{S4P} – eucalyptus coated with custom-made synthesized resins series 4 in pre-steady zone

EUW_{S5} – eucalyptus coated with custom-made synthesized resins series 5

A_{EUS5} – transition point for eucalyptus coated with custom-made synthesized resins series 5

EUW_{S5S} – eucalyptus coated with custom-made synthesized resins series 5 in steady zone

EUW_{S5P} – eucalyptus coated with custom-made synthesized resins series 5 in pre-steady zone

OPW_N - uncoated oil-palm wood

A_{PN} - transition point for uncoated oil-palm wood

OPW_{NS} - uncoated oil-palm wood in steady zone

OPW_{NP} - uncoated oil-palm wood in pre-steady zone

OPW_{AJ} – oil-palm wood coated with commercial adhesive JOWAPUR

A_{PAJ} - transition point for oil-palm wood with commercial adhesive JOWAPUR

OPW_{AJS} – oil-palm wood coated with commercial adhesive JOWAPUR in steady zone

OPW_{AJP} – oil-palm wood coated with commercial adhesive JOWAPUR in pre-steady zone

OPW_{AX} – oil-palm wood coated with adhesive XP 1166

A_{PAX} – transition point for oil-palm wood with adhesive XP 1166

OPW_{AXS} – oil-palm wood coated with adhesive XP 1166 in steady zone

OPW_{AXP} – oil-palm wood coated with adhesive XP 1166 in pre-steady zone

OPW_L – oil-palm wood coated with lasure

A_{PL} - transition point for oil-palm wood with lasure

OPW_{LS} – oil-palm wood coated with lasure in steady zone

OPW_{LP} – oil-palm wood coated with lasure in pre-steady zone

OPW_{S1} – oil-palm wood coated with custom-made synthesized resins series 1

A_{PS1} – transition point for oil-palm coated with custom-made synthesized resins series 1

OPW_{S1S} – oil-palm coated with custom-made synthesized resins series 1 in steady zone

OPW_{S1P} – oil-palm coated with custom-made synthesized resins series 1 in pre-steady zone

OPW_{S2} – oil-palm coated with custom-made synthesized resins series 2

A_{PS2} – transition point for oil-palm with custom-made synthesized resins series 2

OPW_{S2S} – oil-palm coated with custom-made synthesized resins series 2 in steady zone

OPW_{S2P} – oil-palm coated with custom-made synthesized resins series 2 in pre-steady zone

OPW_{S3} – oil-palm coated with custom-made synthesized resins series 3

A_{PS3} – transition point for oil-palm coated with custom-made synthesized resins series 3

OPW_{S3S} – oil-palm coated with custom-made synthesized resins series 3 in steady zone

OPW_{S3P} – oil-palm coated with custom-made synthesized resins series 3 in pre-steady zone

OPW_{S4} – oil-palm coated with custom-made synthesized resins series 4

A_{PS4} - transition point for oil-palm coated with custom-made synthesized resins series 4

OPW_{S4S} – oil-palm coated with custom-made synthesized resins series 4 in steady zone

OPW_{S4P} – oil-palm coated with custom-made synthesized resins series 4 in pre-steady zone

OPW_{S5} – oil-palm coated with custom-made synthesized resins series 5

A_{PS5} – transition point for oil-palm coated with custom-made synthesized resins series 5

OPW_{S5S} – oil-palm coated with custom-made synthesized resins series 5 in steady zone

OPW_{S5P} –oil-palm coated with custom-made synthesized resins series 5 in pre-steady zone

9. References

Amaral, R. C., Rohden, A. B., Garcez, M. R., & Oliveira Andrade, J. J. de. (2022). Reuse of wood ash from biomass combustion in non-structural concrete: mechanical properties, durability, and eco-efficiency Rafaela. *Journal of Material Cycles and Waste Management*, *24*, 2439–2454`. https://doi.org/https://doi.org/10.1007/s10163-022-01493-8

Arno Frühwald. (2017). Oil Palm Trunk Utilization. *International Academy of Wood Science*, 20.

Athawale, V. D., & Nimbalkar, R. V. (2010). Emulsifyable air drying urethane alkyds. *Progress in Organic Coatings*, *67*(1), 66–71. https://doi.org/10.1016/j.porgcoat.2009.09.017

Bekhta, P., Ortynska, G., & Sedliacik, J. (2015). Properties of Modified Phenol-Formaldehyde Adhesive for Plywood Panels Manufactured from High Moisture Content Veneer. *Drvna Industrija*, *65*(4), 293–301. https://doi.org/10.5552/drind.2014.1350

Bomba, J., Šedivka, P., Böhm, M., & Devera, M. (2014). Influence of Moisture Content on the Bond Strength and Water Resistance of Bonded Wood Joints. *BioResources*, *9*(3), 5208–5218. https://doi.org/10.15376/biores.9.3.5208-5218

Caudullo, G., Tinner, W., & De Rigo, D. (2016). Picea abies in Europe: distribution, habitat, usage and threats. In *European Atlas of Forest Tree Species*. Publications Office of the European Union, Luxembourg.

Chaney, W. R. (2000). Water and chemical movement beneath the bark. *Woodl. Steward*, *9*, 1–5.

Chen, C., Kuang, Y., Zhu, S., Burgert, I., Keplinger, T., Gong, A., Li, T., Berglund, L., Eichhorn, S. J., & Hu, L. (2020). Structure–property–function relationships of natural and engineered wood. *Nature Reviews Materials*, *5*(9), 642–666. https://doi.org/10.1038/s41578-020-0195-z

Cheng, Y., Nolan, G., Holloway, D., Kaur, J., Lee, M., & Chan, A. (2021). Flexural Characteristics of Eucalyptus nitens Timber with High Moisture Content. *Bioresources*, *16*(2), 2921–2936.

Chidambaram, R. (1962). Structure of the Hydrogen-Bonded Water Molecule in Crystals. *The Journal of Chemical Physics*, *36*(9), 2361–2365. https://doi.org/10.1063/1.1732889

Chiniforush, A. A., Akbarnezhad, A., Valipour, H., & Malekmohammadi, S. (2019). Moisture and temperature induced swelling/shrinkage of softwood and hardwood glulam and LVL:

An experimental study. *Construction and Building Materials*, *207*, 70–83. https://doi.org/10.1016/j.conbuildmat.2019.02.114

Chiniforush, A. A., Valipour, H., & Akbarnezhad, A. (2019). Water vapor diffusivity of engineered wood : Effect of temperature and moisture content. *Construction and Building Materials*, *224*, 1040–1055. https://doi.org/10.1016/j.conbuildmat.2019.08.013

Christen, S. (1988). *Wood Water Relations*. Springer Berlin, Heidelberg. https://doi.org/https://doi.org/10.1007/978-3-642-73683-4

Clements-croome, D. (2021). Sustainable intelligent buildings for people : A review. *Intelligent Buildings International ISSN:*, *8975*(2011), 67–86. https://doi.org/10.1080/17508975.2011.582313

Csiha, C., & Gurau, L. (2011). Study on the influence of surface roughness on the adhesion of water based PVAC. *Proceedings of International Conference "Wood Science and Engineering", Brasov, Romania*, 411–419.

Csiha, C., Hofmann, T., & Zinad, O. S. (2025). Investigation into Adhesion of Coatings and Adhesives of Eucalyptus and Grey Poplar for Building Applications. *Forests*, *16*(2), 1–14. https://doi.org/10.3390/f16020287

De Meijer, M., & Militz, H. (2000). Moisture transport in coated wood. Part 1: Analysis of sorption rates and moisture content profiles in spruce during liquid water uptake. *Holz Als Roh - Und Werkstoff*, *58*(5), 354–362. https://doi.org/10.1007/s001070050445

Dietsch, P., Franke, S., Franke, B., Gamper, A., & Winter, S. (2015). Methods to determine wood moisture content and their applicability in monitoring concepts. *Journal of Civil Structural Health Monitoring*, *5*(2), 115–127. https://doi.org/10.1007/s13349-014-0082-7

Elkhal, M., Hakam, A., Ez-Zahraouy, H., Hader, A., Tanasehte, M., & Ziani, M. (2022). Mechanical and physical properties of the date palm stem (Phoenix dactylifera L.) in Morocco. *European Journal of Wood and Wood Products*, *80*(3), 693–703.

Fick, A. (1855). On liquid diffusion. *The London, Edinburgh, and Dublin Philosophical Magazine and Journal of Science*, *10*(63), 30–39. https://doi.org/10.1080/14786445508641925

Franke, B., Franke, S., Schiere, M., & Müller, A. (2016). Moisture diffusion in wood - Experimental and numerical investigations. *World Conference on Timber Engineering - WCTEAt: Vienna, AustriaVolume*.

Galka, B., Labaz, B., Bogacz, A., Bojko, O., & Kabala, C. (2014). Conversion of Norway spruce forests will reduce organic carbon pools in the mountain soils of SW Poland. *Geoderma*, *213*, 287–295. https://doi.org/10.1016/j.geoderma.2013.08.029

Ganne-Chedeville, C., Jaaskelainen, A.-S., & , Julien Froidevaux, Mark Hughes, and P. N. (2012). Natural and artificial ageing of spruce wood as observed by FTIR-ATR and UVRR spectroscopy. *Holzforschung*, *66*, 163–170. https://doi.org/10.1515/HF.2011.148

García-Pacios, V., Jofre-Reche, J. A., Costa, V., Colera, M., & Martín-Martínez, J. M. (2013). Coatings prepared from waterborne polyurethane dispersions obtained with polycarbonates of 1,6-hexanediol of different molecular weights. *Progress in Organic Coatings*, *76*(10), 1484–1493. https://doi.org/10.1016/j.porgcoat.2013.06.005

Gardner, D. J. (2018). part 1 : Theories and Mechanisms of Adhesion. In A. P. and K. L. Mittal (Ed.), *Handbook of Adhesive Technology Third Edition* (pp. 3–15). Taylor & Francis.

George, B., Suttie, E., Merlin, A., & Deglise, X. (2005). Photodegradation and photostabilisation of wood - The state of the art. *Polymer Degradation and Stability*, *88*(2), 268–274. https://doi.org/10.1016/j.polymdegradstab.2004.10.018

Gereke, T. (2009). Moisture-induced stresses in cross-laminated wood panels (Doctoral thesis). In *DISS. ETH No. 18427. Department of Civil, Environmental and Geomatic Engineering, ETH Zurich* (Number 18427). University of Leipzig.

Gledhill, R. A., & Kinloch, A. J. (1974). Environmental Failure of Structural Adhesive Joints. *The Journal of Adhesion*, *6*(4), 315–330. https://doi.org/10.1080/00218467408075035

Guindeira, M., Santos, A., & Fernandes, E. O. (2005). Experimental studies on diffusion coefficients of volatile organic compounds for building materials. *Proceedings of the 10 Th International Conference on Indoor Air Quality and Climate*, 1974–2005.

Gunesoglu, S., Cerci, E., & Topalbekiroglu, M. (2017). The improved breathability of polyurethane coated cotton fabric via micro-cracking. *Journal of the Textile Institute*, *108*(10), 1815–1821. https://doi.org/10.1080/00405000.2017.1292647

Gustavsson, L., Madlener, R., Hoen, H. F., Jungmeier, G., Karjalainen, T., Klöhn, S., Mahapatra, K., Pohjola, J., Solberg, B., & Spelter, H. (2006). The role of wood material for greenhouse gas mitigation. *Mitigation and Adaptation Strategies for Global Change*, *11*(5–6), 1097–1127. https://doi.org/10.1007/s11027-006-9035-8

H. K. Burr & A. J. Stamm. (1946). Diffusion In Wood. In *The Journal of physical chemistry* (Vol. 51, Number 1, pp. 240–261). https://doi.org/https://doi.org/10.1021/j150451a019

Han, Y., Yan, X., & Tao, Y. (2022). Effect of Transparent, Purple, and Yellow Shellac Microcapsules on Properties of the Coating on Paraberlinia bifoliolata Surface. *Polymers*, *14*(16). https://doi.org/10.3390/polym14163304

Heinrich, L. A. (2019). Future opportunities for bio-based adhesives-advantages beyond renewability. *Green Chemistry*, *21*(8), 1866–1888. https://doi.org/10.1039/c8gc03746a

Herbst, MARK D., A., & Goldstein, J. H. (1989). A review of water diffusion measurement by NMR in human red blood cells. *American Journal of Physiology-Cell Physiology*, *256*(5), 1097–1104.

Heshmati, M., Haghani, R., & Al-Emrani, M. (2016). Effects of moisture on the long-term performance of adhesively bonded FRP/steel joints used in bridges. *Composites Part B: Engineering*, *92*, 447–462. https://doi.org/10.1016/j.compositesb.2016.02.021

Hofstetter, K., Hinterstoisser, B., & Salme, L. (2006). Moisture uptake in native cellulose – the roles of different hydrogen bonds : a dynamic FT-IR study using Deuterium exchange. *Cellulose*, *13*, 131–145. https://doi.org/10.1007/s10570-006-9055-2

Huacuja-Sánchez, J. E., Müller, K., & Possart, W. (2016). Water diffusion in a crosslinked polyether-based polyurethane adhesive. *International Journal of Adhesion and Adhesives*, *66*, 167–175. https://doi.org/10.1016/j.ijadhadh.2016.01.005

Huang, N., Yan, X., & Han, Y. (2022). Preparation of Melamine-Formaldehyde Resin/Rice Husk Powder Coated Epoxy Resin Microcapsules and Effects of Different Microcapsule Contents on the Properties of Waterborne Coatings on Tilia europaea Surface. *Coatings*, *12*(8). https://doi.org/10.3390/coatings12081213

Hwang, S. W., Chung, H., Lee, T., Ahn, K. S., Pang, S. J., Bang, J., Kwak, H. W., Oh, J. K., & Yeo, H. (2022). Monitoring of Moisture and Dimensional Behaviors of Nail-Laminated Timber (NLT)-Concrete Slab Exposed to Outdoor Air. *Journal of the Korean Wood Science and Technology*, *50*(5), 301–314. https://doi.org/10.5658/WOOD.2022.50.5.301

ISO 12572-1. (2016). *Hygrothermal performance of building materials and products -- Determination of water vapour transmission properties -- Cup method* (Vol. 2016). European Committee for Standardization.

István, K. M., Csilla, C., & Miklós, B. (2023). *A smaragdfa ablakgyártás céljára való alkalmasságának vizsgálata* [University of sopron]. http://diploma.uni-sopron.hu/11144/

Jakes, J. E. (2019). Mechanism for Diffusion through Secondary Cell Walls in Lignocellulosic Biomass [Research-article]. *Journal of Physical Chemistry B*, *123*(19), 4333–4339. https://doi.org/10.1021/acs.jpcb.9b01430

Jankowska, A. (2017). Effect of Extractives on the Equilibrium Moisture Content and Shrinkage of Selected Tropical Wood. *Bioresources Journal*, *12*(1), 597–607. https://doi.org/10.15376/biores.12.1.597-607

Jansson, G., Danusevičius, D., Grotehusman, H., Kowalczyk, J., Krajmerova, D., Skrøppa, T., & Wolf, H. (2013). Norway Spruce (Picea abies (L.) H. Karst.). In *Forest Tree Breeding in Europe: Current State-of-the-Art and Perspectives* (pp. 123–176). Springer.

Joščák, M., Sonderegger, W., Niemz, P., Schnider, T., Oppikofer, R., & Lammar, L. (2012). Influence of the air cavities on thermal conductivity of selected wood based materials and their application for building industry. *Bauphysik*, *34*(1), 32–37. https://doi.org/10.1002/bapi.201200005

Kaboorani, A., & Riedl, B. (2011). Composites : Part A Effects of adding nano-clay on performance of polyvinyl acetate (PVA) as a wood adhesive. *Composites Part A*, *42*(8), 1031–1039. https://doi.org/10.1016/j.compositesa.2011.04.007

Kang, H., & Hart, C. A. (1997). TEMPERATURE EFFECT ON DIFFUSION COEFFICIENT IN DRYING WOOD. *Wood and Fiber Science*, *29*(4), 325–332.

Karagüler, M. E., & Kaya, G. (2017). The effect of relative humidity and moisture to the durability of spruce and laminated timber. *A|Z ITU Journal of the Faculty of Architecture*, *14*(1), 103–110. https://doi.org/https://doi.org/10.5505/itujfa.2017.18480

Kinloch, A. J. (1997). Adhesives in engineering. *Proceedings of the Institution of Mechanical Engineers, Part G: Journal of Aerospace Engineering*, *211*(January), 307–335.

Kläusler, O., Clauß, S., Lübke, L., Trachsel, J., & Niemz, P. (2013). Influence of moisture on stress-strain behaviour of adhesives used for structural bonding of wood. *International Journal of Adhesion and Adhesives*, *44*, 57–65. https://doi.org/10.1016/j.ijadhadh.2013.01.015

Kong, X., Liu, G., & Curtis, J. M. (2011). Characterization of canola oil based polyurethane wood adhesives. *International Journal of Adhesion and Adhesives*, *31*(6), 559–564. https://doi.org/10.1016/j.ijadhadh.2011.05.004

Lana, D. ;, Gonzalez-Alegre, V. ;, Portela, M. ;, & Iniguez-Gonzalez, G. (2022). Cross Laminated Timber (CLT) manufactured with European oak recovered from demolition : Structural properties and non-destructive evaluation. *Construction and Building Materials*, *339*(November 2021). https://doi.org/10.1016/j.conbuildmat.2022.127635

Leger, R., Roy, A., & Grandidier, J. C. (2010). Non-classical water diffusion in an industrial adhesive. *International Journal of Adhesion and Adhesives*, *30*(8), 744–753. https://doi.org/10.1016/j.ijadhadh.2010.07.008

Lennart, S., & Elina, B. (2009). Cellulose structural arrangement in relation to spectral changes in tensile loading FTIR. *Cellulose*, *16*, 975–982. https://doi.org/10.1007/s10570-009-9331-z

Lindh, E. L., Terenzi, C., Salmén, L., & Furó, I. (2017). Water in cellulose: Evidence and identification of immobile and mobile adsorbed phases by 2H MAS NMR. *Physical Chemistry Chemical Physics*, *19*(6), 4360–4369. https://doi.org/10.1039/c6cp08219j

Mannes, D., Sanabria, S., Funk, M., Wimmer, R., Kranitz, K., & Niemz, P. (2014). Water vapour diffusion through historically relevant glutin-based wood adhesives with sorption measurements and neutron radiography. *Wood Science and Technology*, *48*(3), 591–609. https://doi.org/10.1007/s00226-014-0626-3

Mannes, D., Schmidt, J. A., Niemz, P., & Volkmer, T. (2012). Untersuchungen zum Einfluss der Klebstoffart auf den kapillaren Wassertransport in Holz parallel zur Faserrichtung. *Bauphysik*, *34*(2), 61–65. https://doi.org/10.1002/bapi.201200007

Mannes, D., Sonderegger, W., Hering, S., Lehmann, E., & Niemz, P. (2009). Non-destructive determination and quantification of diffusion processes in wood by means of neutron imaging. *Holzforschung*, *63*(5), 589–596. https://doi.org/10.1515/HF.2009.100

Matthews, J. F., Skopec, C. E., Mason, P. E., Zuccato, P., Torget, R. W., Sugiyama, J., Himmel, M. E., & Brady, J. W. (2006). Computer simulation studies of microcrystalline cellulose Iβ. *Carbohydrate Research*, *341*(1), 138–152. https://doi.org/10.1016/j.carres.2005.09.028

Molnár, S., & Bariska, M. (2006). *Magyarország ipari fái: Wood species of Hungary*. Szaktudás Kiadó Ház.

Olek, W., & Weres, J. (2007). Effects of the method of identification of the diffusion coefficient on accuracy of modeling bound water transfer in wood. *Transport in Porous Media*, *66*(1–2), 135–144. https://doi.org/10.1007/s11242-006-9010-6

Opoku, F. Y. (2007). *AN INVESTIGATION INTO THE SUITABILITY OF SELECTED LESSER UTILISED GHANAIAN HARDWOODS FOR USE AS OUTDOOR FURNITURE AND DECKING A thesis submitted for the degree of Master of Philosophy*.

Ozdemir, M. F., Maras, M. murat ;, & Yurtsenven, H. B. (2023). Flexural Behavior of Laminated Wood Beams Strengthened with Novel Hybrid Composite Systems: An Experimental Study. *Journal of the Korean Wood Science and Technology*, *6*(51), 526–541. https://doi.org/https://doi.org/10.5658/WOOD.2023.51.6.526

Pan, P., Yan, X., & Zhao, W. (2022). Effect of Coating Process of Photochromic and Thermochromic Composite Microcapsules on Coating Properties for Basswood. *Coatings*, *12*(9). https://doi.org/10.3390/coatings12091246

Panda, S. S., Panda, B. P., Nayak, S. K., & Mohanty, S. (2018). A Review on Waterborne Thermosetting Polyurethane Coatings Based on Castor Oil: Synthesis, Characterization, and Application. *Polymer - Plastics Technology and Engineering*, *57*(6), 500–522. https://doi.org/10.1080/03602559.2016.1275681

Pokorná, E., Faltus, M., Máchová, P., Zámečník, J., & Fulín, M. (2020). Grey poplar explant acclimation to improve the dehydration tolerance and cryopreservation. *Biologia Plantarum*, *64*(February), 119–128. https://doi.org/10.32615/bp.2019.148

Pournou, Anastasia. (2020). Wood anatomy, chemistry and physical properties. In *Biodeterioration of Wooden Cultural Heritage: Organisms and Decay Mechanisms in Aquatic and Terrestrial Ecosystems* (pp. 1–41). Springer.

Qin, Y., & Yan, X. (2022). Effect of the Addition of Shellac Self-Healing and Discoloration Microcapsules on the Performance of Coatings Applied on Ebiara Solid Board. *Materials Chemistry*, *12*(1627). https://doi.org/10.3390/coatings12111627

Rafsanjani, A., Derome, D., & Carmeliet, J. (2012). The role of geometrical disorder on swelling anisotropy of cellular solids. *Mechanics of Materials*, *55*, 49–59. https://doi.org/10.1016/j.mechmat.2012.08.002

Rafsanjani, A., Stiefel, M., Jefimovs, K., Mokso, R., Derome, D., & Carmeliet, J. (2014). Hygroscopic swelling and shrinkage of latewood cell wall micropillars reveal ultrastructural anisotropy. *Journal of the Royal Society Interface*, *11*(95). https://doi.org/10.1098/rsif.2014.0126

Robert, H. F. (2010). Wood as a Sustainable Building Material. In *Wood Handbook Wood as an Engineering Material Centennial* (pp. 1–6). Forest Products Laboratory • United States Department of Agriculture Forest Service • Madison, Wisconsin.

Sandberg, D. (2016). Additives in wood products—today and future development. *Environmental Footprints and Eco-Design of Products and Processes*, *42*(51), 105–172. https://doi.org/10.1007/978-981-10-0655-5_4

Schadauer, K., & Freudenschuss, A. (2023). *Zwischenauswertung der ÖWI 2016/18-Bund*.

Schwandt, N. W., & Gound, T. G. (2003). Resorcinol-Formaldehyde Resin " Russian Red " Endodontic Therapy. *JOURNAL OF ENDODONTICS*, *29*(2), 435–437. https://doi.org/10.1097/00004770-200307000-00002

Sernek, M., Boonstra, M., Pizzi, A., Despres, A., & Gérardin, P. (2008). Bonding performance of heat treated wood with structural adhesives. *Holz Als Roh - Und Werkstoff*, *66*(3), 173–180. https://doi.org/10.1007/s00107-007-0218-0

Shamaev, V., Russu, A., Medvedev, I., Trubnikov, N., Druzyanova, V., Zadrauskaite, N., & Revyako, S. (2025a). Determination of Factors Influencing the Coefficient of Internal Friction of Natural and Stained Oak. *Journal of the Korean Wood Science and Technology*, *53*(1), 33–48. https://doi.org/10.5658/WOOD.2025.53.1.33

Shamaev, V., Russu, A., Medvedev, I., Trubnikov, N., Druzyanova, V., Zadrauskaite, N., & Revyako, S. (2025b). Determination of Factors Influencing the Coefficient of Internal Friction of Natural and Stained Oak. *Journal of the Korean Wood Science and Technology*, *53*(1), 33–48. https://doi.org/10.5658/WOOD.2025.53.1.33

Sharpe, L. H. (1972). The interphase in adhesion. *The Journal of Adhesion*, *4*(1), 51–64. https://doi.org/10.1080/00218467208072210

Siau, J. F. (1984). Steady-State Moisture Movement. In *Transport Processes in Wood* (pp. 151–174). https://doi.org/10.1007/978-3-642-69213-0_6

Sing, K. S. W., Rouquerol, F., & Rouquerol, J. (1999). *Adsorption by powders and porous solids: principles, methodology, and applications*. Academic Press.

Skaar, C. (1988). Moisture Movement in the Wood Cell Wall BT - Wood-Water Relations. In C. Skaar (Ed.), *Springer Series in Wood Science ((SSWOO))* (pp. 177–206). Springer Berlin Heidelberg. https://doi.org/10.1007/978-3-642-73683-4_5

Skaar, C., Prichananda, C., & Davidson, R. W. (1969). *Some aspects of moisture sorption dynamics in wood.*

Sonderegger, W., Glaunsinger, M., Mannes, D., Volkmer, T., & Niemz, P. (2015). Investigations into the influence of two different wood coatings on water diffusion determined by means of neutron imaging. *European Journal of Wood and Wood Products*, *73*(6), 793–799. https://doi.org/10.1007/s00107-015-0951-8

Sonderegger, W., Hering, S., Mannes, D., Vontobel, P., Lehmann, E., & Niemz, P. (2010). Quantitative determination of bound water diffusion in multilayer boards by means of neutron imaging. *European Journal of Wood and Wood Products*, *68*(3), 341–350. https://doi.org/10.1007/s00107-010-0463-5

Sonderegger, W., Hering, S., & Niemz, P. (2011). Thermal behaviour of Norway spruce and European beech in and between the principal anatomical directions. *Holzforschung*, *65*(3), 369–375. https://doi.org/10.1515/HF.2011.036

Srivaro, S., Matan, N., & Lam, F. (2019). Performance of cross laminated timber made of oil palm trunk waste for building construction : a pilot study. *European Journal of Wood and Wood Products*, *77*(3), 353–365. https://doi.org/10.1007/s00107-019-01403-0

Tang, E., Lisbeth, E., & Thygesen, G. (2013). A critical discussion of the physics of wood – water interactions. *Wood Sci Technol*, *47*, 141–161. https://doi.org/10.1007/s00226-012-0514-7

Temiz, A., Yildiz, U. C., Aydin, I., Eikenes, M., Alfredsen, G., & Çolakoglu, G. (2005). Surface roughness and color characteristics of wood treated with preservatives after accelerated weathering test. *Applied Surface Science*, *250*(1–4), 35–42. https://doi.org/10.1016/j.apsusc.2004.12.019

Tetens, O. (1930). Uber einige meteorologische Begriffe. *Z. Geophys*, *6*, 297–309.

Thomson, W. (1872). 4. On the Equilibrium of Vapour at a Curved Surface of Liquid. *Proceedings of the Royal Society of Edinburgh*, *7*, 63–68. https://doi.org/10.1017/S0370164600041729

Thybring, E. E., Fredriksson, M., Zelinka, S. L., & Glass, S. V. (2022). Water in Wood: A Review of Current Understanding and Knowledge Gaps. *Forests*, *13*(12). https://doi.org/10.3390/f13122051

Thybring, E. E., Thygesen, L. G., & Burgert, I. (2017). Hydroxyl accessibility in wood cell walls as affected by drying and re-wetting procedures. *Cellulose*, *24*(6), 2375–2384. https://doi.org/10.1007/s10570-017-1278-x

Time, B. (1998). *Hygroscopic moisture transport in wood. Dr ing*. Norwegian University of Science and Technology, Trondheim.

Tsushima S., K. Teranishi, Hirai. S. (2005). Water diffusion measurement in fuel-cell SPE membrane by NMR. *Energy*, *30*(2–4), 235–245.

Ülker, O. (2016). Wood Adhesives and Bonding Theory. In *Adhesives - Applications and Properties* (pp. 271–288). https://doi.org/10.5772/65759

Utsumi, Y., Sano, Y., Fujikawa, S., Funada, R., & Ohtani, J. (1998). Visualization of cavitated vessels in winter and refilled vessels in spring in diffuse-porous trees by cryo-scanning electron microscopy. *Plant Physiology*, *117*(4), 1463–1471. https://doi.org/10.1104/pp.117.4.1463

Valent, J., Papp, E., Palla, J., & Csiha, C. (2017). WATER PERMEABILITY OF TWO DIFFERENT WOOD LASURES. *Pro Ligno*, *13*(4), 387–390.

Van Meel, P. A., Erich, S. J. F., Huinink, H. P., Kopinga, K., De Jong, J., & Adan, O. C. G. (2011). Moisture transport in coated wood. *Progress in Organic Coatings*, *72*(4), 686–694. https://doi.org/10.1016/j.porgcoat.2011.07.011

Wadsö, L. (1993). *Studies of water vapor transport and sorption in wood*. Lund University.

Wang, X., Li, X., Xu, L. long, Zhang, Q., & Gu, Y. (2020). Preparation and Corrosion Resistance of γ-aminopropyltriethoxysilane-TiO2-GO/Waterborne Polyurethane Coating. *International Journal of Electrochemical Science*, *15*(11), 11340–11355. https://doi.org/10.20964/2020.11.44

Yang, Z., Han, Y., Peng, W., Wang, L., & Yan, X. (2022). Effect of Fluorane Microcapsule Content on Properties of Thermochroic Waterborne Topcoat on Tilia europaea. *Polymers*, *14*(17). https://doi.org/10.3390/polym14173638

Yin, X., Li, X., & Luo, Y. (2017). Synthesis and characterization of multifunctional two-component waterborne polyurethane coatings: Fluorescence, thermostability and flame retardancy. *Polymers*, *9*(10), 1–15. https://doi.org/10.3390/polym9100492

Zanni-Deffarges, M. P., & Shanahan, M. E. R. (1995). Diffusion of water into an epoxy adhesive: comparison between bulk behaviour and adhesive joints. *International Journal of Adhesion and Adhesives*, *15*(3), 137–142. https://doi.org/10.1016/0143-7496(95)91624-F

Zinad, O. S., & Csiha, C. (2024). Improving sustainability of mortar by wood-ash and Nano-SiO2. *Case Studies in Chemical and Environmental Engineering*, *9*. https://doi.org/10.1016/j.cscee.2023.100597